

1-1-1980

# Interfacial tension theory for low molecular weight and polymer systems.

Claudia I. Poser

*University of Massachusetts Amherst*

Follow this and additional works at: [https://scholarworks.umass.edu/dissertations\\_1](https://scholarworks.umass.edu/dissertations_1)

---

## Recommended Citation

Poser, Claudia I., "Interfacial tension theory for low molecular weight and polymer systems." (1980). *Doctoral Dissertations 1896 - February 2014*. 654.

[https://scholarworks.umass.edu/dissertations\\_1/654](https://scholarworks.umass.edu/dissertations_1/654)

This Open Access Dissertation is brought to you for free and open access by ScholarWorks@UMass Amherst. It has been accepted for inclusion in Doctoral Dissertations 1896 - February 2014 by an authorized administrator of ScholarWorks@UMass Amherst. For more information, please contact [scholarworks@library.umass.edu](mailto:scholarworks@library.umass.edu).

UMASS/AMHERST



312066 0015 5641 7

INTERFACIAL TENSION THEORY FOR LOW  
MOLECULAR WEIGHT AND POLYMER SYSTEMS

A Dissertation Presented

By

CLAUDIA I. POSER

Submitted to the Graduate School of the  
University of Massachusetts in partial fulfillment  
of the requirements for the degree of

DOCTOR OF PHILOSOPHY

February 1980

Polymer Science and Engineering



Claudia Ingrid Poser 1980

All Rights Reserved

National Science Foundation  
Materials Research Laboratory

Project No. 76-80641

INTERFACIAL TENSION THEORY FOR LOW  
MOLECULAR WEIGHT AND POLYMER SYSTEMS

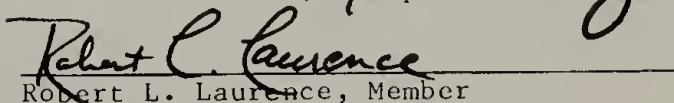
A Dissertation Presented

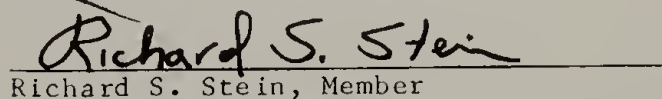
By

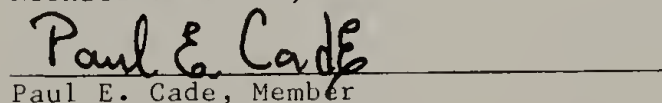
CLAUDIA I. POSER


Approved as to style and content by:

  
Isaac C. Sanchez, Chairperson of Committee

  
Robert L. Laurence, Member

  
Richard S. Stein, Member

  
Paul E. Cade, Member

  
W. J. MacKnight, Department Head  
Polymer Science and Engineering

Für Matthew  
und für meine Eltern

## Acknowledgement

My sincere thanks go to Doctor Isaac Sanchez whose patience and scientific insight were invaluable, and to Professor Laurence, Professor Stein, and Professor Cade for their critical suggestions.

I am also grateful to the staff of the Polymer Division at the National Bureau of Standards, especially Dr. R. K. Eby and Mr. J. P. Colson, for making my stay there as enjoyable as possible. Dr. John W. Cahn also offered useful advice and encouragement. Professor Ted Davis and Bruce Carey at the University of Minnesota generously shared their results and made many helpful suggestions. I would also like to thank Professors Esteban Brignole and Enrique Rotstein at the Universidad Nacional del Sur in Bahia Blanca, Argentina for enabling me to write the bulk of this dissertation in such pleasant company and surroundings.

## ABSTRACT

### Interfacial Tension Theory for Low Molecular Weight and Polymer Systems

February 1980

Claudia I. Poser, B.S., Clemson University

M.S., Ph.D., University of Massachusetts

Directed by: Professor Isaac C. Sanchez

This dissertation reports on the development of an interfacial tension theory applicable to low molecular weight fluids and polymer systems. The theoretical treatment includes a rederivation of the free energy minimization formalism for inhomogeneous systems in the gradient approximation. The gradient approach is then combined with a slightly modified version of the lattice fluid model. The resulting theory describes liquid-vapor and liquid-liquid interfaces of pure and mixed nonpolar and slightly polar systems away from the critical region. The interfacial equations are amenable to numerical evaluation, and the theoretical predictions were tested against experiment for the cases of pure components and binary mixtures.

For one-component liquid-vapor interfaces, a single parameter,  $\tilde{\kappa}$ , which can be related to the range of the attractive part of the intermolecular interaction potential, arises. If the interaction is assumed to be purely dispersive, predicted tension values fall below experimental ones by about 10-15%. A single constant value of  $\tilde{\kappa}$ , determined from a fit of experimental data, reduces this error to about 5% for low molecular weight nonpolar and slightly polar liquids.



The temperature interval over which the theory applies is wide and useful, ranging from the triple point to  $T/T_c = .7$ . ( $T_c$  is the critical temperature.) For polymers, the error is reduced to 10% when a slightly different, but also constant, value of  $\tilde{\kappa}$  is applied. The theory is somewhat less accurate for polymer melts because it overestimates the surface entropy. The molecular weight dependence of the interfacial tension is correctly predicted for the n-alkanes, and is closely related to the dependence of liquid density on molecular weight.

For binary mixtures, the theory contains an additional parameter corresponding to the intermolecular interactions between unlike molecules. This parameter can either be evaluated from the lattice fluid combining rules (using fitted mixing parameters) or it can be approximated from the pure component interfacial parameters by the geometric mean assumption. The latter procedure gives good results for liquid-vapor interfaces in miscible mixtures, but appears to break down for liquid-liquid interfaces. For nonpolar liquid mixtures, the theory can predict the composition dependence of the liquid-vapor interfacial tension to within 5%. Positive deviations from ideal tension behavior as well as strong preferential adsorption at the interface are correctly predicted. The theory suggests that these phenomena arise from size differences, equation of state behavior, and deviations from ideal mixing rules.

For liquid-liquid systems, interfacial tension calculations depend sensitively on the phase diagram predicted by the lattice fluid

theory. The phase diagrams in turn depend on the mixing parameters. For polymer-polymer systems, presently available data is inadequate to accurately evaluate these mixing parameters. Theoretical predictions for polymer-polymer interfaces thus remain qualitative at this time.

TABLE OF CONTENTS

	page
ACKNOWLEDGEMENT . . . . .	v
ABSTRACT . . . . .	vi
LIST OF FIGURES . . . . .	x
LIST OF TABLES . . . . .	xiii
CHAPTER	
I. INTRODUCTION . . . . .	1
II. GRADIENT THEORY OF INHOMOGENEOUS SYSTEMS . . . . .	10
III. LATTICE FLUID THEORY . . . . .	28
IV. PHASE EQUILIBRIA . . . . .	45
V. ONE-COMPONENT SYSTEMS	
A. THEORY . . . . .	73
B. RESULTS . . . . .	76
VI. TWO-COMPONENT SYSTEMS	
A. THEORY . . . . .	122
B. RESULTS . . . . .	128
VII. SUMMARY . . . . .	172
APPENDIX	
NUMERICAL TECHNIQUES . . . . .	184

LIST OF FIGURES

1.	Dependence of the Local Chemical Potential, $\mu(\rho)$ , on Density Through the Interface.....	24
2.	Behavior of the Local Helmholtz Free Energy Density, $a_o$ , and the Excess Helmholtz Free Energy Density, $\Delta a$ , Through the Interface.....	26
3.	Composition Dependence of the Mixing Parameters.....	51
4.	Temperature Dependence of the Mixing Parameters.....	52
5.	Experimental and Calculated Mixing Functions for the System Benzene-n-Heptane at 25°C.....	58
6.	Experimental and Calculated Mixing Functions for the System n-Hexane-2,2-Dimethyl Butane at 25°C.....	60
7.	Map of the Spinodal Equation for the System Cyclohexane-Aniline.....	68
8.	Liquid-Vapor Equilibria for the n-Hexane Benzene System at 25°C.....	70
9.	Temperature-Composition Phase Diagram for the Cyclohexane-Aniline System.....	71
10.	Reduced Interfacial Tension, $\tilde{\gamma}$ , versus Reduced Temperature, $\tilde{T}$ , at Several Values of the Molecular Size Parameter, $r$ .....	77
11.	Reduced Density Profiles at Several Values of the Reduced Temperature, $\tilde{T}$ , and Molecular Size Parameter, $r$ ...	79
12.	Dependence of the Reduced Interfacial Tension, $\tilde{\gamma}$ , on Reduced Temperature, $\tilde{T}$ , Near the Critical Temperature, $\tilde{T}_c$ .....	81
13.	Comparison of Experimental and Theoretical Tensions versus Temperature for n-Hexane with $\tilde{\kappa} = .5$ .....	83
14.	Values of $\tilde{\kappa}$ Required to Fit the Experimental Tension for n-Alkanes versus Temperature Reduced by the Experimental Critical Temperature.....	85
15.	Comparison of Experimental and Theoretical Tensions versus Temperature for n-Hexane and n-Decane with $\tilde{\kappa} = .61$ ..	87
16.	Comparison of Experimental and Theoretical Tensions versus Temperature for Chlorobenzene and Diethyl Ether with $\tilde{\kappa} = .62$ .....	89
17.	Reduced Tension, $\tilde{\gamma}$ , versus Reduced Interfacial Thickness, $\tilde{t}$ , for n-Heptane at Two Values of $\tilde{\kappa}$ .....	93
18.	Reduced Interfacial Tension, $\tilde{\gamma}$ , and Thickness, $\tilde{t}$ , as a Function of $\tilde{T}/\tilde{T}_c$ for n-Heptane with $\tilde{\kappa} = .62$ .....	96
19.	Reduced Interfacial Thickness, $\tilde{t}$ , versus the Molecular Size Parameter, $r$ , for Several Liquids at Constant Ratio of the Reduced Temperature to the Reduced Theoretical Critical Temperature.....	97
20.	Molecular Weight Dependence of the Interfacial Tension for n-Alkanes.....	100
21.	Effect of $\gamma^*$ on the Calculated Tension for n-Alkanes.....	102

22.	Effect of $\epsilon^*$ on the Calculated Tension for n-Alkanes.....	104
23.	Reduced Interfacial Tension versus Reduced Temperature for Polymers.....	106
24.	Interfacial Tension versus Temperature for Branched Polyethylene and Poly(Vinyl Acetate).....	108
25.	Interfacial Tension versus Temperature for Polystyrene and Linear Polyethylene.....	109
26.	Comparison of the Theory to Empirical Predictions for Poly(Dimethyl Siloxane).....	118
27.	Comparison of the Theory to Empirical Predictions for Polystyrene.....	119
28.	Comparison of the Theory to Empirical Predictions for Linear Polyethylene.....	120
29.	Comparison of the Theory to Empirical Predictions for Polyisobutylene.....	121
30.	Interfacial Tension versus Mole Fraction for Benzene-n- Hexane at 25°C.....	129
31.	Interfacial Tension versus Mole Fraction for Cyclo- hexane-n-Hexane at 20°C.....	130
32.	Interfacial Tension versus Mole Fraction for Benzene- Cyclohexane at 20°C.....	131
33.	Interfacial Tension versus Mole Fraction for Benzene- n-Dodecane at 40°C.....	132
34.	Interfacial Tension versus Mole Fraction for Benzene- Cyclohexane at 20°C with Fitted End-Points.....	133
35.	Interfacial Profiles for Benzene-n-Hexane at 25°C.....	138
36.	Excess Interfacial Tension of n-Hexane with Three Pentanes.....	141
37.	Interfacial Tension versus Mole Fraction for Toluene- Chlorobenzene at 20°C.....	143
38.	Interfacial Tension versus Mole Fraction for n-Dodecane- n-Hexane at 30°C.....	145
39.	Interfacial Tension versus Mole Fraction for Benzene-n- Dodecane at 40°C.....	146
40.	Effect of the Mixing Parameters on Interfacial Profiles for Benzene-n-Dodecane at 40°C.....	147
41.	Interfacial Tension versus Volume Fraction for Toluene- Poly(Dimethyl Siloxane) at 24°C.....	149
42.	Interfacial Tension versus Volume Fraction for Tetralin- Poly(Dimethyl Siloxane) at 30°C.....	150
43.	Interfacial Profiles for Tetralin-Poly(Dimethyl Siloxane) at 30°C.....	153
44.	Interfacial Profiles for Benzene-Polyisobutylene at 30°C....	157
45.	Interfacial Profiles for Cyclohexane-Aniline at 9°C.....	159
46.	Interfacial Tension and Thickness as a Function of Molecular Weight for Linear Polyethylene-Polystyrene at 140°C.....	162
47.	Schematic Representation of a Common Polymer-Polymer Temperature-Composition Diagram.....	163

48.	Dependence of the Interfacial Tension on the Mixing Parameter $\zeta$ for Linear Polyethylene-Polystyrene at 140°C.....	165
49.	Dependence of the Interfacial Tension on the Mixing Parameter $\zeta$ for Poly(Dimethyl Siloxane)-Polyisobutylene at 140°C.....	166
50.	Dependence of the Interfacial Tension on the Mixing Parameter $\zeta$ for Poly(Dimethyl Siloxane)-Polystyrene at 140°C.....	167
51.	Dependence of the Interfacial Tension on the Mixing Parameter $\zeta$ for Poly(Dimethyl Siloxane)-Poly(Vinyl Acetate) at 140°C.....	168
52.	Dependence of the Interfacial Thickness on the Mixing Parameter $\zeta$ for Linear Polyethylene-Polystyrene at 140°C.....	169
53.	Schematic Representation of a Solution Path for a Liquid-Vapor Interface.....	198

## LIST OF TABLES

1.	Lattice Fluid Parameters of Low Molecular Weight Liquids....	32
2.	Lattice Fluid Parameters for Polymers.....	34
3.	Mixing Parameters for the $\Delta P^*$ Combining Rules.....	53
4.	Mixing Parameters for the General Combining Rules.....	54
5.	Errors between Calculated and Experimental Tensions for Low Molecular Weight Liquids.....	90
6.	Surface Entropy of n-Alkanes.....	111
7.	Surface Entropy of Polymers .....	112
8.	Comparison of Surface Entropy Error to MacLeod's Exponent...	114
9.	Interfacial Tension of Benzene-Cyclohexane at 20°C for Different Values of the Mixing Parameters.....	135
10.	Comparison of the Geometric Mean Approximation to Eq. VI.8.	136
11.	Calculated and Experimental Excess Interfacial Tensions for n-Hexane-n-Dodecane at 30°C.....	140
12.	Thickness and $\zeta$ for Some Polymer Systems.....	170

## CHAPTER I

### INTRODUCTION

The theoretical description of interfaces between fluid phases has a long and active history dating back to the differing approaches formulated by Gibbs<sup>1</sup> and van der Waals.<sup>2</sup> Gibbs treated the fluid interface as a discontinuity, constructing a hypothetical dividing surface with which he associated a superficial Helmholtz free energy. Van der Waals based his derivation on the concept that the interface arises from and can be described by the principle of free energy minimization. In addition, he introduced the idea that the free energy in the inhomogeneous region may be expressed as a function of the local density and its spatial derivatives. Although van der Waals' interfacial theory was forgotten until a similar derivation for binary systems by Cahn and Hilliard<sup>3</sup> in 1958, his "free energy" approach contained the seeds of the modern gradient theory of inhomogeneous systems.

Cahn and Hilliard used a concentration gradient formulation in conjunction with the regular solution model to derive expressions for the interfacial tensions and concentration profiles of low molecular weight binary mixtures. Subsequently, Widom<sup>4,5</sup> reformulated the theory for a fluid in the neighborhood of its critical point where the gradient approximation was thought to be exclusively applicable. McCoy and Davis<sup>6</sup> have recently shown that the gradient theory is fairly accurate even for sharp interfaces, although Abraham<sup>7</sup> demonstrated that results for a liquid-vapor interface of a Lennard-Jones fluid



are erroneous at the triple point.

In the rigorous form of the free energy theory, which was developed by Yang, Fleming, and Gibbs,<sup>8</sup> the gradient expansion is applied to the total Helmholtz free energy density. This theory leads to intractable integral equations for the density distributions. Bongiorno, Scriven, and Davis<sup>9</sup> derived their interfacial theory by applying the gradient expansion to the potential energy density only. The resulting tractable expressions for the tensions and profiles require the use of an unspecified equation of state. These authors have obtained reasonable results for simple fluids by combining their gradient theory with the van der Waals' equation of state.<sup>10</sup> For polyatomic low molecular weight fluids the semi-empirical Peng-Robinson equation has been used successfully.<sup>11,12</sup> All of the more rigorous molecular theories require the two-body distribution functions in the interface, which has eluded evaluation even for argon.<sup>13</sup> Thus, the gradient approximation combined with a mean field equation of state holds the most promise for predicting interfacial properties of complex molecules such as polymers.

Systems containing polymers have historically been treated separately from low molecular weight liquids. This separation may be traced back to early observations of the break-down of ideal mixing equations when applied to polymer solutions, which led to the recognition of the influence of macromolecular size and flexibility. The Flory-Huggins theory provided a successful explanation of unique polymer solution behavior primarily by evaluating the configurational entropy of mixtures.<sup>14</sup> These historical developments may serve to

explain why most of the previous work on polymer interfaces concentrates on binary systems and on the entropic effects of an interface on polymer conformation. The focus on polymer-polymer interfaces has been further motivated by the fact that phase separation and immiscibility are the rule rather than the exception for polymer pairs which is again due to the comparatively small entropy of mixing.

For the reasons cited above, descriptions of the surface tension for pure polymers have remained at the semi-empirical stage.<sup>15</sup> The most sophisticated of these approaches was developed by Patterson and coworkers.<sup>16,17</sup> In this treatment an empirical correlation serves to connect the surface tension to the equation of state parameters of Prigogine's<sup>18</sup> corresponding states theory. Errors in predicted values for this and other methods (based on solubility parameters and the parachor method<sup>15</sup>) are in the range of 15% for nonpolar and slightly polar polymer melts.

The effort applied to the description of binary systems containing polymers has been more extensive. A brief review is given below. More detailed discussions of theoretical predictions will be presented in the main body of this dissertation where applicable. Existing theories generally fall into two categories: those dealing with the liquid-vapor interface of polymer solutions, and those dealing with the liquid-liquid interfaces between the two phases of a demixed polymer solution or polymer-polymer system. The former category consists essentially of Prigogine and Marechal's monolayer theory,<sup>19</sup> its modifications by Gaines,<sup>20</sup> and the multilayer formula-

tions by Roe<sup>21</sup> and Helfand.<sup>22</sup> The original version of the monolayer theory is based on the athermal Flory-Huggins solution theory. The system consists of bulk liquid and one lattice layer of a different composition. The polymer molecules in this monolayer are restricted to conformations lying parallel to the surface. Gaines modified this treatment by introducing energetic interactions into the bulk phase, while still assuming the surface layer to behave athermally. The interaction parameter is then used as a fitting parameter which leads to good agreement for the concentration dependence of surface tension for a variety of polymer solutions.<sup>20,23,24</sup> The use of the monolayer together with the requirement of conformations parallel to the surface remains conceptually unsatisfying, however.

The lattice theories proposed independently by Helfand and Roe, seek to remove these restrictions. The number of lattice layers whose composition differs from the bulk is not specified. Both of these theories use a random heat of mixing and concentrate on formulating the system's entropy. The interfacial profile is obtained by minimization of the resulting free energy. The results of the two authors differ due to different assumptions used in the entropy formulation. The expressions obtained by Helfand are very difficult to solve numerically,<sup>25</sup> and have not been compared to experimental data. Roe's results are somewhat simpler to solve. Predictions of the interfacial tension's concentration dependence for polymer solutions are similar to those obtained by Gaines, although different values of the fitting parameter  $\chi$  are required.<sup>21</sup> Roe also found that the concentrations obtained for the top-most (surface) layer were almost

identical to those calculated in the monolayer approach, and that the succeeding layers had very little effect on the tension.

The first theory which was proposed for polymer-containing liquid-liquid interfaces is due to Vrij,<sup>26</sup> who combined the gradient approximation with a solution model due to Debye<sup>27</sup> to describe two-phase polymer solutions near a critical solution temperature. The model was tested for a demixed solution of two different polymers in a common solvent. Although Vrij made some drastic assumptions (the polymers were assumed to have identical segment sizes and radii of gyration), the predicted dependence of the interfacial tension on concentration agreed qualitatively with experimental results. Recently, Vrij<sup>28</sup> has published a revised theory for demixed systems consisting of a single solvent and polymer. Debye's solution model was replaced by the Flory-Huggins entropy of mixing with two different expressions for the energy of mixing, the regular solution form and an empirical relation due to Koningsveld.<sup>29</sup> Due to the details of the model, solutions for the interfacial profile exist only within about 1% of the critical temperature.

Nose,<sup>30</sup> in an extension of Vrij's approach applicable to polymer solutions and polymer-polymer systems, has added an elastic free energy term to the Flory-Huggins free energy of mixing in order to account for distortions of the polymer segment distributions at an interface. One of the interesting predictions of this theory is a first order transition from a diffuse to a sharp interface near the critical temperature,  $T_c$ . Nose claims that this prediction is borne

out by the change in the dependence of the interfacial tension on  $T_c - T$  which he has observed experimentally.<sup>31</sup> Numerical predictions of the tension have the right order of magnitude and qualitative behavior near a critical solution temperature.

Several theories have been derived for polymer-polymer systems away from the critical temperature. The first two of these are extensions of the multilayer lattice models of Helfand<sup>32</sup> and Roe.<sup>33</sup> As in the polymer solution versions of these theories, the calculations consist of deriving an expression for the entropy in the interface which corresponds to the minimum free energy. Results of the two theories again differ due to different assumptions used in the entropy formulation. Predictions of these theories remain primarily qualitative, since several parameters arise whose values cannot be unambiguously established.<sup>15</sup>

A numerically more successful theory, though somewhat less rigorous, was proposed by Helfand and Sapse.<sup>34</sup> The explicit consideration of the concentrations in each lattice layer is here abandoned. The interface is considered as an area in which interdiffusion of segments takes place, so that the probability of finding a segment in the interface may be described by a modified diffusion equation. The segments are assumed to be in an average molecular environment (mean field) and to follow Gaussian random walk statistics. The calculated values of the tension seem to agree very well with experimental data at 140°C, but this agreement must be considered somewhat fortuitous, since the temperature dependence cannot be predicted. All quantities in the final expression for the tension which would be expected to

contribute to the variation with temperature are evaluated from experimental data, and are considered to be constant.

The most recent treatment to appear on polymer-polymer interfaces again relies on a combination of the gradient approximation and the Flory-Huggins theory.<sup>35</sup> The concentration expansion, however, is here applied to the total free energy of mixing. As a result, the theory contains a number of undefined parameters. In order to obtain numerical results, the interfacial tension must be fitted at one temperature. In that case, the surface entropy (the temperature derivative of the tension) can be predicted as a function of another parameter.

From this brief review of the literature, some general features emerge. Small molecules are treated separately from macromolecules, and, in general, polymer solutions are treated separately from polymer-polymer mixtures. In addition, many of the theories dealing with polymers are either empirical (as in the case of pure polymers), restricted to a special region of the phase diagram (polymer solutions near a critical solution temperature), or difficult to connect to real systems (lattice theories of Helfand and Roe). The basic motivations leading to the work presented in this dissertation follow directly from these observations. A unified theory applicable to the range of molecular weights is clearly desirable. In addition, the theory should be able to describe pure substances, homogeneous mixtures, and phase-separated mixtures within the same framework. Furthermore, the parameters required should be unambiguously definable. In order to derive practical benefits from such a consistent approach, calculations

necessary to evaluate the predictions should be straightforward.

In view of such considerations, the approach which appeared most likely to be rewarding was to construct a theory combining the elements of the gradient approximation with the lattice fluid<sup>36-39</sup> (LF) model. The lattice fluid theory fulfills the present criteria for a molecular model, since it is able to describe the thermodynamic properties of both low and high molecular weight fluids semi-quantitatively. Moreover, generalization to systems of more than one component is straightforward. The gradient approximation was selected on the basis of the promising results which have been obtained through its use as discussed above.

The work presented here is organized into seven chapters and a numerical appendix. In Chapter II a different and more direct derivation of the gradient theory is presented. The treatment is confined to a planar interface and results are given for an n-component system. The final equations are identical to those obtained by Bongiorno et al.,<sup>9</sup> and reduce to those of Cahn and Hilliard<sup>3</sup> for a special case. Chapter III contains a discussion of the LF theory with special emphasis on some modifications made in adapting this formalism to the description of interfaces. These modifications consist of including long-range intermolecular interactions instead of exclusively nearest neighbor interactions. This change does not alter the homogeneous form of the LF theory due to its mean field nature. In addition, the combining rules employed in the extension to mixtures differ from those originally proposed.

Since the description of an interface between two phases requires

the knowledge of the equilibrium properties of those phases, Chapter IV will describe how the phase behavior of the different types of systems was analyzed. Chapters V and VI pertain to one and two component systems, respectively. Each of these chapters is divided into two sections. In the first section the general interfacial tension theory is specialized to the case under consideration. The second section presents numerical results and discusses them in the light of experimental results, empirical correlations, and predictions from other theoretical work. A summary which includes some suggestions for future work is contained in Chapter VII. The Numerical Appendix is intended to serve as an outline of techniques applied to the calculation of equilibrium phases, interfacial tensions, and profiles. Copies of specific programs are not included, since they tend to be of limited use. Most of the methods are well established in the field of numerical analysis. The Appendix will thus be useful as a guide to those techniques which were successful, especially when alternate approaches can be used.



## CHAPTER I I

## GRADIENT THEORY OF INHOMOGENEOUS SYSTEMS

Recent statistical mechanical theories of interfaces are based on two different approaches: the momentum balance formalism which requires mechanical equilibrium across the interface, and the free energy approach based on the principle of free energy minimization. Both of these approaches can be used at various levels of approximation. In order to justify the particular free energy formalism chosen for this work, a review of the basic statistical mechanical formulations follows.

The momentum balance approach was developed by Kirkwood and Buff<sup>40</sup> using the mechanical definition of the interfacial tension,  $\gamma$ , as the excess stress transmitted across a strip of unit width normal to the interface. For a planar interface, the result of this theory is

$$\gamma = \int_{-\infty}^{+\infty} [P_{xx} - P_{zz}] dx \quad (II.1)$$

$$= \sum_{i,j} \frac{1}{2} \int_{-\infty}^{+\infty} \frac{(s_z^2 - s_x^2)}{s} \frac{du_{ij}}{ds} \rho_2^{ij}(\tilde{R}, \tilde{R}+s) d^3 \tilde{s} dx .$$

$x$  is the direction normal to the interface, and  $P_{xx}$  and  $P_{zz}$  are components of the pressure tensor. In order to satisfy the requirements of hydrostatic equilibrium,  $P_{xx}$  must be constant and  $P_{yy}$  and  $P_{zz}$  must be equal and functions of  $x$ .  $du_{ij}/ds$  represents the force acting between particles of type  $i$  and  $j$ ,  $\rho_2^{ij}$  is the doublet density distribution function, and  $\tilde{R}$  and  $\tilde{R}'$  are position vectors.

The following definitions also apply:

$$\underline{s} = \underline{R} - \underline{R}' \quad ; \quad s = |\underline{s}| \quad . \quad (\text{II.2})$$

$s_z$  and  $s_x$  are the z and x components of  $\underline{s}$ . The density profiles are determined by the Yvon-Born-Green set of integro-differential equations.

Since

$$\rho_2^{ij}(\underline{R}, \underline{R} + \underline{s}) \equiv \rho_1^i(\underline{R}) \rho_1^j(\underline{R} + \underline{s}) g_{ij}(\underline{R}, \underline{R} + \underline{s}) \quad (\text{II.3})$$

where  $\rho_1^i$  and  $\rho_1^j$  represent the singlet density distribution functions, evaluation of the interfacial tension requires the inhomogeneous pair distribution function  $g_{ij}$ , which is generally unknown. In the original paper, the planar liquid-vapor interface was approximated by a step-function with the vapor density set equal to zero. The pair distribution function was equated to that of a homogeneous liquid.

One of the less drastic forms of approximation recently proposed<sup>41</sup> involves the application of the gradient expansion to the singlet densities and the pair distribution function. The effect of the gradient expansion is to change the equation for the density profile from an integral to a differential form. The local inhomogeneous pair distribution is then estimated by the homogeneous pair distribution at a mean density (mean field approximation). With these assumptions, tractable equations can be obtained. However, numerical results still require the homogeneous pair distribution function and the pair potential which are not available for most liquids.

The free energy approach, as mentioned previously, is based on

minimizing the Helmholtz free energy density of the inhomogeneous system. The exact model used determines whether the density profiles are given by integral or differential equations. The exact formulation recently given by Yang, Fleming and Gibbs<sup>8</sup> requires the direct homogeneous correlation function and leads to intractable integral expressions for the profile. Since the modern gradient theory grew out of the original formulation by van der Waals<sup>2</sup> an examination of his assumptions is conceptually useful.

The planar interface under consideration in van der Waals' theory is that of a pure liquid in equilibrium with its vapor. The two homogeneous phases thus differ only in their densities. Van der Waals postulated that the density in the interfacial region changes continuously in the direction perpendicular to the interface, and that the density profile adopted by the system is that which minimizes the total free energy. Further, the energy at a given point in the inhomogeneous region not only depends on the density at that point, but is influenced by the densities at all points lying within the range of the intermolecular forces. This is the concept which leads to the expression of the free energy in the inhomogeneous region as the sum of the local free energy and terms consisting of density gradients scaled by intermolecular force contributions. An additional approximation invoked in the theory is that the entropy in the inhomogeneous region is a function of the local density only. This approximation appears to be quite successful for small molecules,<sup>6</sup> and has been retained in recent treatments of such systems.<sup>3,9,12</sup> Basically, the van der Waal's

theory introduced the free energy approach to fluid interfaces and simultaneously proposed the gradient approximation as a means for including the nonlocal contributions to the free energy density in the presence of a density variation. This approach, in combination with the van der Waals fluid model, resulted in a solvable differential equation whose predictions are qualitatively correct.

The free energy approach has since been reformulated in the absence of the gradient approximation<sup>6,10</sup> allowing this approximation's domain of validity to be examined for several molecular models. For the van der Waals fluid, the tensions predicted by the integral and gradient versions of the theory agreed within 10% over the entire liquid-vapor coexistence range,<sup>9</sup> while the disagreement appears to be slightly larger at low temperatures for the Modified Van der Waals and the Approximate Density Functional models.<sup>6</sup> The mathematical simplicity gained through the application of the gradient approximation is considerable.

As pointed out previously, a particular model for the Helmholtz free energy density is required in order to use the free energy formalism. Since the goal of the present theory is to predict interfacial properties of complex polyatomic fluids, a rigorous molecular theory is precluded by the current state of knowledge of liquid structure. The model selected is a mean field description based on a compressible lattice which will be discussed in detail in the next chapter. A general derivation of the interfacial tension theory in the mean field approximation, which forms the basis of the work presented in this thesis, is given below.

In the free energy approach, one may define the interfacial tension,  $\gamma$ , of a planar interface by

$$\gamma \equiv (A - A_e) / S_o \quad (\text{II.4})$$

where  $S_o$  is the surface area,  $A$  is the inhomogeneous system's Helmholtz free energy, and  $A_e$  is the Helmholtz free energy of a hypothetical homogeneous system of the same density and composition. In order to evaluate  $A$ , we adopt the assumption first made by van der Waals<sup>2</sup> that the entropy of the inhomogeneous system depends only on the local density. Although this assumption is standard for small molecules,<sup>3,9,12</sup> its validity is expected to be limited for polymers, and its effect will be examined in a later section.

The quantity to be evaluated for an inhomogeneous system is then the potential energy,  $E$ . In the mean field approximation, the potential energy per unit volume,  $V$ , at position  $\tilde{R}$  for an  $n$ -component system can be written

$$E(\tilde{R})/V = \frac{1}{2} \sum_i^n \sum_j^n \epsilon_{ij}(\tilde{R}) \quad (\text{II.5})$$

where  $\epsilon_{ij}$  is the interaction energy of components  $i$  and  $j$  and is given by:

$$\epsilon_{ij}(\tilde{R}) = \rho_i(\tilde{R}) \int \rho_j(\tilde{R}+s) g_{ij}(s) u_{ij}(s) ds \quad (\text{II.6})$$

$\rho_i(\tilde{R})$  and  $\rho_j(\tilde{R}+s)$  are the number densities of components  $i$  and  $j$  at positions  $\tilde{R}$  and  $\tilde{R}+s$ , respectively,  $s \equiv |s|$  is the intermolecular distance,  $g_{ij}(s)$  the pair distribution function, and  $u_{ij}(s)$  is the intermolecular interaction potential. We may further ignore

short-range correlations in the mean field approximation, such that

$$g_{ij}(\underline{s}) = \begin{cases} 0 & s < \sigma_{ij} \\ 1 & s > \sigma_{ij} \end{cases} \quad (11.7)$$

where  $\sigma_{ij}$  is the parameter which characterizes the hard core portion of the pair potential  $u_{ij}$ . In addition,  $u_{ij}$  is assumed to be spherically symmetric; i.e. a function of  $s$  and not  $\underline{s}$ .

In the gradient approximation,  $\rho_j(\underline{R}+\underline{s})$  is expanded in a Taylor's series around  $\underline{s} = \underline{0}$ :

$$\rho_j(\underline{R}+\underline{s}) = \rho_j(\underline{R}) + (\nabla \rho_j \cdot \underline{s})_{\underline{s}=\underline{0}} + \frac{1}{2!} (\nabla \rho_j \cdot \underline{s})_{\underline{s}=\underline{0}}^2 + \dots \quad (11.8)$$

to account for the effect on the potential energy of the concentration and density gradients present in an inhomogeneous system. Since all of the above derivatives are evaluated at  $\underline{s}=\underline{0}$ , they are functions of the  $x$ ,  $y$ , and  $z$  components of  $\underline{R}$  only. Substitution of eq. 11.8 into eq. 11.6 and subsequent integration yields:

$$\epsilon_{ij} = -\rho_i(\underline{R})\rho_j(\underline{R})\kappa_0^{ij} + \rho_i(\underline{R}) \int \{(\nabla \rho_j \cdot \underline{s}) + \frac{1}{2}(\nabla \rho_j \cdot \underline{s})^2 + \dots\} u_{ij}(s) ds \quad (11.9)$$

with

$$\kappa_0^{ij} = -4\pi \int_{\sigma_{ij}}^{\infty} s^2 u_{ij}(s) ds. \quad (11.10)$$

Since  $u_{ij}$  is spherically symmetric, it is an even function of  $s_x$ ,  $s_y$ , and  $s_z$ , so that the integral in eq. 11.9 has the following properties:

$$\int (\nabla_{\rho_j} \cdot \tilde{s})^b u_{ij}(\tilde{s}) d\tilde{s} \quad \begin{cases} = 0 & \text{if } b \text{ is odd} \\ \neq 0 & \text{if } b \text{ is even} \end{cases} \quad (\text{II.11})$$

If the expansion is truncated after the third term, the  $b=2$  term is the only one remaining. The integral in eq. II.9 can be further reduced:

$$\int \frac{1}{2} (\nabla_{\rho_j} \cdot \tilde{s})^2 u_{ij}(\tilde{s}) d\tilde{s} = -\nabla_{\rho_j}^2 \kappa_2^{ij} \quad (\text{II.12})$$

where

$$\kappa_2^{ij} = -\frac{2\pi}{3} \int_{\sigma_{ij}}^{\infty} s^4 u_{ij}(s) ds. \quad (\text{II.13})$$

This simplification is again based on the spherical symmetry of  $u_{ij}$  which implies

$$\int s_x^2 u_{ij}(s) ds_x = \int s_y^2 u_{ij}(s) ds_y = \int s_z^2 u_{ij}(s) ds_z = \frac{4\pi}{3} \int s^4 u_{ij}(s) ds. \quad (\text{II.14})$$

The components of the integrand in eq. II.12 may be grouped as

$$\frac{1}{2} \iiint \left\{ \frac{\partial^2 \rho_j}{\partial s_x^2} s_x^2 + \frac{\partial^2 \rho_j}{\partial s_y^2} s_y^2 + \frac{\partial^2 \rho_j}{\partial s_z^2} s_z^2 \right\} u_{ij}(s) ds_x ds_y ds_z +$$

$$\iiint \left\{ \frac{\partial^2 \rho_j}{\partial s_x \partial s_y} s_x s_y + \frac{\partial^2 \rho_j}{\partial s_x \partial s_z} s_x s_z + \frac{\partial^2 \rho_j}{\partial s_y \partial s_z} s_y s_z \right\} u_{ij}(s) ds_x ds_y ds_z. \quad (\text{II.15})$$

The first integral reduces to the right-hand side of eq. II.12 through the use of eq. II.14, while the second integral, whose terms

are of the form

$$\frac{\partial^2 \rho_j}{\partial s_x \partial s_y} \int s_x \int s_y u_{ij}(s) ds_y ds_x + \text{similar terms}, \quad (II.16)$$

goes to zero due to the considerations set forth in eq. II.11.

Eq. II.9 thus becomes

$$\epsilon_{ij} = -\rho_i(R) \rho_j(R) \kappa_o^{ij} - \rho_i(R) \nabla^2 \rho_j \kappa_2^{ij}. \quad (II.17)$$

Substitution of eq. II.17 into II.5 yields the following result for the Helmholtz free energy density

$$a(R) = -\frac{1}{2} \sum_i \sum_j \{ \rho_i(R) \rho_j(R) \kappa_o^{ij} - \rho_i(R) \nabla^2 \rho_j \kappa_2^{ij} \} - \quad (II.18)$$

$$T \frac{S}{V} (\rho_1, \rho_2, \dots, \rho_n)$$

where T is the temperature and S the entropy. Defining the local Helmholtz free energy density as

$$a_o(R) \equiv -\frac{1}{2} \sum_i \sum_j \rho_i(R) \rho_j(R) \kappa_o^{ij} - T \frac{S}{V} (\rho_1, \rho_2, \dots, \rho_n), \quad (II.19)$$

we may also write

$$a(R) = a_o(R) - \frac{1}{2} \sum_i \sum_j \rho_i(R) \nabla^2 \rho_j \kappa_2^{ij}. \quad (II.20)$$

The total Helmholtz free energy, A, of the system is given by

$$A = \iiint_V a(R) d^3R. \quad (II.21)$$

For a system with a planar interface of cross-sectional area  $S_o$  and volume  $LS_o$  ( $L \rightarrow \infty$ )



$$A = S_o \int_{-L/2}^{L/2} a(x) dx \quad (\text{II.22})$$

where  $x$  is the direction perpendicular to the interface. Substitution of eq. II.20 into II.22 yields

$$A = S_o \int_{-L/2}^{L/2} \left\{ a_o(x) - \frac{1}{2} \sum_i \sum_j \rho_i(x) \frac{d^2 \rho_j}{dx^2} \kappa_2^{ij} \right\} dx \quad (\text{II.23})$$

Integration of the second term in the integrand by parts, using the boundary condition that  $d\rho_i/dx \rightarrow 0$  as  $x \rightarrow \pm \infty$  leads to

$$A = S_o \int_{-L/2}^{L/2} \left\{ a_o(x) + \frac{1}{2} \sum_i \sum_j \kappa_2^{ij} \frac{d\rho_i}{dx} \frac{d\rho_j}{dx} \right\} dx \quad (\text{II.24})$$

The interfacial tension, as defined by eq. II.4, is then given by

$$\gamma = \int_{-\infty}^{\infty} \left\{ \Delta a + \frac{1}{2} \sum_i \sum_j \kappa_2^{ij} \frac{d\rho_i}{dx} \frac{d\rho_j}{dx} \right\} dx \quad (\text{II.25})$$

where

$$\Delta a \equiv a_o(x) - A_e/V \equiv a_o(x) - a_e \quad (\text{II.26})$$

The limits of integration have been extended to infinity since both  $\Delta a$  and the  $x$ -derivatives on the number densities go to 0 as  $L \rightarrow \infty$ . As mentioned previously,  $A_e$  represents the Helmholtz free energy of a hypothetical system containing the same number densities of the components, but lacking an interface. The quantity may be expressed in terms of the equilibrium chemical potentials  $\mu_i^e$  and the external

pressure  $P_e$  :

$$A_e = \sum_i N_i \mu_i^e - P_e V \quad (\text{II.27})$$

$$a_e = \sum_i \rho_i(x) \mu_i^e - P_e .$$

$\Delta a$  thus represents the excess Helmholtz free energy density of a fluid at the local composition  $\rho_1, \rho_2, \dots, \rho_n$  in the absence of density gradients, and the double sum in eq. II.25 represents, to the lowest order, the additional free energy density contribution due to the presence of such gradients.

In order to obtain the equilibrium interfacial tension, eq. II.25 must be minimized which results in  $n$  coupled differential equations:

$$\frac{\partial \Delta a}{\partial \rho_i} - \sum_j \kappa_2^{ij} d^2 \rho_j / dx^2 = 0 . \quad (\text{II.28})$$

This set of equations forms the conditions subject to which the integral in eq. II.25 must be evaluated. Multiplying the differential equations by  $d\rho_i/dx$  and summing over species  $i$  gives an expression which upon integration results in

$$\Delta a = \frac{1}{2} \sum_i \sum_j \kappa_2^{ij} (d\rho_i/dx)(d\rho_j/dx) . \quad (\text{II.29})$$

The equilibrium tension can thus be written as

$$\gamma = \sum_i \sum_j \kappa_2^{ij} \int_{-\infty}^{\infty} (d\rho_i/dx)(d\rho_j/dx) dx = 2 \int_{-\infty}^{\infty} \Delta a dx . \quad (\text{II.30})$$

This equation was first derived by Bongiorno, Scriven, and Davis<sup>9</sup>

for a more general theory of interfaces by a different procedure. In their theory the pair distribution function  $g_{ij}(\vec{s})$  is not assumed to be given by eq. II.7, but rather is approximated by the homogeneous pair distribution function evaluated at a mean density. This has the effect of allowing short-range correlations to be taken into account in evaluating the local energy terms in the interfacial region. However, the effect of short-range correlations on the local entropy is not considered.

The theoretical development given above is quite general, and the results can be used with any mean field theory of fluids. We will now proceed to demonstrate the correspondence of the present theory to the well-known Cahn-Hilliard theory for the special case of a single component liquid-vapor interface. The original Cahn-Hilliard theory was derived for a two-component system of constant density containing a liquid-liquid interface.<sup>3</sup> As a result the inhomogeneity could be expressed in terms of a single variable, the concentration of one of the components. Applying the Cahn-Hilliard derivation to a pure component in the presence of a density gradient is straightforward. The initial assumption of the CH formalism is that the Helmholtz free energy density may be written in terms of an expansion in density and its derivatives:

$$a(\rho, \nabla\rho, \nabla^2\rho, \dots) = a_o(\rho) + \kappa_1 \nabla^2\rho + \kappa_2 (\nabla\rho)^2 + \dots \quad (\text{II.31})$$

with

$$\kappa_1 = \left. \frac{\partial a}{\partial \nabla^2 \rho} \right|_o ; \kappa_2 = \frac{1}{2} \left. \frac{\partial^2 a}{(\partial |\nabla\rho|)^2} \right|_o \quad (\text{II.32})$$

where  $a_o(\rho)$  is again the free energy density of a uniform fluid of density  $\rho$ , and the subscripts  $o$  in eq. II.32 indicate that the derivatives are to be evaluated in the limit of  $\nabla\rho$  and  $\nabla^2\rho$  going to zero. If the density variation is sufficiently slow, so that the expansion may be truncated after the 2nd order terms, the resulting expression for the total Helmholtz free energy of the system is

$$A = \int_V \{a_o(\rho) + \kappa'(\nabla\rho)^2\} dV \quad (\text{II.33})$$

where

$$\kappa' = -d\kappa_1/d\rho + \kappa_2 \quad (\text{II.34})$$

Using these relations and the definition of the interfacial tension given in eq. II.4 the result for a planar interface is

$$\gamma = \int_{-\infty}^{\infty} \{\Delta a + \kappa'(d\rho/dx)^2\} dx \quad (\text{II.35})$$

where  $\Delta a$  has the same meaning as in the present theory. For a single component, eq. II.25 reduces to

$$\gamma = \int_{-\infty}^{\infty} \{\Delta a + \frac{1}{2} \kappa_2''(d\rho/dx)^2\} dx \quad (\text{II.36})$$

where

$$\frac{1}{2}\kappa_2'' = -\frac{\pi}{3} \int_{o_i}^{\infty} s^4 u(s) ds \quad (\text{II.37})$$

The value of  $\kappa'$  in the Cahn-Hilliard formulation is obtained by carrying out an expansion of the potential energy for a lattice model. The expression obtained for  $\kappa'$  is identical to that of  $\frac{1}{2}\kappa''$  given above.<sup>42</sup>

In concluding this section on the gradient theory of interfaces, a qualitative discussion of the thermodynamic significance of the results is in order. The following remarks will be confined to a one-component system for purposes of simplicity. We will further drop the subscripts on the factor multiplying the gradient term so that eq. II.36 becomes

$$\gamma = \int_{-\infty}^{\infty} \left\{ \Delta a + \frac{1}{2} \kappa (d\rho/dx)^2 \right\} dx \quad (\text{II.38})$$

subject to

$$\frac{\partial \Delta a}{\partial \rho} - \kappa \frac{d^2 \rho}{dx^2} = 0 . \quad (\text{II.39})$$

Recalling the definition of  $\Delta a$  given in eqs. II.26 and II.27, we obtain

$$\frac{\partial \Delta a}{\partial \rho} = \frac{\partial}{\partial \rho} \{ a_o - \rho \mu^e + P_e \} = \mu(\rho) - \mu^e \quad (\text{II.40})$$

where  $\mu(\rho)$  is the local chemical potential and is a function of the density. The relationship which must be satisfied in order to minimize the interfacial tension is therefore

$$\mu^e = \mu(\rho) - \kappa \frac{d^2 \rho}{dx^2} . \quad (\text{II.41})$$

In a liquid-vapor system, the requirement of a continuous density profile implies that the density must pass from the liquid density to the vapor density via the thermodynamically unstable densities between the two. One thus makes the tacit assumption in the gradient theory, that the expressions obtained for the equilibrium chemical

potentials may be extended into the unstable region. Fig. 1 illustrates the behavior of  $\mu(\rho)$  through the interfacial region. Since  $\mu(\rho)$  is a thermodynamically unstable quantity over the greater portion of the interface, a constant chemical potential can only be maintained throughout the system through the influence of the density curvature term. If one examines the alternate form of the minimization condition

$$\Delta a - \frac{1}{2}\kappa \left( \frac{d\rho}{dx} \right)^2 = 0 \quad (\text{II.42})$$

the relationship between the density profile and the energy requirements of the system becomes even more apparent. Fig. 2 shows the qualitative behavior of  $a_0$  and  $\Delta a$  in the inhomogeneous system. The excess free energy arising from the thermodynamically unfavorable densities through which the system passes, can be thought of as a driving force leading to the mechanical response of a density gradient. The magnitude of  $\kappa$  is crucial in determining the nature of the density profile. If  $\kappa$  were equal to zero, the only possible density profile would be a step-function, since  $\Delta a$  must equal zero also in such a case. Further, as the value of  $\kappa$  increases, the density profile required to satisfy eq. II.41 or II.42 becomes less steep.

A satisfying feature of the theory is that it predicts the proper behavior for the density profile and interfacial tension as the temperature increases. As the critical point is approached the free energy curve illustrated in Fig. 2.a. changes its shape. The two minima move closer together and the maximum flattens out, until at the critical point only a single shallow minimum exists. As a result

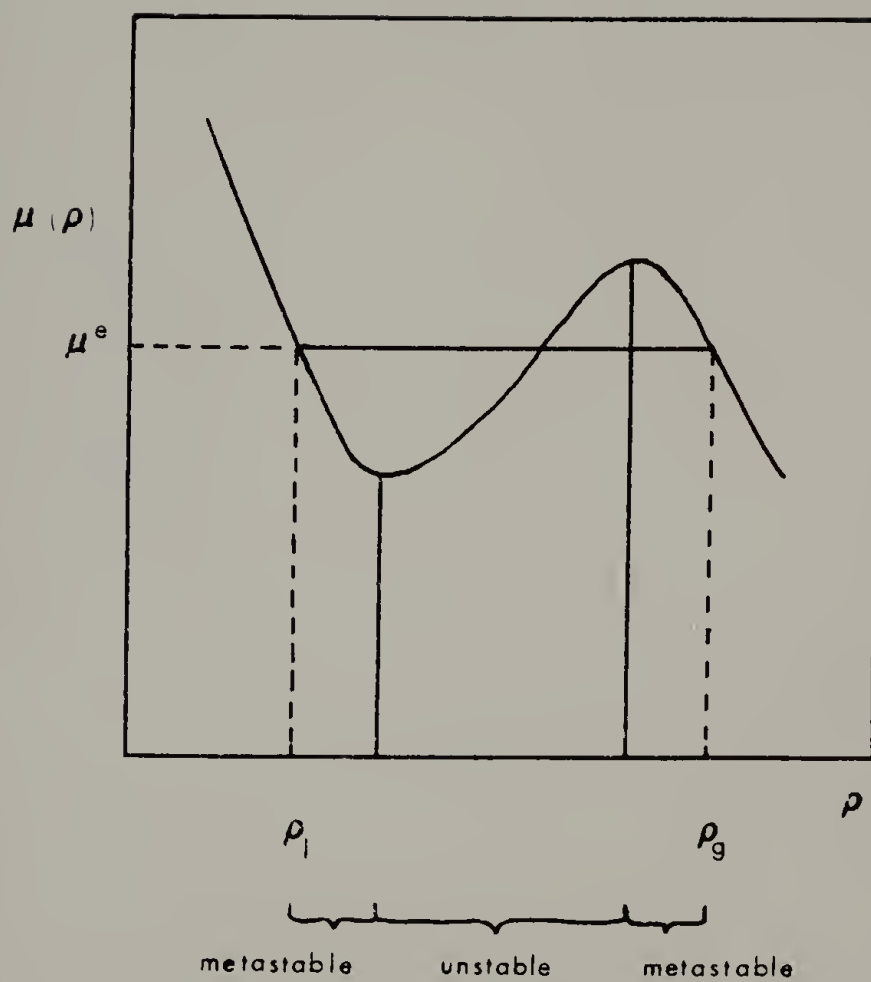
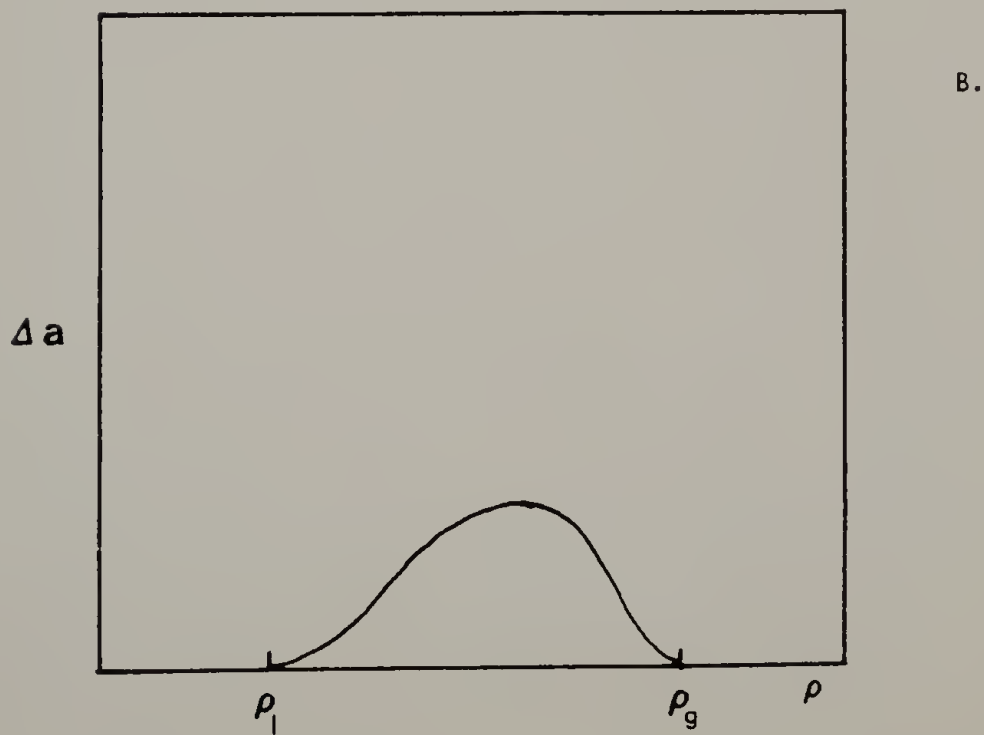
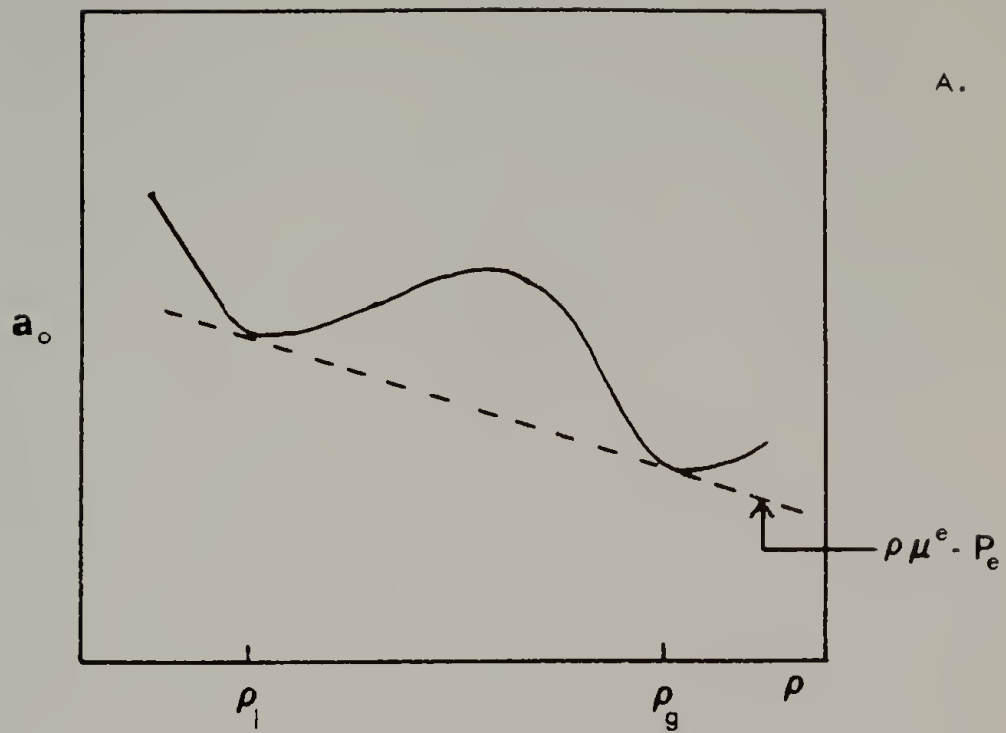


Figure 1. Dependence of the local chemical potential,  $\mu(\rho)$ , on density through the interface.  $\rho_l$  and  $\rho_g$  are the liquid and gas densities, respectively, and  $\mu^e$  is the equilibrium chemical potential.

Figure 2. Behavior of the local Helmholtz free energy density,  $a_0$ , and the excess Helmholtz free energy density,  $\Delta a$ , through the interface. The broken line represents the free energy density of the hypothetical homogeneous reference system.





of this behavior, the magnitude of  $\Delta a$  decreases, and the area under the curve in Fig. 2.b also gets smaller. As a result, the density gradient required to satisfy eq. II.42 decreases, and the density profile broadens. Simultaneously, the interfacial tension which is proportional to the weighted area under the  $\Delta a$  curve, decreases. This proportionality can be clearly seen when eq. II.42 is used to effect a change of variables in eq. II.38 via

$$dx = \sqrt{\kappa/2\Delta a} \, d\rho \quad (\text{II.43})$$

to yield

$$\gamma = 2 \int_{\rho_g}^{\rho_l} \sqrt{\frac{1}{2}\kappa\Delta a} \, d\rho \quad (\text{II.44})$$

$\kappa$ , which is a measure of the strength and range of the intermolecular interactions, is thus crucial in determining the magnitude of the interfacial tension as well as the nature of the density profile.

In summary, the free energy approach in the mean field gradient approximation has been chosen for the present theory of interfaces, because a more rigorous approach would require pair distribution functions which would preclude application to polyatomic fluids. In addition, the gradient approximation has been shown to be quite accurate over the entire coexistence range. The present derivation is direct, and the resulting equations can be used in conjunction with any mean field molecular model. Furthermore, the qualitative predictions of the theory are in accord with fluid behavior, and the equations will be seen to be amenable to numerical solution.

## CHAPTER III

### LATTICE FLUID THEORY

In the previous chapter, a general theory of interfaces was developed which requires the use of a molecular equation of state for quantitative predictions. Since the goal of this thesis is to develop a unified model applicable to the range of molecular weights, the selected fluid model must provide a tractable and accurate description of such systems. The lattice fluid model<sup>36-39</sup> provides such a description. A brief review of the one-component model will be followed by a more detailed discussion of the two-component form. Use of the theory to calculate phase equilibria will be discussed in the subsequent chapter.

The LF model is similar to the Flory-Huggins theory,<sup>13</sup> except that instead of assuming a filled lattice, vacant lattice sites are included. This has the important effect of rendering the lattice compressible. Thus one can describe the thermodynamic properties of pure components. In addition, the LF theory can predict density-related features of binary phase diagrams which cannot be described by a model based on a fully occupied lattice. In the pure fluid case,  $N$   $r$ -mers occupy the lattice (each mer occupying one site), and there are  $N_0$  vacant sites. The configurational partition function is evaluated by assuming random mixing of  $r$ -mers and vacant sites.

The reduced chemical potential,  $\tilde{\mu}$ , of a pure component is given

$$\tilde{\mu} \equiv \mu / (N r \epsilon^*) = -\tilde{\rho} + \tilde{P}\tilde{v} + \tilde{T}[(\tilde{v}-1)\ln(1-\tilde{\rho}) + \frac{1}{r} \ln \tilde{\rho}] \quad (\text{III.1})$$

to within an additive constant.  $\tilde{T}$ ,  $\tilde{P}$ ,  $\tilde{v}$ , and  $\tilde{\rho}$  are the reduced temperature, pressure, volume and density defined as

$$\tilde{T} \equiv T/T^* \quad T^* \equiv \epsilon^*/k \quad (\text{III.2})$$

$$\tilde{P} \equiv P/P^* \quad P^* \equiv \epsilon^*/v^* \quad (\text{III.3})$$

$$\tilde{v} \equiv 1/\tilde{\rho} \equiv V/V^* \quad V^* \equiv N(rv^*) \equiv N(M/\rho^*). \quad (\text{III.4})$$

$\epsilon^*$  is the total interaction energy per mer,  $v^*$  is the close-packed mer volume (or hard core volume of the mer),  $V^*$  is the close-packed volume of the  $N$   $r$ -mers, and  $M$  is the molecular weight.  $T$ ,  $P$ , and  $V$  are the temperature, pressure and volume, respectively.

In the original derivation of the model fluid's potential energy, only nearest neighbor interactions were taken into account. This approach is acceptable for the pure LF since the mean field potential energy will always be of a van der Waals form if the attractive part of the pair potential is sufficiently short range. Bulk thermodynamic properties are therefore not sensitive to the specific form of the pair potential. Interfacial properties, on the other hand, are very sensitive to the range of intermolecular forces, as evidenced by the importance of the  $\kappa$ 's in the gradient theory. In order to be consistent, long range interactions must therefore be included in the bulk theory.

Since one of the stipulations of the LF model is that only one mer can occupy a given lattice site at a time, we shall assume a Sutherland type pair potential (hard core plus attractive tail):

$$u(s) = \begin{cases} \infty & s/\sigma < 1 \\ -\epsilon_0 (\sigma/s)^m & s/\sigma > 1. \end{cases} \quad (\text{III.5})$$

where  $s$  is the separation between mers,  $\sigma$  the distance associated with the repulsive core volume (which is identified as  $\sigma = v^*{}^{1/3}$ ), and  $\epsilon_0$  is the depth of the potential energy minimum. Note that this interaction potential acts between mers, not molecules. The characteristic LF interaction energy is then given by

$$\epsilon^* = 2\pi\epsilon_0/m-3 . \quad (\text{III.6})$$

This definition is different from the original one, and is the only modification which arises from the use of eq. III.5. In practice,  $\epsilon^*$  is determined from a fit of experimental data, as discussed below, so that changing the form of the intermolecular interaction has no effect on the homogeneous LF.

The chemical potential (III.1) is at a minimum at equilibrium and satisfies the following equation of state

$$\tilde{\rho}^2 + \tilde{P} + \tilde{T} \left[ \ln(1-\tilde{\rho}) + \left(1 - \frac{1}{r}\right)\tilde{\rho} \right] = 0 . \quad (\text{III.7})$$

The equation of state defines the value of  $\tilde{\rho}$  (or two  $\tilde{\rho}$ 's in the two-phase region) which minimizes the free energy at a given  $\tilde{T}$  and  $\tilde{P}$ .

From eqs. III.2-4, one obtains that three parameters, either  $\epsilon^*$ ,  $v^*$ , and  $r$  or  $T^*$ ,  $P^*$ , and  $\rho^*$ , suffice to characterize a fluid. For low molecular weight liquids, these parameters can be obtained by performing a non-linear least squares fit of the equation of state to saturated vapor pressure data,<sup>36</sup> which are readily available in the literature. Alternate methods have also been discussed.<sup>39</sup> For a polymer liquid,  $r \rightarrow \infty$  and the equation of state reduces to a corresponding states equation which can be fitted to experimental liquid density data to

determine the parameters.<sup>38</sup> A partial list of low molecular weight liquid and polymer liquid parameters is given in Table 1 and 2, respectively. Also included in Tables 1 and 2 is a parameter,  $\gamma^*$ , which is defined as  $\epsilon^*/v^{*2/3}$ .  $\gamma^*$  will later be used to reduce the interfacial tension.

A discussion of the physical significance of the molecular parameters has been given,<sup>39</sup> and will be briefly summarized here. The parameter  $\rho^*$  may be identified as the close-packed density of the fluid state. This is a disordered, not a crystalline state, so that  $\rho^*$  should be lower than the crystalline density of the compound. In keeping with this view, the values of  $\rho^*$  obtained for low molecular weight liquids are generally about 10% smaller than their known crystal densities. Eq. III.4 thus leads to the identification of  $rv^*$  as the close-packed molecular volume of the disordered fluid.

The product  $r\epsilon^*$  which represents the total molecular interaction energy has been examined as a function of chain-length for the n-alkanes from  $C_3$  to  $C_{14}$  and found to increase systematically. One may identify  $r\epsilon^*$  as the energy required to convert one mole of fluid in the close-packed state ( $\tilde{\rho}=1$ ) to a vapor of negligible density ( $\tilde{\rho}=0$ ). This identification leads to a simple interpretation of the ratio  $\epsilon^*/v^*$ , defined as the characteristic pressure  $P^*$ . Since the cohesive energy density, CED, may be defined as

$$\text{CED} \equiv \Delta E_{\text{vap}}/V = r\epsilon^*/rv^* \equiv P^* \quad (\text{III.8})$$

where  $\Delta E_{\text{vap}}$  is the energy of vaporization,  $P^*$  provides a measure of the strength of the fluid's intermolecular interactions.

Table 1

## LATTICE FLUID PARAMETERS FOR LOW MOLECULAR WEIGHT LIQUIDS

	$T^*$	$P^*$	$v^*$	$\rho^*$	$r$	$\gamma^*$
	K	mN/m <sup>2</sup>	m <sup>2</sup> /mol x 10 <sup>-6</sup>	kg/m <sup>3</sup> x 10 <sup>-3</sup>		mN/m
methane	224	248	7.52	0.50	4.26	57.6
ethane	815	327	8.00	0.64	5.87	77.7
propane	371	313	9.84	0.69	6.50	79.6
n-butane	403	322	10.40	0.736	7.59	83.4
isobutane	398	288	11.49	0.72	7.03	77.0
n-pentane	441	310	11.82	0.755	8.09	83.7
isopentane	424	308	11.45	0.765	8.24	82.3
neopentane	415	266	12.97	0.744	7.47	74.0
n-hexane	476	298	13.28	0.775	8.37	83.7
2,2 dimethylbutane	455	275	13.77	0.773	8.10	78.0
2,3 dimethylbutane	463	289	13.31	0.781	8.29	81.2
cyclohexane	497	383	10.79	0.902	8.65	100
n-heptane	487	309	13.09	0.80	9.57	86.3
n-octane	502	308	13.55	0.815	10.34	87.0
n-nonane	517	307	14.00	0.828	11.06	87.6
n-decane	530	304	14.47	0.837	11.75	87.9
n-undecane	542	303	14.89	0.846	12.40	88.2
n-dodecane	552	301	15.28	0.854	13.06	88.4
n-tridecane	560	299	15.58	0.858	13.79	88.4
n-tetradecane	570	296	15.99	0.864	14.36	88.4
n-hexadecane	578	284	16.93	0.840	15.92	86.4
n-heptadecane	596	287	17.26	0.88	15.83	87.9

benzene	523	444	9.80	0.994	8.02	112
chlorobenzene	585	437	11.14	1.206	8.38	116
bromobenzene	608	454	11.13	1.616	8.73	120
toluene	543	402	11.22	0.996	8.50	107
m-xylene	560	385	12.11	0.952	9.21	105
o-xylene	571	394	12.03	0.965	9.14	107
p-xylene	561	381	12.24	0.949	9.14	104
tetralin	621	315	16.37	0.935	9.03	98.3
carbon tetrachloride	535	813	11.69	1.788	7.36	102
chloroform	512	456	9.33	1.688	7.58	113
methylene chloride	487	559	7.23	1.538	7.64	128
diethyl ether	431	363	9.88	0.870	8.62	92.3
aniline	614	629	8.11	1.115	10.30	150



Table 2

## LATTICE FLUID PARAMETERS FOR POLYMERS

	$T^*$ K	$P^*$ MN/m <sup>2</sup>	$v^*$ m <sup>3</sup> /mol $\times 10^{-6}$	$\rho^*$ kg/m <sup>3</sup> $\times 10^{-3}$	$\gamma^*$ mN/m
poly(dimethyl siloxane)	476	302	13.1	1.104	84.3
poly(vinyl acetate)	590	509	9.64	1.283	128
poly(isobutylene)	643	354	15.1	0.974	104
polyethylene (linear)	649	426	12.7	0.904	118
polyethylene (branched)	673	358	15.6	0.887	106
polystyrene (atactic)	735	358	17.1	1.105	109

In the generalization of a pure component model to a multicomponent one, "combining rules" must be invoked to describe the intermolecular interaction between unlike molecules. In a binary mixture, a relationship must be found for the hard core parameter ( $\sigma_{12}$ ) and the parameter proportional to the depth of the potential well ( $\epsilon_{12}^*$ ). In the original LF mixture theory, the following combining rule for  $\sigma_{12}$  was used

$$\sigma_{12}^3 = (\sigma_{11}^3 + \sigma_{22}^3) / 2 \quad (\text{III.9})$$

which results in simple additivity of molecular volumes at  $T=0$ .

The second relationship was

$$\epsilon^* = \phi_1^2 \epsilon_{11}^* + 2\phi_1\phi_2\zeta \sqrt{\epsilon_{11}^* \epsilon_{22}^*} + \phi_2^2 \epsilon_{22}^* \quad (\text{III.10})$$

where  $\zeta$  is an adjustable parameter. This set of combining rules, unfortunately, fails to provide a sufficiently accurate description of thermodynamic mixture properties. Since, ultimately, the LF model will be extended to inhomogeneous systems, a more quantitative theory for bulk systems is crucial. Two sets of alternate combining rules were considered.

The first set of combining rules<sup>39</sup> retains the stipulation of simple additivity of close-packed volumes which may also be expressed as

$$v^* = r_1 N_1 v_1^* + r_2 N_2 v_2^* = (r_1' N_1 + r_2' N_2) v^* \quad (\text{III.11})$$

$$r_i v_i^* = r_i' v^* \quad (\text{III.12})$$

The superscript ' refers to the value in the mixture (note that

$r_i \neq r_i'$  in general). We also retain the requirement that the total number of pair interactions in the close-packed mixture equals the sum of the pair interactions of the components in their close-packed states. As a consequence:

$$r_1 N_1 + r_2 N_2 = r_1' N_1 + r_2' N_2 = rN \quad (\text{III.13})$$

where

$$r \equiv x_1 r_1 + x_2 r_2 \equiv x_1 r_1' + x_2 r_2' \quad (\text{III.14})$$

$$x_1 \equiv N_1/N = 1-x_2 \quad (\text{III.15})$$

$$N \equiv N_1 + N_2 \quad (\text{III.16})$$

Both of these rules were imposed in the original LF model of mixtures.<sup>37</sup>

In addition, we specify that the characteristic pressures be pairwise additive in the close-packed mixture:

$$P^* = \phi_1' P_1^* + \phi_2' P_2^* - \phi_1' \phi_2' \Delta P^* \quad (\text{III.17})$$

$$\Delta P \equiv P_1^* + P_2^* - 2P_{12}^* \quad (\text{III.18})$$

$$\phi_1' = r_1' N_1 / rN = 1 - \phi_2' \quad (\text{III.19})$$

As a result of this requirement, the mer-mer interaction energies,  $\epsilon_{ij}^*$ , are no longer pair-wise additive as they were in the original paper.  $\epsilon^*$  is now expressed as

$$\epsilon^* = P^* v^* = (\phi_1' P_1^* + \phi_2' P_2^* - \phi_1' \phi_2' \Delta P^*) (\phi_1 v_1^* + \phi_2 v_2^*) \quad (\text{III.20})$$

where

$$\phi_1 = r_1 N_1 / rN = 1 - \phi_2 \quad (\text{III.21})$$

If the reduced temperature, pressure and density are defined analogously to those of the pure case, substituting the mixture definitions for  $P^*$ ,  $\epsilon^*$ ,  $v^*$ , and  $V^*$ , the configurational Gibbs free energy is

$$\begin{aligned} \tilde{G} \equiv G/rN\epsilon^* = & -\tilde{\rho} + \tilde{P}\tilde{v} + \tilde{T}[(1-\tilde{\rho})\ln(1-\tilde{\rho}) + \tilde{\rho}/r \ln \tilde{\rho}] + \\ & \tilde{T}\left[\frac{\phi'_1}{r'_1} \ln \phi'_1 + \frac{\phi'_2}{r'_2} \ln \phi'_2\right] . \end{aligned} \quad (\text{III.22})$$

The chemical potential for component 1 can be obtained by direct analogy to the derivation used with the old combining rules and is

$$\begin{aligned} \mu_1 = kT \left[ \ln \phi'_1 + (1-r_1/r'_2)\phi'_2 + r_1\tilde{\rho} X_1\phi'^2_2 \right] + \\ r_1 kT \left\{ -\tilde{\rho}/\tilde{T}_1 + \tilde{P}_1\tilde{v}/\tilde{T}_1 + \tilde{v}[(1-\tilde{\rho}) \ln(1-\tilde{\rho}) + \tilde{\rho}/r_1 \ln \rho] \right\} \end{aligned} \quad (\text{III.23})$$

with

$$X_1 \equiv (\Delta P^* v_1^*)/kT . \quad (\text{III.24})$$

$\Delta P^*$  thus represents the adjustable parameter for this version of the mixture theory. We will thus subsequently refer to this set of combining rules as the  $\Delta P^*$  combining rules.

The second set of combining rules is more general and will be discussed in detail, since it was selected for use in the interfacial theory. We first make the assumption that

$$r_1 = r'_1 \quad (\text{III.25})$$

so that the number of sites occupied by a molecule in the pure and

mixed states is the same. In effect, this removes the assumption of simple volume additivity in the close-packed state.  $\epsilon^*$  can now be obtained without recourse to further assumptions from the properties of the model.<sup>39</sup> The energy per unit volume of the n-component LF is written

$$E/V = \frac{1}{2} \sum_i^n \sum_j^n \rho_i \rho_j \int u_{ij}(s) g_{ij}(s) ds . \quad (\text{III.26})$$

$g_{ij}(s)$  will be defined as eq. (II.7), and  $u_{ij}(s)$  is analagous to the one-component interaction potential. Using the following definition:

$$\rho_i \equiv r_i N_i / V = \tilde{\rho} \frac{\phi_i}{v^*} \quad (\text{III.27})$$

results in

$$E = -rN\tilde{\rho}\epsilon^* \quad (\text{III.28})$$

with

$$\epsilon^* \equiv \frac{1}{v^*} \sum_i^n \sum_j^n \phi_i \phi_j \epsilon_{ij}^* \sigma_{ij}^3 . \quad (\text{III.29})$$

$v^*$ , the average close-packed volume of a mer in the mixture, is not explicitly defined. Making the additional assumption

$$v^* = \sum_i^n \sum_j^n \phi_i \phi_j \sigma_{ij}^3 , \quad (\text{III.30})$$

completes the description of the mixture; however,  $\epsilon_{ij}^*$  and  $\sigma_{ij}$  remain undefined. We shall cast them in the form of the Lorentz-Berthelot rules, modified by adjustable parameters:

$$\epsilon_{ij}^* = \zeta \sqrt{\epsilon_{ii}^* \epsilon_{jj}^*} \quad (\text{III.31})$$

and

$$\sigma_{ij}^3 = \Delta(\sigma_{ii}^3 + \sigma_{jj}^3)/2 \quad . \quad (\text{III.32})$$

When  $\Delta$  is set equal to one, simple close-packed volume additivity is recovered and the definition of  $\epsilon^*$  for the binary system can be shown to be equivalent to eq. (III.20).

It is useful to define

$$\delta = \Delta - 1 \quad , \quad (\text{III.33})$$

since the close-packed volume of a binary mixture may then be written

$$v^* = \phi_1 v_1^* + \phi_2 v_2^* - \phi_1 \phi_2 \delta (v_1^* + v_2^*) \quad (\text{III.34})$$

where the identification  $v_i^* = \sigma_{ii}^3$  has been made. The parameter  $\delta$  has the physical significance of measuring the deviation of close-packed mixing from the ideal value

$$\delta \begin{cases} < 0 & v^* < v_{\text{ideal}}^* \\ = 0 & v^* = v_{\text{ideal}}^* \\ > 0 & v^* > v_{\text{ideal}}^* \end{cases} \quad (\text{III.35})$$

where

$$v_{\text{ideal}}^* = \phi_1 v_1^* + \phi_2 v_2^* \quad . \quad (\text{III.36})$$

The use of the general combining rules allows a more elegant derivation of the chemical potential for the multicomponent LF.

The total number of mers in an n-component mixture is given by

$$rN = \sum_i^n r_i N_i \quad (\text{III.37})$$

The Gibbs free energy per mer of such a system can be divided into a combinatorial,  $g_c$ , and a noncombinatorial,  $g_{nc}$ , part:

$$G/rN = g_c + g_{nc} \equiv g \quad (III.38)$$

where

$$g_c = kT \sum_i^n \phi_i / r_i \ln \phi_i \quad (III.39)$$

$$g_{nc} = -\tilde{\rho}\epsilon^* + P\tilde{v}^* + kT\tilde{V}[(1-\tilde{\rho}) \ln(1-\tilde{\rho}) + \tilde{\rho}/r \ln \tilde{\rho}] \quad (III.40)$$

The following definitions apply:

$$\phi_i \equiv r_i N_i / rN \quad (III.41)$$

$$1/r \equiv \sum_i^n \phi_i / r_i \quad (III.42)$$

$$v^* \equiv \sum_i^n \sum_j^n \phi_i \phi_j^3 \sigma_{ij} \quad (III.43)$$

$$\epsilon^* \equiv \sum_i^n \sum_j^n \phi_i \phi_j^3 \sigma_{ij} \epsilon_{ij}^* / v^* \quad (III.44)$$

The equation of state of the mixture is obtained from

$$\left. \frac{\partial g}{\partial v} \right)_{T,P,\phi} = \left. \frac{\partial g_{nc}}{\partial v} \right)_{T,P,\phi} = 0 \quad (III.45)$$

and has the form

$$\tilde{\rho}^2 + \tilde{P} + \tilde{T}[\ln(1-\tilde{\rho}) + (1-\frac{1}{r})\tilde{\rho}] = 0 \quad (III.46)$$

This equation is formally identical to that obtained for the pure component; the difference lies in the definitions of  $r$ ,  $v^*$ , and  $\epsilon^*$

which for the mixture are given by eqs. III.42-44.

The chemical potential of component  $i$  in the system is defined as

$$\mu_i \equiv \left( \frac{\partial G}{\partial N_i} \right)_{T,P,N'} = r_i g + r N \left( \frac{\partial g}{\partial N_i} \right)_{N'} . \quad (\text{III.47})$$

$N'$  indicates that all  $N_j$  except  $N_i$  are held constant. Use of eq.

III.38 leads to

$$\mu_i = r_i \left[ g + \frac{N_i}{\phi_i} \left( \frac{\partial g}{\partial N_i} \right)_{N'} \right] . \quad (\text{III.48})$$

If we consider  $g$  at constant  $T$  and  $P$  to be a function of the  $n+1$  variables  $\phi_1, \phi_2, \dots, \phi_n$ , and  $\tilde{\rho}$ , we can write

$$dg = \sum_i^n \left( \frac{\partial g}{\partial \phi_i} \right)_{T,P,\phi',\tilde{\rho}} d\phi_i + \left( \frac{\partial g}{\partial \tilde{\rho}} \right)_{T,P,\phi} d\tilde{\rho} . \quad (\text{III.49})$$

At equilibrium the  $\partial g / \partial \tilde{\rho}$  term is equal to the equation of state (c.f. III.45), and therefore goes to zero.

We can thus write:

$$\left( \frac{\partial g}{\partial N_i} \right)_{N'} = \sum_j^n \left( \frac{\partial g}{\partial \phi_j} \right)_{\phi',\tilde{\rho}} \left( \frac{\partial \phi_j}{\partial N_i} \right)_{N'} \quad (\text{III.50})$$

and since

$$\left( \frac{\partial \phi_j}{\partial N_i} \right)_{N'} = \begin{cases} \phi_i(1-\phi_i)/N_i & i=j \\ -\phi_i\phi_j/N_i & i \neq j \end{cases} \quad (\text{III.51})$$

we obtain

$$\mu_i = r_i \left\{ g + \left( \frac{\partial g}{\partial \phi_i} \right)_{\phi',\tilde{\rho}} - \sum_j^n \phi_j \left( \frac{\partial g}{\partial \phi_j} \right)_{\phi',\tilde{\rho}} \right\} . \quad (\text{III.52})$$



If we now separate  $g$  into  $g_c$  and  $g_{nc}$ :

$$\mu_i = kT \left[ \ln \phi_1 + (1-r_i/r) \right] + r_i \left[ g_{nc} + \frac{\partial g_{nc}}{\partial \phi_i} \right]_{\phi', \tilde{\rho}} - \sum_j^n \phi_j \left[ \frac{\partial g_{nc}}{\partial \phi_j} \right]_{\phi', \tilde{\rho}} \quad (III.53)$$

Before substituting in eq. III.40, we note that  $\epsilon^*, 1/r, v^*$  are homogeneous functions of  $\phi_j$  of order zero, one, and two, respectively. Therefore we can use the general property of a function  $f(x_1, x_2, \dots, x_n)$  of order  $a$  that

$$\sum_j^n x_j \left( \frac{\partial f}{\partial x_j} \right)_{x'} = a f(x_1, x_2, \dots, x_n) \quad (III.54)$$

to obtain

$$\sum_j^n \phi_j \left( \frac{\partial g_{nc}}{\partial \phi_j} \right)_{\phi', \tilde{\rho}} = 2P\tilde{v}v^* + kT \ln \tilde{\rho}/r. \quad (III.55)$$

Substituting III.40 and III.55 into III.52 results in

$$\mu_i = kT \left[ \ln \phi_i + (1-r_i/r) \right] + r_i \left\{ -\tilde{\rho} \left[ \epsilon^* + \frac{\partial \epsilon^*}{\partial \phi_i} \right]_{\phi'} + P\tilde{v} \left[ \frac{\partial v^*}{\partial \phi_i} \right]_{\phi'} - v^* \right\} + kT\tilde{v} \left[ (1-\tilde{\rho}) \ln (1-\tilde{\rho}) + \tilde{\rho}/r_i \ln \tilde{\rho} \right]. \quad (III.56)$$

For the special case of a binary mixture, we can show that

$$\epsilon^* + \frac{\partial \epsilon^*}{\partial \phi_1} \phi_2 = \epsilon_{11}^* - X_{12} \phi_2^2 \quad (III.57)$$

and

and

$$\frac{\partial v^*}{\partial \phi_1} \phi_2 - v^* = v_1^* + (v_1^* + v_2^*) \delta \phi_2^2 \quad (\text{III.58})$$

where

$$X_{12} = (P_1^* P_2^*)^{\frac{1}{2}} v_1^* \left( \frac{v_2^*}{v^*} \right)^2 [a + b_{12} \delta + c_{12} \delta^2] \quad (\text{III.59})$$

$$a = (\tau/v)^{\frac{1}{2}} + (v/\tau)^{\frac{1}{2}} - (v^{\frac{1}{2}} + v^{-\frac{1}{2}}) \zeta \quad (\text{III.60})$$

$$b_{12} = \{ \phi_1 (2 + v \phi_1) (\tau^{\frac{1}{2}} - \zeta) - \phi_2^2 (\zeta - \tau^{-\frac{1}{2}}) \} (v^{\frac{1}{2}} + v^{-\frac{1}{2}}) \quad (\text{III.61})$$

$$c_{12} = \phi_2^2 (\tau^{\frac{1}{2}} - \zeta) (1+v) (v^{\frac{1}{2}} + v^{-\frac{1}{2}}) \quad (\text{III.62})$$

$$\tau \equiv \epsilon_{11}^* / \epsilon_{22}^* \quad ; \quad v \equiv v_1^* / v_2^* \quad . \quad (\text{III.63})$$

The chemical potential may then also be written:

$$\mu_1 = kT \{ \ln \phi_1 + (1-r_1/r_2) \phi_2 + r_1 X_{12} \phi_2^2 \} \quad (\text{III.64})$$

with

$$X_{12} = \tilde{\rho} X_{12} / kT + \frac{\tilde{\rho}_1 \tilde{v}}{\tilde{T}_1} (1 + v^{-1}) \delta + \quad (\text{III.65})$$

$$1/\phi_2^2 \{ -\tilde{\rho}/\tilde{T}_1 + \tilde{P}_1 \tilde{v}/\tilde{T}_1 + \tilde{v} [ (1-\tilde{\rho}) \ln(1-\tilde{\rho}) + \tilde{\rho}/r_1 \ln \tilde{\rho} ] \}.$$

Exchanging subscripts in eqs. III.59-III.65 will result in the chemical potential of component 2. Although eq. III.64 looks like the Flory-Huggins chemical potential, there are some crucial differences. First,  $X_{12} \neq X_{21}$ . In addition,  $X_{12}$  is not only explicitly temperature and pressure dependent, but is also a function of composition.

Further differences lie in the LF theory's ability to describe volume changes on mixing, as well as lower critical solution temperatures which are common features of polymer containing systems. These improvements are solely due to the compressible nature of the model.

## CHAPTER IV

### PHASE EQUILIBRIA

Before the LF theory can be applied to the interface between two phases in equilibrium, the equilibrium properties of the two phases must be calculated. For one-component systems, this problem reduces to calculating the equilibrium vapor pressure and densities of the two phases at a given temperature. For binary mixtures, the situation becomes much more complicated. First the mixing parameter(s) need to be evaluated. Then the phase diagram must be determined. For homogeneous liquid mixtures, one requires the vapor pressure and the concentrations of the liquid and vapor phases at a given temperature. In a liquid-liquid system, the pressure can be equated to the external pressure, so that, at a fixed temperature, the concentrations of the two liquid phases must be calculated.

The equilibrium vapor pressure,  $\tilde{P}_e$ , for a pure fluid at a given temperature can be evaluated from the condition:

$$\mu[\tilde{T}, \tilde{P}_e, \tilde{\rho}_l(\tilde{T}, \tilde{P}_e)] = \mu[\tilde{T}, \tilde{P}_e, \tilde{\rho}_g(\tilde{T}, \tilde{P}_e)] \quad (\text{IV.1})$$

This equation can be solved in one of several ways. The method employed in this thesis has been described elsewhere in detail.<sup>36,43</sup>

Basically, the spinodal densities can be evaluated at a given temperature from<sup>36</sup>

$$\tilde{\rho}_s = \frac{1}{2} \left\{ -\frac{\tilde{T}}{2} \left(1 - \frac{1}{r}\right) + 1 \pm \sqrt{\left[ \frac{\tilde{T}}{2} \left(1 - \frac{1}{r}\right) - 1 \right]^2 - \frac{2\tilde{T}}{r}} \right\} . \quad (\text{IV.2})$$

Substitution of the two reduced spinodal densities into the equation of state yields two corresponding values of the reduced pressure which

serve as upper and lower bounds on the solution of eq. IV.1. This method allows one to obtain  $\tilde{\rho}_l, \tilde{\rho}_g$  and  $\tilde{P}_e$  efficiently. For polymer liquids, the vapor density and pressure are too small to be numerically accessible, so that both can be set equal to zero.

The first step in describing binary mixtures is to select a set of combining rules and determine the applicable mixture parameter(s). As mentioned previously, two forms of the binary mixture theory were investigated. When using the  $\Delta P^*$  combining rules, only one adjustable parameter must be determined, while use of the general combining rules requires two. Determination of the parameters can be accomplished in several ways, and the methods used were selected based on the type of literature data most readily available. For low molecular weight miscible mixtures, excess functions, particularly heats and volumes of mixing have been reported for a range of liquids. Furthermore, obtaining  $\Delta P^*$  or alternately  $\delta$  and  $\zeta$  from heat and volume of mixing data turns out to be a fairly simple numerical procedure.

The heat of mixing,  $\Delta H_m$ , of a binary system for the  $\Delta P^*$  combining rules is given by:

$$\Delta H_m / rN = v^* \{ -\tilde{\rho} P^* + \phi_1 P_1^* \tilde{\rho}_1 + \phi_2 P_2^* \tilde{\rho}_2 \} + P \frac{\Delta V}{rN} \quad (IV.3)$$

We shall assume that  $P \approx 0$ , so that the last term in eq. IV.3 may be neglected. In that case, the unknown quantities in this equation are  $\tilde{\rho}$  and  $P$ , since the  $\tilde{\rho}_j$ 's can be calculated from the equation of state using the pure component parameters of  $j$ . Given an experimental value of  $\Delta H_m$ , eq. IV.3 can be rearranged so as to calculate  $\tilde{\rho} P^*$ .

The equation of state, at zero pressure, can then be rewritten as

$$\frac{1}{P^*} = c \{ 1 - \exp \left[ -c \frac{1}{P^*} \left( \frac{c v^*}{kT} + 1 - \frac{1}{r} \right) \right] \} \quad (\text{IV.4})$$

where

$$c \equiv \tilde{\rho} P^*$$

which can be solved by simple iteration to yield  $P^*$ .  $\Delta P^*$  is then obtained from eq. III.17. The values of the temperature and compositions used in this calculation must, of course, correspond to those at which  $\Delta H_m$  was measured. The concentrations are normally given in the literature in terms of mole fractions,  $x_i$ , and are related to  $\phi_i'$  by

$$\phi_i' = \frac{m_i / \rho_i^*}{\sum_j m_j / \rho_j^*} \quad (\text{IV.5})$$

$$m_i = \frac{x_i M_i}{\sum_j x_j M_j},$$

where the  $m_j$ 's are the mass fractions.

The general combining rules result in two mixing parameters  $\delta$  and  $\zeta$ , thus their use requires two experimental quantities. The heat of mixing for this case is given by:

$$\Delta H_m / rN = -\tilde{\rho} \epsilon^* + \phi_1 \tilde{\rho}_1 \epsilon_{11}^* + \phi_2 \tilde{\rho}_2 \epsilon_{22}^* + P \frac{\Delta V}{rN} \quad (\text{IV.7})$$

and the volume of mixing,  $\Delta V_m$ , equals:

$$\Delta V_m / rN = v^* \tilde{v} - \phi_1 v_1^* \tilde{v}_1 - \phi_2 v_2^* \tilde{v}_2 \quad (IV.8)$$

If we again assume that  $P \approx 0$ , the unknowns in these equations occur in the following combinations:  $\tilde{\rho} \epsilon^*$  and  $v^* \tilde{v}$  (recall that  $\tilde{\rho} = 1/\tilde{v}$ ).

The mer fractions,  $\phi_i$ , are here related to the  $x_i$  by

$$\phi_i = \frac{r_i x_i}{\sum_j r_j x_j} \quad (IV.9)$$

The term  $v^* \tilde{v}$  can be directly calculated from eq. (IV.8). The result can be used in the following rearranged version of eq. (IV.7):

$$\epsilon_o^* = v^* \tilde{v} \left[ \phi_1 \tilde{\rho}_1 \epsilon_{11}^* + \phi_2 \tilde{\rho}_2 \epsilon_{22}^* - \frac{\Delta H}{rN} \right] \quad (IV.10)$$

where

$$\epsilon_o^* \equiv \epsilon^* v^* \quad (IV.11)$$

The equation of state at  $P \approx 0$  can be written

$$\tilde{\rho}^2 + kT \tilde{\rho} (v^* \tilde{v}) / \epsilon_o^* \left[ \ln(1 - \tilde{\rho}) + \left(1 - \frac{1}{r}\right) \tilde{\rho} \right] = 0 \quad (IV.12)$$

and solved for  $\tilde{\rho}$ . The values of  $\tilde{\rho}$ ,  $\epsilon_o^*$ , and  $v^* \tilde{v}$  then allow determination of  $\epsilon^*$  and  $v^*$  for the mixture, from which  $\delta$  and  $\zeta$  may be obtained using eq. III.22 and III.23 with the combining rules.

The values of  $\Delta P^*$ ,  $\delta$ , and  $\zeta$  obtained in practice are not unique, but depend to some extent on the temperature and composition. Fig. 3 illustrates the compositional dependence of the parameters for the

system benzene-toluene at 25°C. Not surprisingly, the best overall fit between theoretical and experimental excess functions was obtained with mixing parameters calculated at the composition at which the excess functions' extrema occurred. In order to standardize the determination of the mixing parameters, we chose to calculate them at .5 (in mole fraction), since this composition is usually close to where extrema arise for the relatively nonpolar low molecular weight liquids under consideration. The temperature dependence of the mixing parameters is more difficult to evaluate, since excess functions are usually measured at only one temperature. For the benzene-toluene system, measurements have been carried out over a 20° interval.<sup>44</sup>

The values of the parameters determined at three different temperatures are shown in Fig. 4. The variation for this system in this temperature range is not severe compared to the compositional variation.

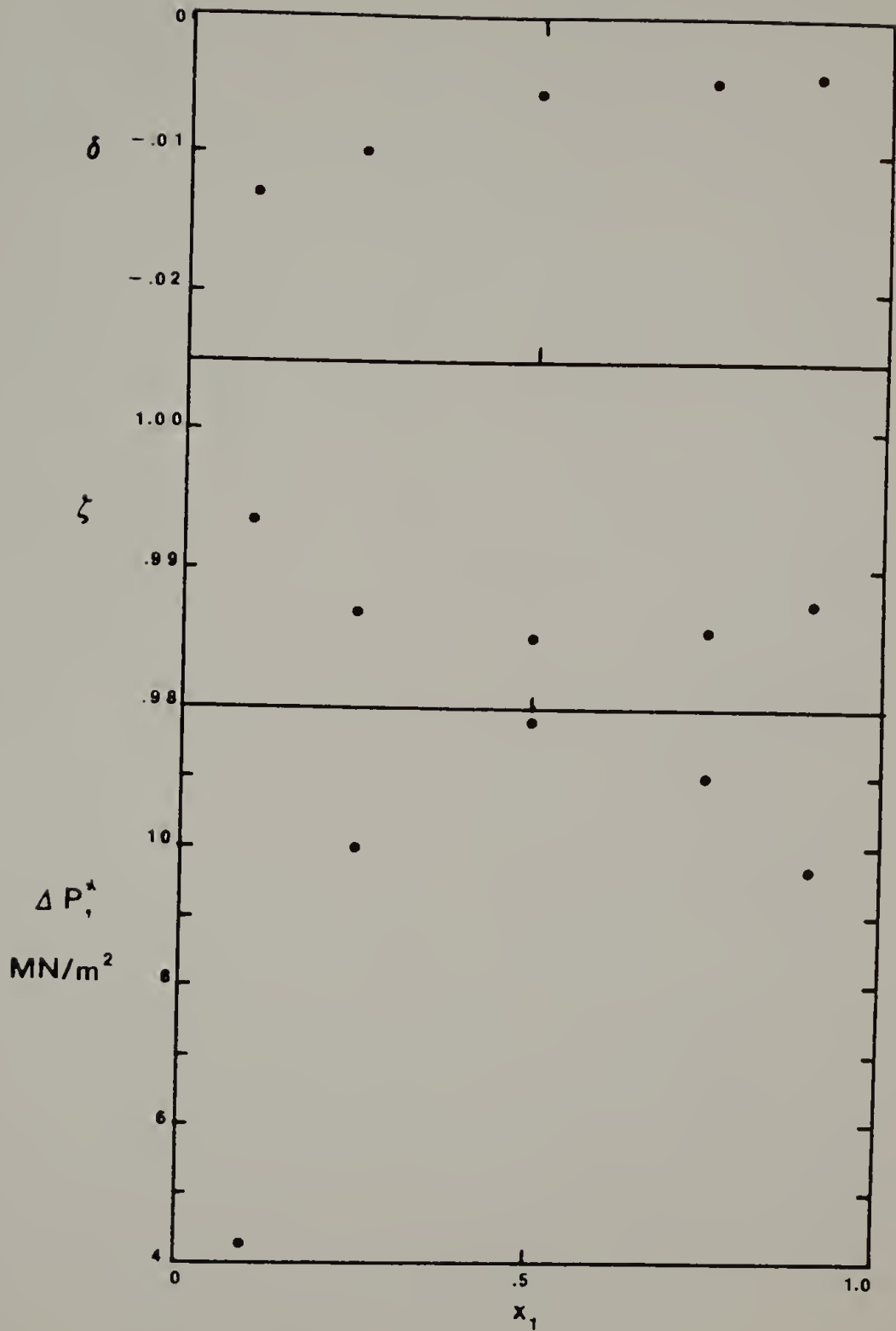
Tables 3 and 4 contain compilations of  $\Delta P^*$ 's and  $\delta$  and  $\zeta$  parameters calculated for a variety of mixtures. In order to evaluate the relative performance of the two sets of combining rules, the parameters obtained at  $x = .5$  were used to calculate the excess functions over the composition range and compared to the experimental curves. These comparisons were made for heat and volume of mixing curves, as well as for the free energy of mixing. The free energy of mixing can be obtained from:

$$\Delta G_m / rN = \Delta H_m / rN - T \Delta S_m / rN \quad . \quad (\text{IV.13})$$

For the  $\Delta P^*$  combining rules:



Figure 3. Composition dependence of the mixing parameters. The parameters shown were calculated for benzene-toluene mixtures at 20°C. Benzene is component 1.



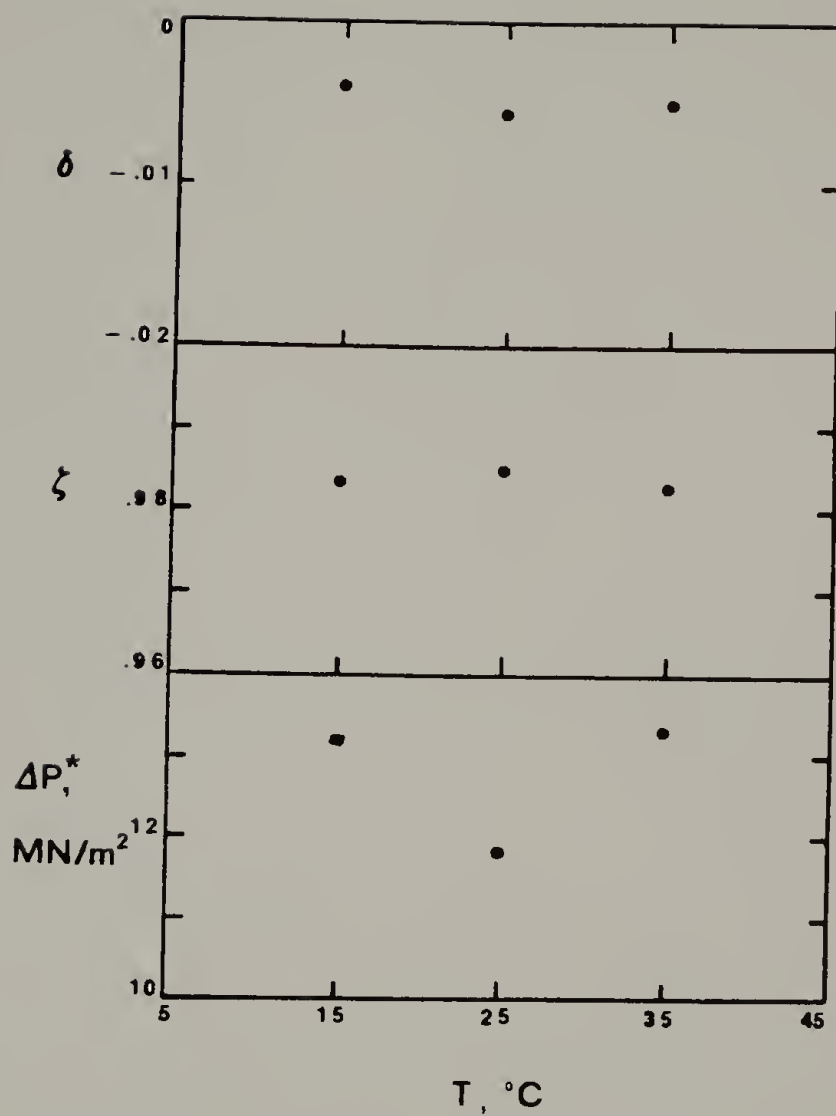


Figure 4. Temperature dependence of the mixing parameters. The parameters shown were calculated for benzene-toluene mixtures at mole fractions of .5 .

Table 3

MIXING PARAMETERS FOR THE  $\Delta P^*$  COMBINING RULES

	$\Delta P^*$ MN/m <sup>2</sup>	data from reference
n-hexane/2,2 dimethylbutane	0.4	45
n-hexane/benzene	28.9	46
n-hexane/CCl <sub>4</sub>	11.3	47
n-heptane/toluene	17.9	48
n-heptane/CCl <sub>4</sub>	11.2	47
n-heptane/benzene	31.9	48
benzene/toluene	11.8	44

Table 4  
MIXING PARAMETERS FOR THE GENERAL COMBINING RULES

	$\delta$	$\zeta$	data from reference
n-hexane/2,2 dimethylbutane	.0006	1.0001	45, 49
n-hexane/cyclohexane	-.0041	.9917	50, 51
benzene/n-pentane	.0103	.9770	48
benzene/n-hexane	-.0027	.9688	46, 52
benzene/cyclohexane	.0004	.9635	53, 51
benzene/n-heptane	-.0018	.9632	48
benzene/n-octane	-.0048	.9642	46, 52
benzene/n-decane	-.0066	.9579	46, 52
benzene/n-dodecane	-.0070	.9521	46, 52
benzene/n-tetradecane	-.0073	.9469	46, 52
benzene/n-hexadecane	-.0086	.9422	46, 52
benzene/toluene	-.0057	.9853	44
benzene/o-xylene	.0014	.9861	54
benzene/m-xylene	.0016	.9864	54
benzene/p-xylene	.0007	.9888	54
benzene/chloro-benzene	.0016	.9969	55, 56
benzene/bromo-benzene	.0025	.9944	55, 56
toluene/n-pentane	.0136	.9862	48
toluene/n-hexane	.0086	.9770	48
toluene/cyclohexane	.0025	.9709	53, 57
toluene/n-octane	.0022	.9783	48

	$\delta$	$\zeta$	data from reference
toluene/o-xylene	.0004	.9972	54
toluene/m-xylene	.0003	.9976	54
toluene/p-xylene	0	.9985	54
toluene/chlorobenzene	.0006	1.0038	55, 56
toluene/bromobenzene	.0014	1.0036	55, 56
chlorobenzene/n-heptane	.0002	.9817	58
CCl <sub>4</sub> /n-hexane	.0010	.9887	47
CCl <sub>4</sub> /n-heptane	.0009	.9875	47
CCl <sub>4</sub> /n-octane	.0012	.9861	59, 60
CCl <sub>4</sub> /toluene	-.0011	.9981	44
CCl <sub>4</sub> /o-xylene	.0016	1.0003	61
CCl <sub>4</sub> /m-xylene	.0022	.9983	61
CCl <sub>4</sub> /p-xylene	.0016	1.0003	44
CHCl <sub>3</sub> /n-hexane	-.0038	.9681	47
CHCl <sub>3</sub> /n-heptane	-.0037	.9661	47
CHCl <sub>2</sub> /n-hexane	-.0143	.9346	47
CHCl <sub>2</sub> /n-heptane	-.0161	.9304	47
o-xylene/m-xylene	-.0001	.9996	62
o-xylene/p-xylene	-.0001	.9998	62
m-xylene/p-xylene	-.0003	.9997	62
cyclohexane/n-dodecane	0	.9765	45, 63

$$\Delta S/rN = -k \left\{ \frac{\phi_1'}{r_1'} \ln \phi_1' + \frac{\phi_2'}{r_2'} \ln \phi_2' + \right. \\ \left. \tilde{v} [(1-\tilde{\rho}) \ln (1-\tilde{\rho}) + \frac{\tilde{\rho}}{r} \ln \tilde{\rho}] \right\} + \quad (IV.14)$$

$$\frac{k}{\phi_1' + v\phi_2'} \left\{ \phi_1' \tilde{v}_1 [(1-\tilde{\rho}_1) \ln (1-\tilde{\rho}_1) + \frac{\tilde{\rho}_1}{r_1} \ln \tilde{\rho}_1] + \right. \\ \left. v\phi_2' \tilde{v}_2 [(1-\tilde{\rho}_2) \ln (1-\tilde{\rho}_2) + \frac{\tilde{\rho}_2}{r_2} \ln \tilde{\rho}_2] \right\}$$

where  $v = v_1^*/v_2^*$  and  $k$  is the Boltzmann constant. For the general combining rules:

$$\Delta S/rN = k \left\{ -\frac{\phi_1}{r_1} \ln \phi_1 - \frac{\phi_2}{r_2} \ln \phi_2 + \right. \\ \left. \tilde{v} [(1-\tilde{\rho}) \ln (1-\tilde{\rho}) + \frac{\tilde{\rho}}{r} \ln \tilde{\rho}] + \phi_1 \tilde{v}_1 [(1-\tilde{\rho}_1) \ln (1-\tilde{\rho}_1) \right. \\ \left. + \frac{\tilde{\rho}_1}{r_1} \ln \tilde{\rho}_1] + \phi_2 \tilde{v}_2 [(1-\tilde{\rho}_2) \ln (1-\tilde{\rho}_2) + \frac{\tilde{\rho}_2}{r_2} \ln \tilde{\rho}_2] \right\}. \quad (IV.15)$$

When the calculated mixing functions are compared to the experimental ones for a number of mixtures, the agreement for the free energy and enthalpy functions is approximately the same for both sets of combining rules. However, the general combining rules yield better volume of mixing curves, as one might expect. Fig. 5 and 6 illustrate the types of results obtained.

Since the general combining rules offer the advantage of improving the fit to the volume of mixing curve, they were exclusively adopted

Figure 5. Experimental and calculated mixing functions for the system benzene-n-heptane at 25°C. Data are represented by filled circles and were taken from correlations given in reference 58. Broken lines were calculated with  $\Delta P^* = .0076 \text{ MN/m}^2$ , and solid lines represent results for  $\delta = -.0018$  and  $\zeta = .9632$ . The heat of mixing curves are coincident for the two sets of combining rules.



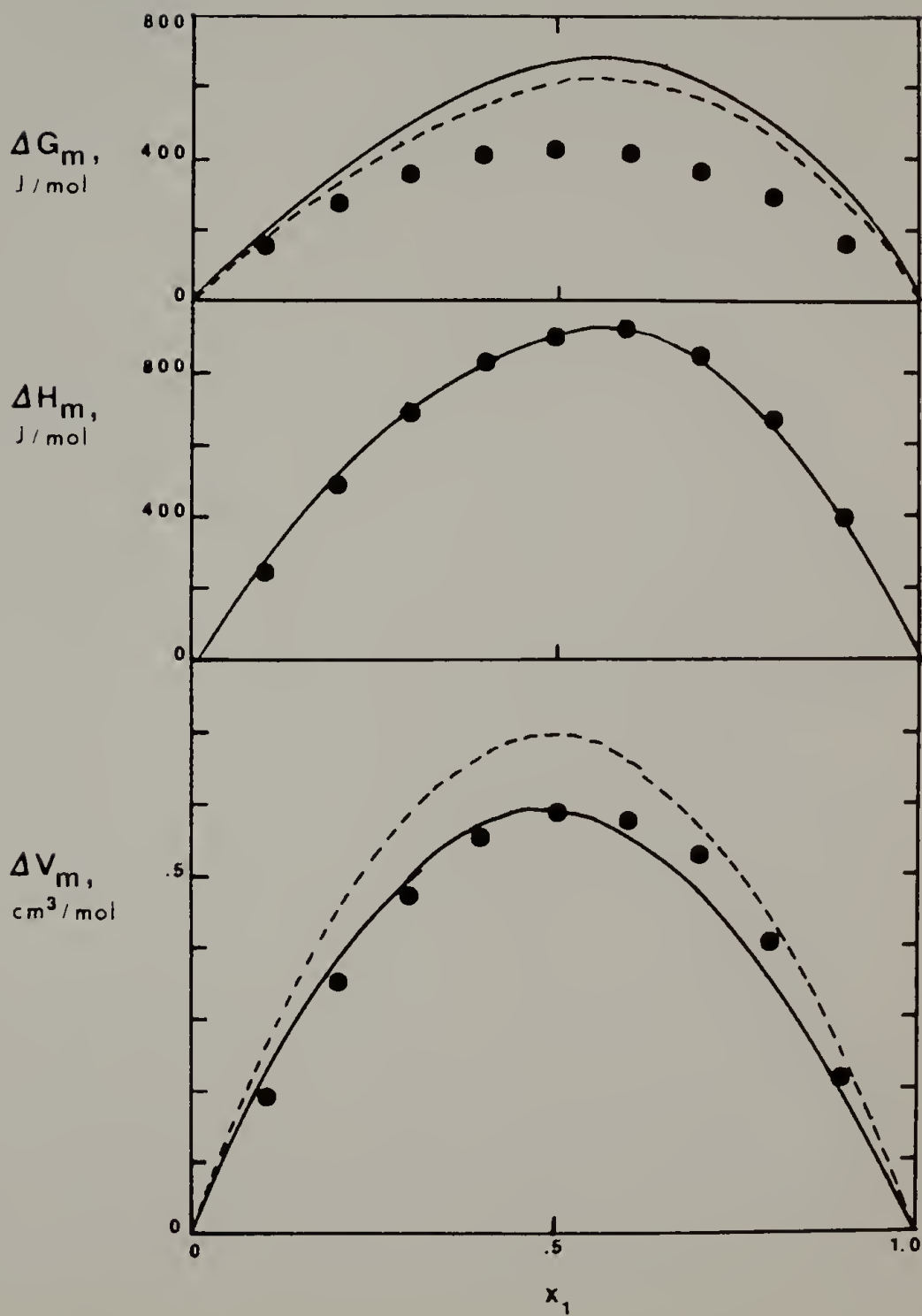
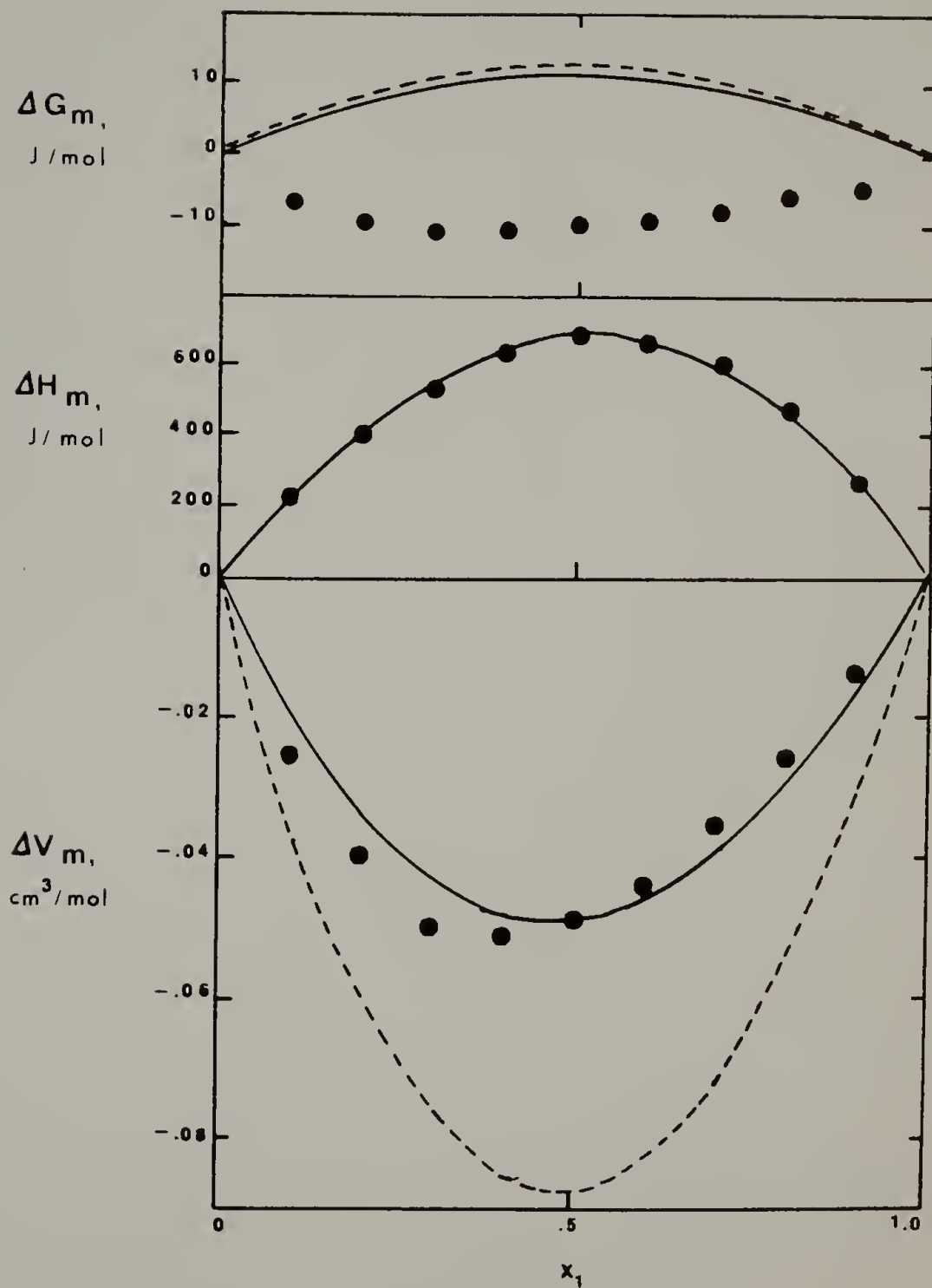


Figure 6. Experimental and calculated mixing functions for the system n-hexane-2,2-dimethyl butane at 25°C. Data are represented by filled circles and were taken from references 45 and 49. Broken lines were calculated with  $\Delta P^* = .0001 \text{ MN/m}^2$ , and solid lines are results for  $\delta = .0006$  and  $\zeta = 1.000$ . The heat of mixing curves are coincident for the two sets of combining rules.



for subsequent work. Additional benefits are gained through the use of these rules. A one-parameter mixture theory can easily be recovered by setting  $\delta$  equal to the arithmetic mean value (0) or to the appropriate geometric mean value. Thus the same equations may be applied in the event that only one piece of mixing data is available. In addition, the algebraic manipulation of the theoretical equations is simpler when using these combining rules. Finally, the two mixing parameters allow more flexibility in fitting liquid-liquid phase diagrams which will become important for partially miscible mixtures.

The most prevalent type of data for phase-separated binary liquids consists of critical temperatures and critical compositions. A totally different method for determining the mixing parameters,  $\delta$  and  $\zeta$ , is therefore necessary. The critical conditions for phase separation can be written:

$$\frac{d^2 g}{d\phi_1^2} = 0 \quad (\text{IV.16})$$

$$\frac{d^3 g}{d\phi_1^3} = 0 \quad (\text{IV.17})$$

where  $g = G/rN$ . Eq. IV.16 is commonly called the spinodal condition. If  $dg/d\phi_1$  is treated as a function of two independent variables  $\phi_1$  and  $\tilde{v}$  while the temperature and pressure are held constant, we obtain:

$$\frac{d^2(g/kT)}{d\phi_1^2} = \frac{\partial^2(g/kT)}{\partial\phi_1^2} + \frac{\partial^2(g/kT)}{\partial\phi_1\partial\tilde{v}} \frac{d\tilde{v}}{d\phi_1} \quad (\text{IV.18})$$

In addition, we can show:

$$\frac{d\tilde{v}}{d\phi_1} = -\tilde{v}\tilde{T}P^{*\beta} \left[ \frac{\partial^2(g/kT)}{\partial\phi_1\partial\tilde{v}} \right] \quad (\text{IV.19})$$

so that

$$\frac{d^2(g/kT)}{d\phi_1^2} = \frac{\partial^2(g/kT)}{\partial\phi_1^2} - \tilde{v}\tilde{T}P^{*\beta} \left[ \frac{\partial^2(g/kT)}{\partial\phi_1\partial\tilde{v}} \right]^2. \quad (\text{IV.20})$$

$\beta$  is the isothermal compressibility, and

$$\tilde{T}P^{*\beta} = \tilde{v} \left[ \frac{1}{\tilde{v}-1} + \frac{1}{r} - \frac{2}{\tilde{v}\tilde{T}} \right]. \quad (\text{IV.21})$$

Furthermore,

$$\frac{\partial^2(g/kT)}{\partial\phi_1^2} = -\tilde{\rho} \frac{d^2\frac{1}{\tilde{T}}}{d\phi_1^2} + \tilde{v} \frac{d^2\frac{\tilde{P}}{\tilde{T}}}{d\phi_1^2} + \ln\tilde{\rho} \frac{d^2\frac{1}{r}}{d\phi_1^2} + \frac{1}{\phi_1 r_1} + \frac{1}{\phi_2 r_2} \quad (\text{IV.22})$$

and

$$\frac{\partial^2(g/kT)}{\partial\phi_1\partial\tilde{v}} = \tilde{\rho}^2 \frac{d\frac{1}{\tilde{T}}}{d\phi_1} + \frac{d\frac{\tilde{P}}{\tilde{T}}}{d\phi_1} - \tilde{\rho} \frac{d\frac{1}{r}}{d\phi_1} \equiv \tilde{\rho} \Psi. \quad (\text{IV.23})$$

The derivatives in eqs. IV.22 and 23 are defined by:

$$\frac{d\frac{1}{r}}{d\phi_1} = \frac{1}{r_1} - \frac{1}{r_2} \quad (\text{IV.24})$$

$$\frac{d^2\frac{1}{r}}{d\phi_1^2} = 0 \quad (\text{IV.25})$$

$$\frac{d\tilde{P}/\tilde{T}}{d\phi_1} = \frac{Pv'}{kT}; \quad v' = v_1^* - v_2^* + (\phi_2 - \phi_1) \Delta v \quad (\text{IV.26})$$

$$\frac{d^2 \tilde{P}/\tilde{T}}{d\phi_1^2} = -\frac{2P}{kT} \Delta v \quad (\text{IV.27})$$

$$\frac{d \frac{1}{\tilde{T}}}{d\phi_1} = \frac{1}{kT} \frac{d\epsilon^*}{d\phi_1} = \frac{1}{kT} (\epsilon_{11}^* - \epsilon_{22}^* - X_{12}\phi_2^2 + X_{21}\phi_1^2) \quad (\text{IV.28})$$

$$\frac{d^2 \frac{1}{\tilde{T}}}{d\phi_1^2} = 2X_{12}\phi_2 + 2X_{21}\phi_1 - \phi_2^2 \frac{dX_{12}}{d\phi_1} + \phi_1^2 \frac{dX_{21}}{d\phi_1} \equiv X \quad (\text{IV.29})$$

where  $\Delta v = \delta(v_1^* + v_2^*)$  and  $X_{12}$  and  $X_{21}$  are defined by eqs. III.59-63.

$$\frac{dX_{12}}{d\phi_1} = 2X_{12} \left\{ \frac{D_{12}\delta}{a_{12} + b_{12}\delta + c_{12}\delta^2} - \frac{v_1^* - v_2^* + (\phi_2 - \phi_1)\Delta v}{v^*} \right\} \quad (\text{IV.30})$$

with

$$D_{12} = [(1+v\phi_1)(\tau^{\frac{1}{2}-\zeta}) - \phi_2(\tau^{-\frac{1}{2}-\zeta})]/(1+v) + (c_{12}/\phi_1)\delta. \quad (\text{IV.31})$$

$\frac{dX_{21}}{d\phi_1}$  can be obtained by exchanging subscripts in eqs. III.59-63 and IV.30.  $D_{21}$  is not given by exchanging subscripts in eq. IV.31

but by

$$D_{21} = [\phi_1(\tau^{\frac{1}{2}-\zeta}) - (1+v^{-1}\phi_2)(\tau^{-\frac{1}{2}-\zeta})]/(1+v^{-1}) - (c_{21}/\phi_2)\delta. \quad (\text{IV.32})$$

The final result for the spinodal condition may then be written:

$$\frac{1}{\phi_1 r_1} + \frac{1}{\phi_2 r_2} - \left[ \frac{2\tilde{P}\Delta v\tilde{v}}{\tilde{T}v^*} + \tilde{\rho}(X + \tilde{T}P^*\beta\psi^2) \right] = 0 \quad (\text{IV.33})$$

The spinodal condition represents the limit of stability for a homogeneous system. Since this equation, though complicated in appearance, is

straightforward to solve, it is a useful tool in the analysis of liquid-liquid phase behavior.

To derive the form of eq. IV.17, we proceed analogously. Taking the derivative with respect to  $\phi_1$  of eq. IV.18 and using results obtained in the derivation of the spinodal equation leads us to write:

$$\begin{aligned} \frac{d^3(g/kT)}{d\phi_1^3} = & -\frac{1}{\phi_1^2 r_1} + \frac{1}{\phi_2^2 r_2} - \tilde{\rho} \frac{d\tilde{X}}{d\phi_1} + \tilde{\rho}\psi \frac{\partial}{\partial\phi_1} \frac{d\tilde{v}}{d\phi_1} - \\ & \tilde{\rho}\tilde{T}P^{*\beta}\psi \left[ \tilde{\rho}\tilde{X} - \frac{2\Delta v\tilde{v}P}{kT} + \frac{\partial\psi}{\partial\phi_1} - \tilde{T}P^{*\beta}\psi \left( -\tilde{\rho}\psi + \frac{\partial\psi}{\partial\tilde{v}} \right) + \right. \\ & \left. \psi \frac{\partial}{\partial\tilde{v}} \frac{d\tilde{v}}{d\phi_1} \right] . \end{aligned} \quad (\text{IV.34})$$

The following derivatives complete the evaluation:

$$\frac{\partial\psi}{\partial\phi_1} = \tilde{\rho}\tilde{X} - \frac{2\Delta v\tilde{v}P}{kT} \quad (\text{IV.35})$$

$$\frac{\partial\psi}{\partial\tilde{v}} = -\tilde{\rho}^2 \frac{d\tilde{T}}{d\phi_1} + \frac{d\tilde{P}/\tilde{T}}{d\phi_1} \quad (\text{IV.36})$$

$$\frac{\partial}{\partial\tilde{v}} \frac{d\tilde{v}}{d\phi_1} = -\tilde{T}P^{*\beta} \frac{\partial\psi}{\partial\tilde{v}} - \psi \frac{\partial\tilde{T}P^{*\beta}}{\partial\tilde{v}} \quad (\text{IV.37})$$

$$\frac{\partial}{\partial\phi_1} \frac{d\tilde{v}}{d\phi_1} = -\tilde{T}P^{*\beta} \frac{\partial\psi}{\partial\phi_1} - \psi \frac{\partial\tilde{T}P^{*\beta}}{\partial\phi_1} \quad (\text{IV.38})$$

$$\frac{\partial^2\tilde{T}P^{*\beta}}{\partial\tilde{v}^2} = \tilde{\rho}\tilde{T}P^{*\beta} \{ 1 + \tilde{T}P^{*\beta} [ (\tilde{v}-1)^{-2} - 2\tilde{v}^{-2} \tilde{T}^{-1} ] \} \quad (\text{IV.39})$$

$$\frac{\partial\tilde{T}P^{*\beta}}{\partial\phi_1} = -\tilde{\rho}(\tilde{T}P^{*\beta})^2 \left[ \frac{1}{r_1} - \frac{1}{r_2} - 2\tilde{\rho} \frac{d\tilde{T}}{d\phi_1} \right] \quad (\text{IV.40})$$

$$\frac{dX}{d\phi_1} = \frac{2}{kT} \{ X_{12} [ 4\phi_2 Y_{12}^{-1-2\phi_2} Y_{12}^2 - \phi_2^2 \frac{dY_{12}}{d\phi_1} ] + X_{21} [ 4\phi_1 Y_{21}^{+1+2\phi_1} Y_{21}^2 + \phi_1^2 \frac{dY_{21}}{d\phi_1} ] \} \quad (\text{IV.41})$$

$$Y_{12} \equiv \frac{1}{2X_{12}} \frac{dX_{12}}{d\phi_1} \quad (\text{IV.42})$$

$$\frac{dY_{12}}{d\phi_1} = \frac{D'_{12}\delta}{a_{12} + b_{12}\delta + c_{12}\delta^2} - 2(Y_{12} + \frac{v'}{v^*})^2 + \frac{2\Delta v}{v^*} + (\frac{v'}{v^*})^2 \quad (\text{IV.43})$$

where

$$D'_{12} = [v(\tau^{\frac{1}{2}} - \zeta) + (\tau^{-\frac{1}{2}} - \zeta)] / (1+v) + (\tau^{\frac{1}{2}} - \zeta)\delta \quad (\text{IV.44})$$

$Y_{21}$  and  $\frac{dY_{21}}{d\phi_1}$  can again be obtained by exchanging subscripts.

The mixture parameters for a binary system can now be evaluated from eqs. IV.33 and 34 by inserting the experimental value for the critical temperature and composition, and solving for  $\delta$  and  $\zeta$ . Some care must be taken in this procedure, since both upper and lower critical solution temperatures (UCST's and LCST's) may appear in the theoretical phase diagram. Therefore it is possible that the calculated values of the mixing parameters could represent those needed to produce an LCST at the specified temperature and concentration rather than the UCST which is experimentally observed. The spinodal equation can be used to advantage here. As mentioned before, the spinodal (i.e. the locus of points for which eq. IV.33 equals



zero as a function of  $\phi_1$  and  $T$  at constant  $P$ ) represents the limit of stability. If  $d^2g/d\phi_1^2 > 0$ , the binary mixture is stable or metastable as a single phase, while a single phase is unstable for  $d^2g/d\phi_1^2 < 0$ . One can therefore determine the nature of the phase diagram at constant pressure by calculating  $d^2g/d\phi_1^2$ . The most efficient way to examine the phase diagram in this manner is to "map" the function  $d^2g/d\phi_1^2$ . An example of such a map is shown in Fig. 7. The digit "1" is printed whenever  $d^2g/d\phi_1^2 > 0$ , while "2" corresponds to negative values. This kind of map is useful whenever a general view of the theoretical phase behavior is desired. The locus of equilibrium points (the binodal) always lies in the  $d^2g/d\phi_1^2 > 0$  region outside the spinodal, except at the critical temperature where the binodal and spinodal coincide.

Once the mixing parameters,  $\delta$  and  $\zeta$ , have been calculated, the properties of the equilibrium phases need to be evaluated. For both liquid-vapor and liquid-liquid equilibria, the governing equations are

$$\mu_1^I(\tilde{T}, \tilde{P}, \phi_1^I) = \mu_1^{II}(\tilde{T}, \tilde{P}, \phi_1^{II}) \quad (\text{IV.45})$$

$$\mu_2^I(\tilde{T}, \tilde{P}, \phi_1^I) = \mu_2^{II}(\tilde{T}, \tilde{P}, \phi_1^{II}) \quad (\text{IV.46})$$

along with the equation of state. The superscripts <sup>I</sup> and <sup>II</sup> refer to the two phases. There are four independent variables in the system,  $\tilde{T}$ ,  $\tilde{P}$ ,  $\phi_1^I$ , and  $\phi_1^{II}$ , and only two equations, so that two variables must be fixed. For the case of liquid-vapor equilibrium

Figure 7. Map of the spinodal equation for the system cyclohexane-aniline. A value of 2 was printed when the spinodal equation evaluated at the appropriate temperature,  $T$ , and mer fraction,  $\phi$ , was negative. A single phase is therefore unstable in this region. Calculations were carried out using the following values of the mixing parameters:  $\delta = -.0505$  and  $\zeta = .9592$ .



the temperature and liquid composition were set and the equations were solved for the vapor pressure and composition. Numerically, this was accomplished using a Simplex algorithm, discussed briefly in the appendix on numerical methods. Fig. 8 shows an example of a liquid-vapor equilibrium calculation for n-hexane and benzene. Although the n-hexane enrichment of the vapor phase is somewhat over-estimated at low liquid phase concentrations, the theory satisfactorily predicts the shape of the curve as well as the existence of an azeotrope at high concentrations of n-hexane.

The analysis for liquid-liquid equilibria was carried out in one of two ways. In the first case, one sets the temperature and pressure and calculates the phase compositions. When this method is employed with the Simplex algorithm, one finds that the compositions converge to the same value, i.e. the trivial result of a single phase obtains. There are two ways to deal with this problem: one is to substitute a Newton-Raphson algorithm, and the other is to instead fix the pressure and composition difference between phases. Both methods have proved equally useful. Some complications which arise when one component is only marginally represented in one of the phases are also discussed in the numerical appendix. Fig. 9 shows the calculated binodal for cyclohexane-aniline ( $\delta = -.0152$ ;  $\zeta = .9598$ ) compared to experimental data. This figure illustrates a general feature of the LF model; the predicted region of immiscibility in a phase diagram is generally narrower than is experimentally observed.

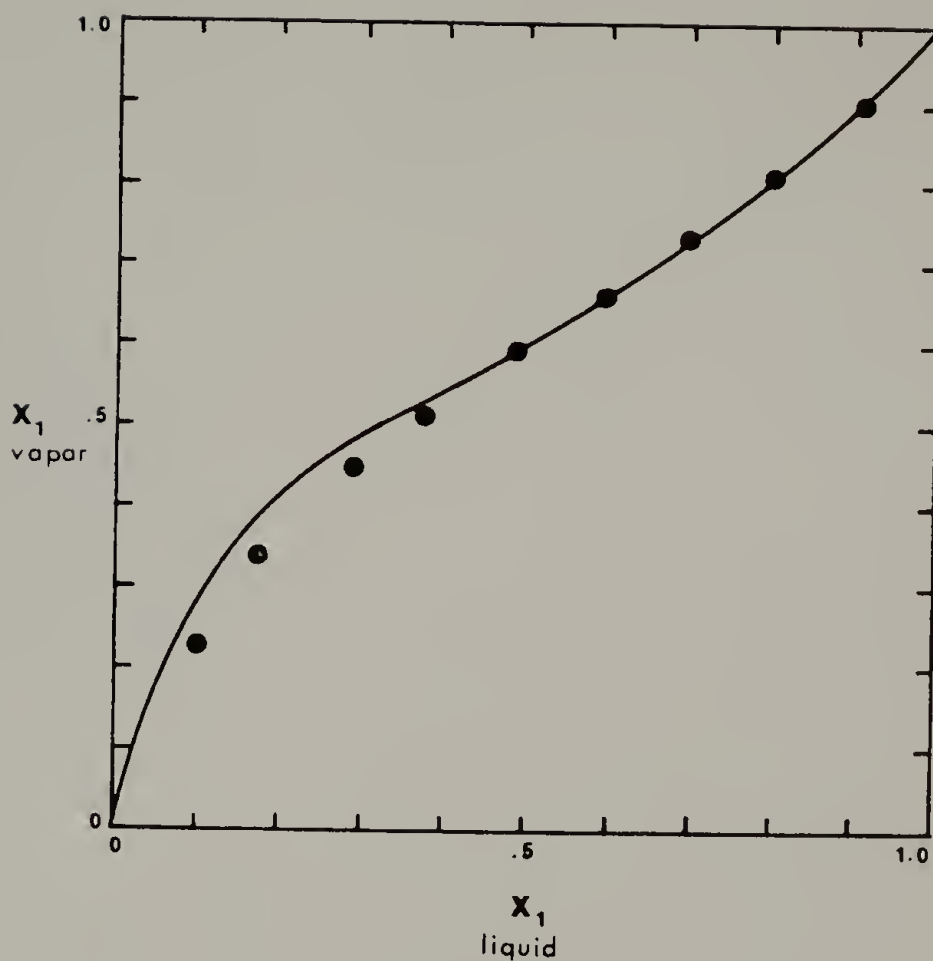


Figure 8. Liquid-vapor equilibria for the n-hexane-benzene system at 25°C. Liquid and vapor composition is plotted in terms of the mole fraction of n-hexane. Data (filled circles) were taken from reference 64, and the theoretical line was calculated with  $\delta = -.0027$  and  $\zeta = .9688$ .

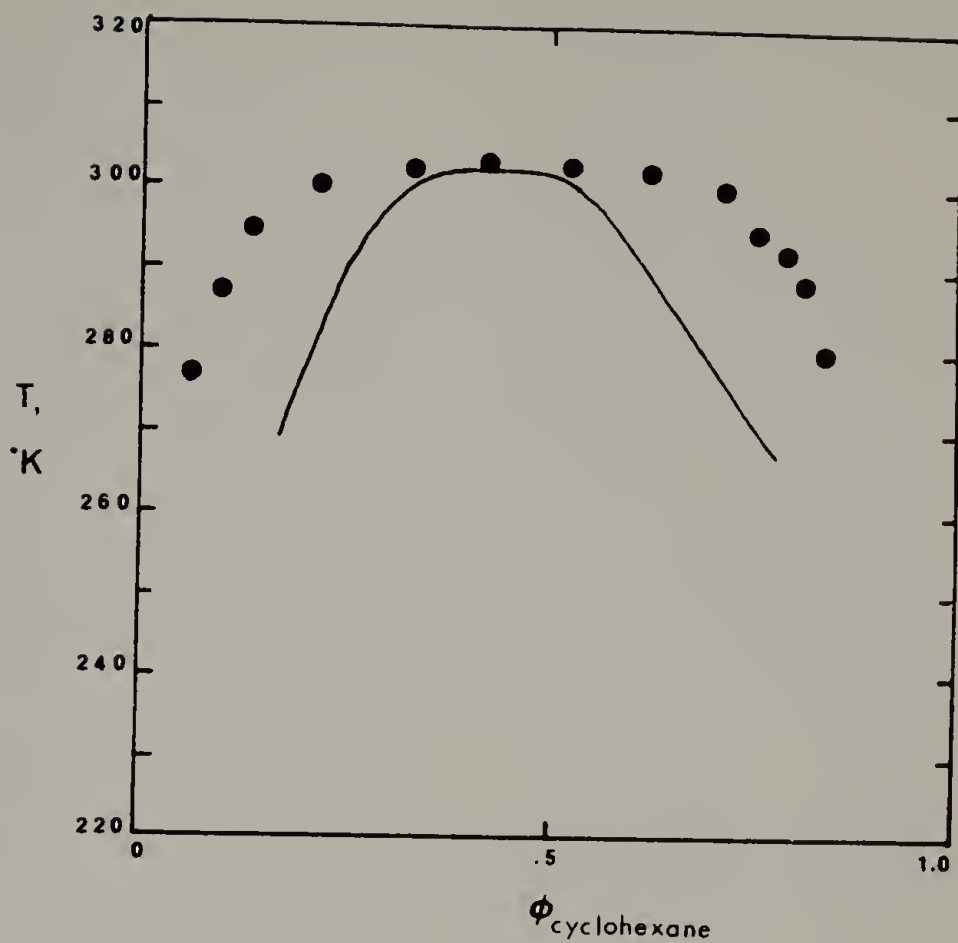


Figure 9. Temperature-composition phase diagram for the cyclohexane-aniline system. Data points were taken from reference 65 and the theoretical binodal line was calculated with  $\delta = -.0152$  and  $\zeta = .9598$ .  $\phi$  is the mer fraction.

One would thus expect to underestimate the interfacial tensions, since the concentration difference between the theoretical phases is less than the experimental difference.

Once the equilibrium properties of a liquid system have been analyzed, calculations of the surface properties can be carried out. Results obtained for pure systems will be discussed in the next chapter, while binary systems will be the subject of Chapter VI.

CHAPTER V  
ONE-COMPONENT SYSTEMS

A. Theory

In Chapter II, the general gradient theory of interfaces was developed. Now we shall combine this formulation with the lattice fluid theory for the case of a pure component liquid-vapor interface. The governing equation is

$$\gamma = \int_{-\infty}^{\infty} \left\{ \Delta a + \frac{1}{2} \kappa \left( \frac{d\rho}{dx} \right)^2 \right\} dx \quad (V.1)$$

subject to

$$\Delta a = \frac{1}{2} \kappa \left( \frac{d\rho}{dx} \right)^2 \quad (V.2)$$

where the subscripts on  $\kappa$  have been dropped. Recall that

$$\kappa = - \frac{2\pi}{3} \int_{\sigma}^{\infty} s^4 u(s) ds \quad (V.3)$$

As mentioned previously, eq. V.2 may be rearranged to allow a change of variables

$$dx = \sqrt{\kappa/2\Delta a} d\rho \quad (V.4)$$

which leads to the more convenient expression

$$\gamma = 2 \int_{\rho_g}^{\rho_l} \sqrt{\frac{1}{2} \kappa \Delta a} d\rho \quad (V.5)$$

where  $\rho_g$  and  $\rho_l$  are the equilibrium gas and liquid densities. This equation is preferable since the domain of integration is now bounded.



Eq. V.4 can also be formally integrated to

$$x-x_0 = \int_{\rho_0}^{\rho} \sqrt{\kappa/2\Delta a} \, d\rho \quad , \quad (\text{V.6})$$

from which form the interfacial profile may be calculated. The values of  $x_0$  and  $\rho_0$  may be arbitrarily set anywhere in the interface. From these equations, it is apparent that the following quantities are required for a numerical evaluation of the interfacial properties:  $\kappa$ , or equivalently the intermolecular interaction potential,  $\Delta a$  and the equilibrium gas and liquid densities. These quantities will be obtained from the LF model.

To evaluate  $\kappa$ , we identify  $\sigma = v^*{}^{1/3}$  as before and use eq. III.5 for  $u(s)$ . Eq. V.3 then becomes

$$\kappa = \frac{2\pi}{3} \int_{v^*{}^{1/3}}^{\infty} s^{4-m} \epsilon_0 v^{*m/3} \, ds \quad . \quad (\text{V.7a})$$

Upon integration, assuming  $m > 5$ :

$$\begin{aligned} \kappa &= \frac{2\pi\epsilon_0}{3} \frac{1}{m-5} v^{*m/3} v^{*(5-m)/3} \\ &= \frac{1}{3} \epsilon^* v^{*5/3} \frac{m-3}{m-5} \end{aligned} \quad (\text{V.7b})$$

where the definition of  $\epsilon^*$  given in eq. III.6 has been used. The value of  $\kappa$  is thus set for a given value of  $m$ , which measures the range of the attractive part of the potential.

In order to determine the form of  $\Delta a$ , we recall the definition

$$\Delta a \equiv a_0 - a_e = a_0 - \rho \mu^e + P_e \quad . \quad (\text{V.8})$$

which we can rewrite as

$$\begin{aligned}\Delta a &= \rho \mu(\rho, P_e) - P_e - \rho \mu^e + P_e \\ &= [\rho(\mu, P_e) - \mu^e] .\end{aligned}\quad (\text{V.9})$$

The number density of mers in the LF is

$$\rho = \frac{1}{V} = \frac{\tilde{\rho}}{rNv^*} . \quad (\text{V.10})$$

Substituting eq. V.10 and III.1 into V.9 yields

$$\Delta a = \frac{\epsilon^*}{v^*} \tilde{\rho} \{ -\tilde{\rho} + \tilde{P}_e \tilde{v} + \tilde{T} [ (\tilde{v}-1) \ln(1-\tilde{\rho}) + \frac{1}{r} \ln \tilde{\rho} ] - \tilde{\mu}^e \} \quad (\text{V.11})$$

The equilibrium vapor pressure,  $\tilde{P}_e$ , and the equilibrium densities  $\tilde{\rho}_g$  and  $\tilde{\rho}_l$  are obtained from phase equilibria as described in the previous chapter.

Due to the form of eq. V.11, the interfacial problem can be expressed entirely in reduced form as

$$\tilde{\gamma} = 2 \int_{\tilde{\rho}_g}^{\tilde{\rho}_l} \sqrt{\tilde{\kappa} \tilde{\Delta} \tilde{a}} \, d\tilde{\rho} \quad (\text{V.12})$$

using the following definitions:

$$\tilde{\gamma} = \gamma / \gamma^* \quad ; \quad \gamma^* = \epsilon^* / v^{*2/3} \quad (\text{V.13})$$

$$\tilde{\kappa} = \frac{1}{2} \kappa / v^{*2/3} \quad (\text{V.14})$$

$$\tilde{\Delta} \tilde{a} = \Delta a v^* / \epsilon^* . \quad (\text{V.15})$$

Eq. V.6 becomes in reduced form

$$\tilde{x} - \tilde{x}_0 = \int_{\tilde{\rho}_0}^{\tilde{\rho}} \sqrt{\tilde{\kappa}/\Delta\tilde{a}} \, d\tilde{\rho} \quad (\text{V.16})$$

with

$$\tilde{x} = x/v^*{}^{1/3} \quad (\text{V.17})$$

Once the phase equilibrium has been calculated at a given temperature, the interfacial tension and profile can be obtained by straightforward numerical integration of eqs. V.12 and V.16 or alternately eqs. V.5 and V.6.

## B. Results

The first requirement placed on any theory is that the predicted trends as a function of the input variables should be in agreement with experimental observation. In order to evaluate the qualitative predictions, the potential exponent  $m$  will be set equal to 6, the traditional value associated with pure dispersion forces.  $\kappa$  is thus equal to  $\frac{1}{2}$ . There are two variables in which we are primarily interested: the temperature and the molecular weight. A plot of the reduced interfacial tension vs. the reduced temperature at various values of the LF parameter  $r$  ( $r$  is roughly proportional to molecular weight) is given in Fig. 10. In the LF model, the reduced critical temperature,  $\tilde{T}_c$ , is given by

$$\tilde{T}_c = 2r/(1 + \sqrt{r})^2 \quad (\text{V.18})$$

i.e. it is a function of  $r$ . As can be seen in Fig. 10, at a given value of  $r$ , the reduced interfacial tension decreases and goes to zero at a reduced temperature which is equal to  $\tilde{T}_c$ . The figure also

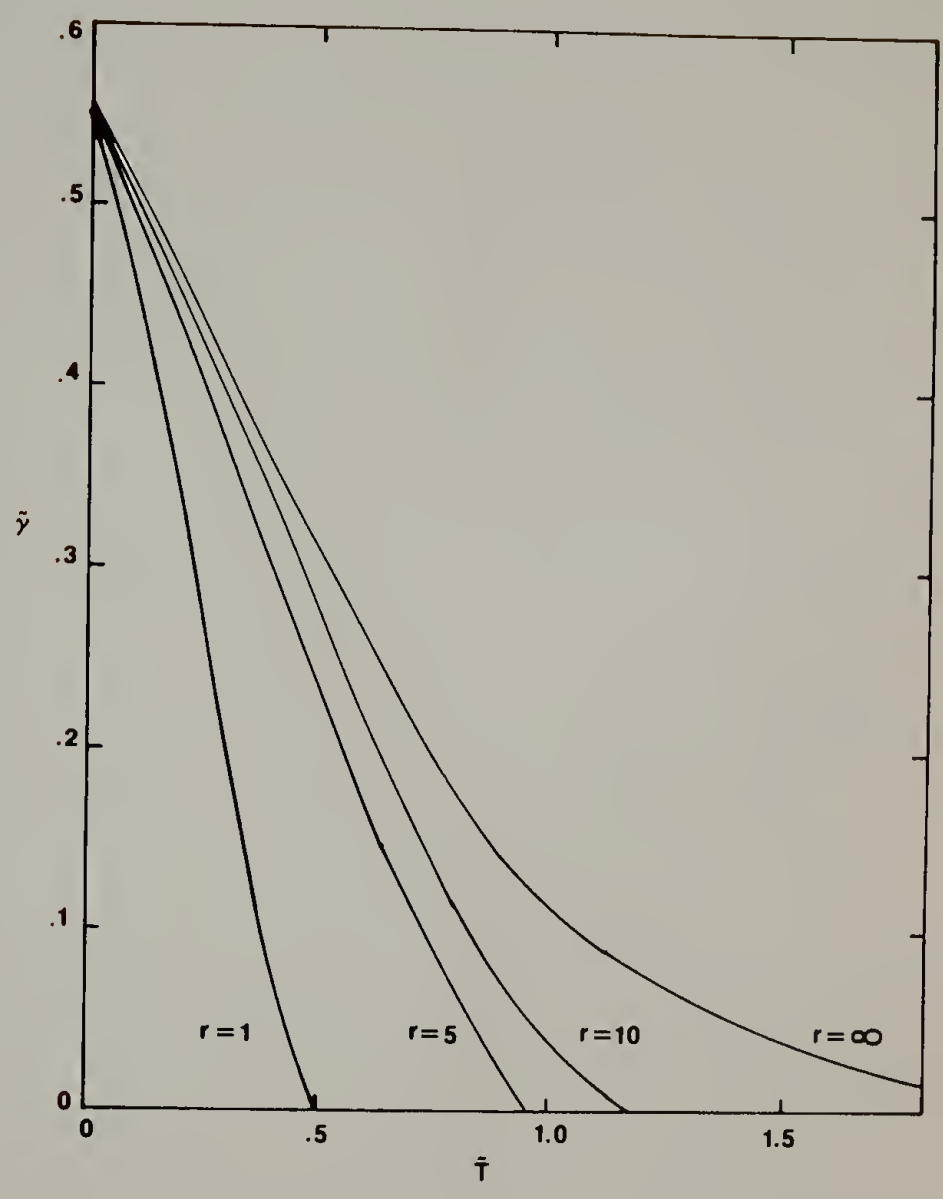


Figure 10. Reduced interfacial tension,  $\tilde{\gamma}$ , versus reduced temperature,  $\tilde{T}$ , at several values of the molecular size parameter,  $r$ .

demonstrates that for a homologous series of liquids, the tension increases as a function of molecular weight at a given temperature. The surface entropy ( $-d\gamma/dT$ ) can be seen to decrease with increasing molecular weight.

Fig. 10 provides in addition a check on the accuracy of the numerical integration procedure. In the limit of  $T$  going to zero, eq. V.12 reduces to

$$\begin{aligned} \lim_{\tilde{T} \rightarrow 0} \tilde{\gamma} &= \frac{2}{\sqrt{2}} \int_0^1 \sqrt{\tilde{\rho} - \tilde{\rho}^2} d\tilde{\rho} \\ &= \frac{\pi}{4\sqrt{2}} \approx .5554 . \end{aligned} \tag{V.19}$$

Note that the calculated curves in Fig. 10 converge to this value as  $\tilde{T}$  goes to zero.

Figure 11 illustrates the behavior of the reduced density profiles for three values of  $r$  at three reduced temperatures. As expected, the profiles for a given  $r$  flatten as the temperature increases, becoming straight lines at  $\tilde{T}_c$  (not shown). In addition, steeper profiles are obtained at a given  $\tilde{T}$  as a function of increasing  $r$ . The density profiles for  $r = 5$  and  $r = 10$  appear to exhibit an approximate common point of intersection at a density corresponding to the reduced critical density. Bongiorno and Davis<sup>10</sup> and other workers<sup>66,67</sup> have observed the occurrence of such intersections for their theories, but they located the  $x$ -origins of their density profiles so as to correspond to the Gibbs dividing surface. The  $x$ -origin in Fig. 11 is arbitrarily located at a density of  $(\tilde{\rho}_l + \tilde{\rho}_g)/2$ . The observation of an approximate

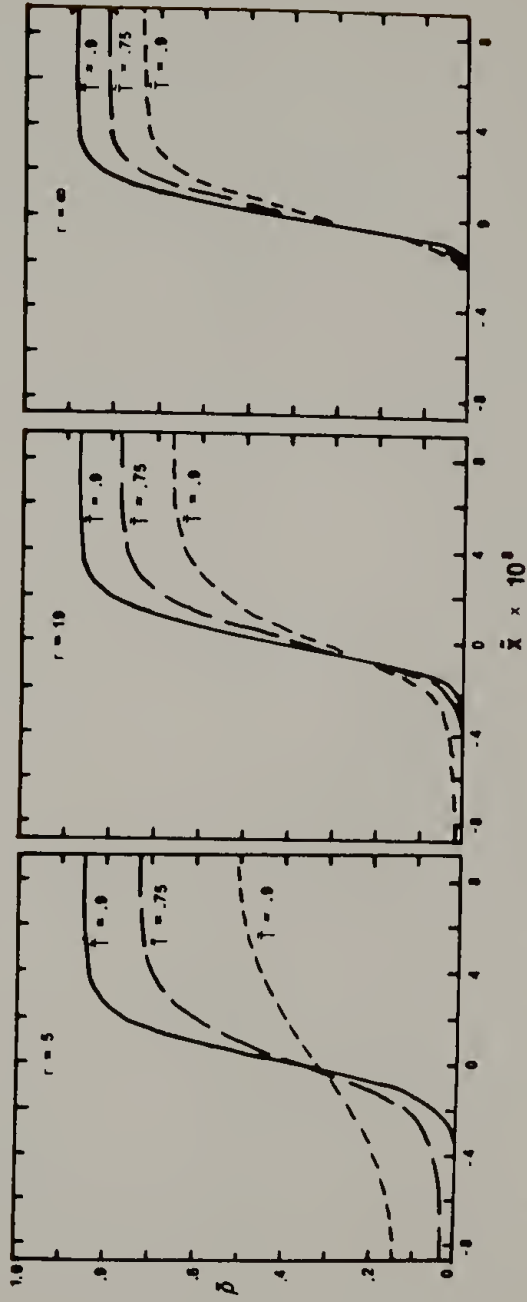


Figure 11. Reduced density profiles at several values of the reduced temperature,  $\bar{T}$ , and molecular size parameter,  $r$ . The reduced distance,  $\bar{x}$ , has its origin arbitrarily located at the average of the reduced liquid and gas densities.

common point of intersection must thus be considered coincidental; it may arise from the fact that the density,  $\rho(\rho_l > \rho > \rho_g)$ , where  $\mu^o$  crosses  $\mu^e$  (see Fig. 1) shifts only very slightly over the range of temperature.

The present theory thus predicts the qualitative relationship between  $\gamma$ ,  $T$ , and  $r$  satisfactorily. The decrease in tension and concomitant flattening of the density profile as the temperature rises are, of course, due to the increasing similarity of the phases as the critical point is approached. The relationship between  $\tilde{\gamma}$  and the distance from the critical temperature,  $\tilde{T}_c - \tilde{T}$ , is often expressed as

$$\tilde{\gamma} = \tilde{\gamma}_0 (\tilde{T}_c - \tilde{T})^p, \quad (\text{V.20})$$

where  $p$  is a critical exponent. A plot of  $\ln \tilde{\gamma}$  vs.  $\ln (\tilde{T}_c - \tilde{T})$  is shown in Fig. 12. The slope of this line yields  $p = 1.5$ , which is identical to the value predicted by the van der Waals model. The experimental value of  $p$  is approximately 1.2.<sup>68</sup> The fact that the present theory does not yield the correct result for a critical exponent is not surprising. Although the gradient approximation should be best near the critical point, this is precisely the region in which a mean field theory like the LF theory should fail. In the mean field, molecular correlations are neglected, and such correlations become very important in critical phenomena. As a result the LF model generally overestimates the critical temperature. Other evidence of the unsatisfactory nature of the model in the critical region has

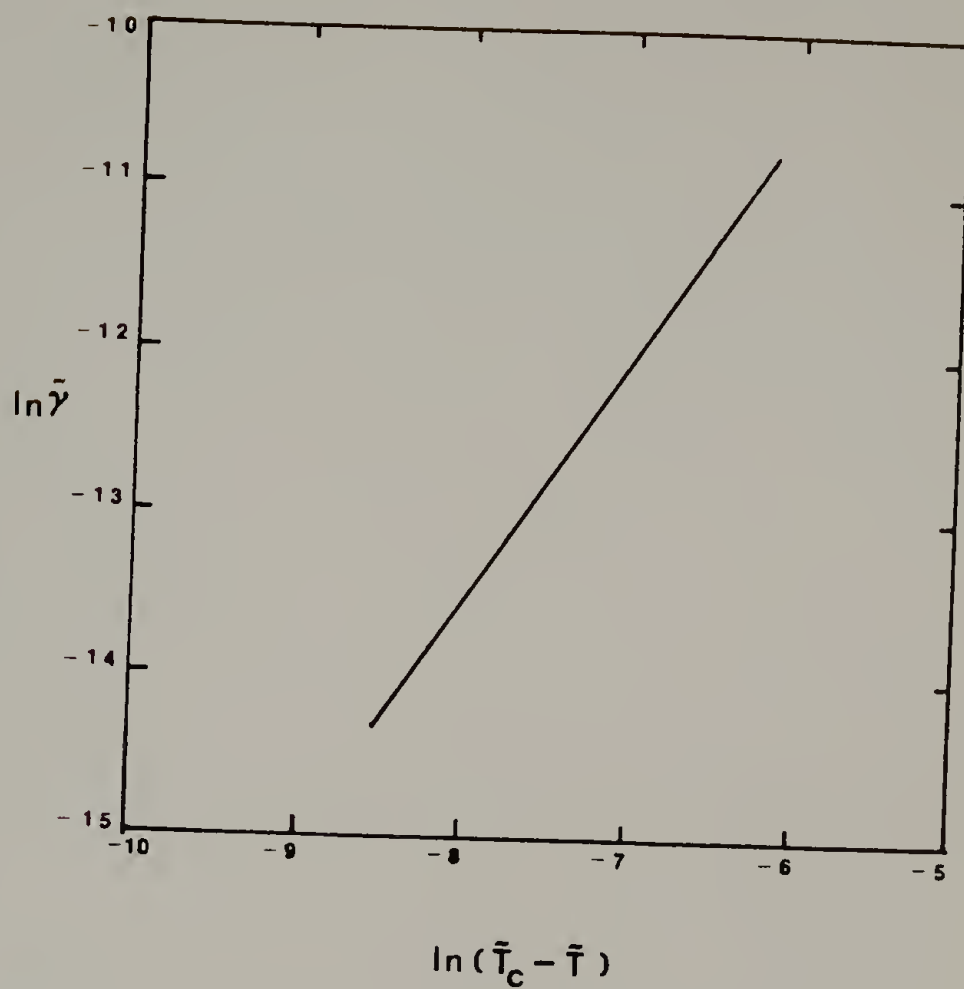


Figure 12. Dependence of the reduced interfacial tension,  $\tilde{\gamma}$ , on reduced temperature,  $\tilde{T}$ , near the critical temperature,  $\tilde{T}_c$ . The slope of this line is 1.5.



been discussed elsewhere.<sup>36</sup> For this reason, we shall concentrate on the region away from the critical point, where the LF model gives good predictions for fluid behavior.

If one uses the a priori value of  $\tilde{\kappa} = .5$ , the calculation of the tension and profile contains no adjustable parameters. The pure component LF parameters are determined solely by bulk properties. The result of such a calculation for hexane is shown in Fig. 13. Although the tension vs. temperature curve is qualitatively correct, the value of the tension is underestimated by about 10% across the temperature range. The same type of result is obtained for other (nonpolar or slightly polar) low molecular weight liquids. The ability of the present theory to predict tensions of polyatomic fluids within 10% of the experimental values without the use of adjustable parameters is satisfying. As mentioned previously, more rigorous theories are limited in their description to simpler fluids.

Since a 10% error was obtained with remarkable consistency for a number of low molecular weight liquids, the possibility of reducing the error by using a  $\tilde{\kappa}$  obtained from a fit of the data was investigated. Such pure component  $\tilde{\kappa}$ 's would form a superior basis for the subsequent mixture calculations. In Fig. 14, the  $\tilde{\kappa}$  required to exactly reproduce the experimental tension at a given temperature is plotted vs. the temperature reduced by the experimental critical temperature for n-alkanes ranging from n-pentane to n-heptadecane. The data used in these calculations were taken from a compilation by Timmermans.<sup>69</sup> The values of  $\tilde{\kappa}$  fall into a narrow range over a wide

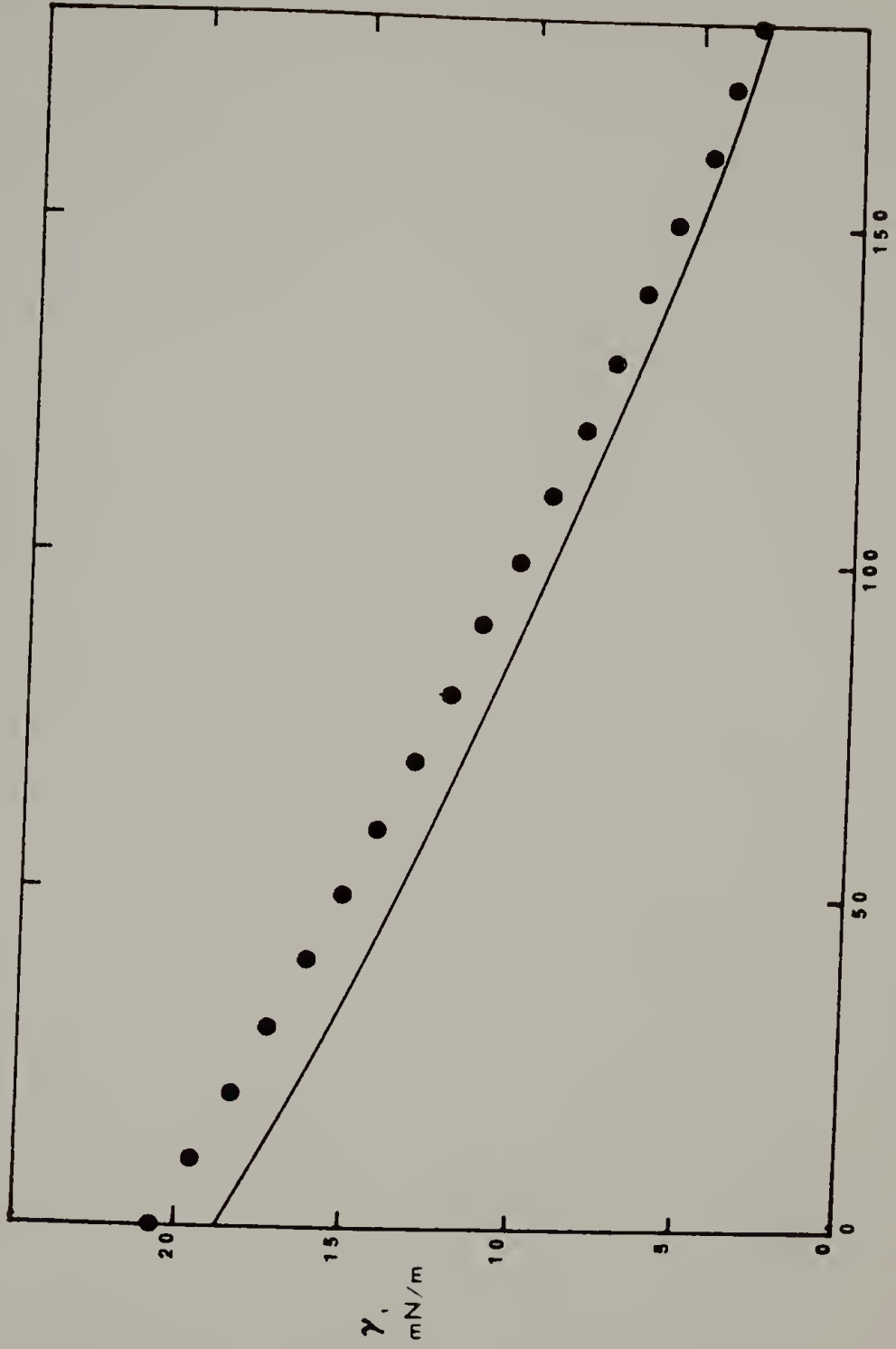
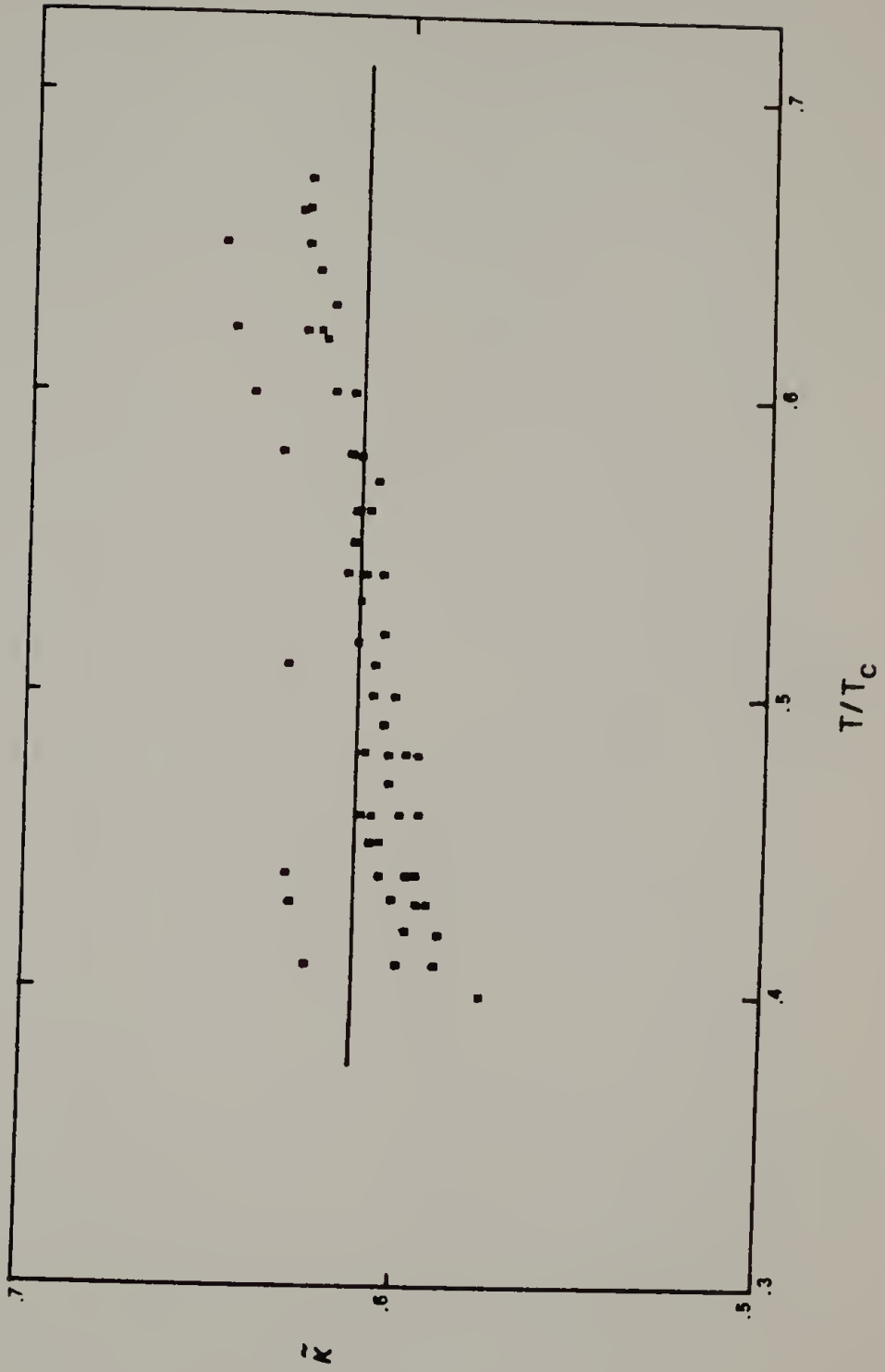


Figure 13. Comparison of experimental and theoretical tensions versus temperature for n-hexane with  $\tilde{\kappa} = .5$ . Data points are from reference 70.

Figure 14. Values of  $\tilde{\kappa}$  required to fit the experimental tension for n-alkanes versus temperature reduced by the experimental critical temperature. Data points are from reference 69, and the line represents the average value of  $\tilde{\kappa}$ .



range of temperature ( $.4 < T/T_c < .7$ ). Obviously, the points do not appear to lie about a horizontal line but rather about a line with a slight positive slope. The average value of  $\tilde{\kappa}$  is  $0.61 \pm .03$ , indicated by the line in Fig. 14. This constant average value, rather than the temperature dependent  $\tilde{\kappa}$  obtained from a least-squares fit was selected for use, for two reasons. First, the  $T/T_c$  dependence of  $\tilde{\kappa}$  can be seen to be quite small, so that introducing this dependence into the theory would increase the complexity without yielding important benefits. Second, while the average value of  $.61$  for  $\tilde{\kappa}$  was also obtained using other sets of data,<sup>70</sup> and was furthermore relatively insensitive to the number of data points used, the least-squares parameters varied widely. (The slope of the line varied from  $.01$  to  $2 \times 10^{-8}$ .) The use of an average value for  $\tilde{\kappa}$  thus seemed indicated. Between  $T/T_c$  of  $0.7$  and  $1.0$ , the fitted values of  $\tilde{\kappa}$  begin to deviate more and more from this average value, which is due to the unsatisfactory nature of the LF near the critical point. Within the wide and useful temperature range of  $.4 < T/T_c < .7$ , tensions for the n-alkanes can be fitted with an error of about 3% using  $\tilde{\kappa} = .61$  ( $T/T_c = .4$  is near the freezing point for most alkanes).

Fig. 15 illustrates the excellent agreement between calculated and experimental tensions for n-hexane and n-decane obtained with  $\tilde{\kappa} = .61$ . For n-hexane,  $T/T_c = .7$  occurs at approximately  $90^\circ\text{C}$ . Note that the agreement does not drastically break down at this temperature, but the calculated curve gradually loses accuracy above this temperature. The tensions obtained with the fitted value of  $\tilde{\kappa}$  represent a marked

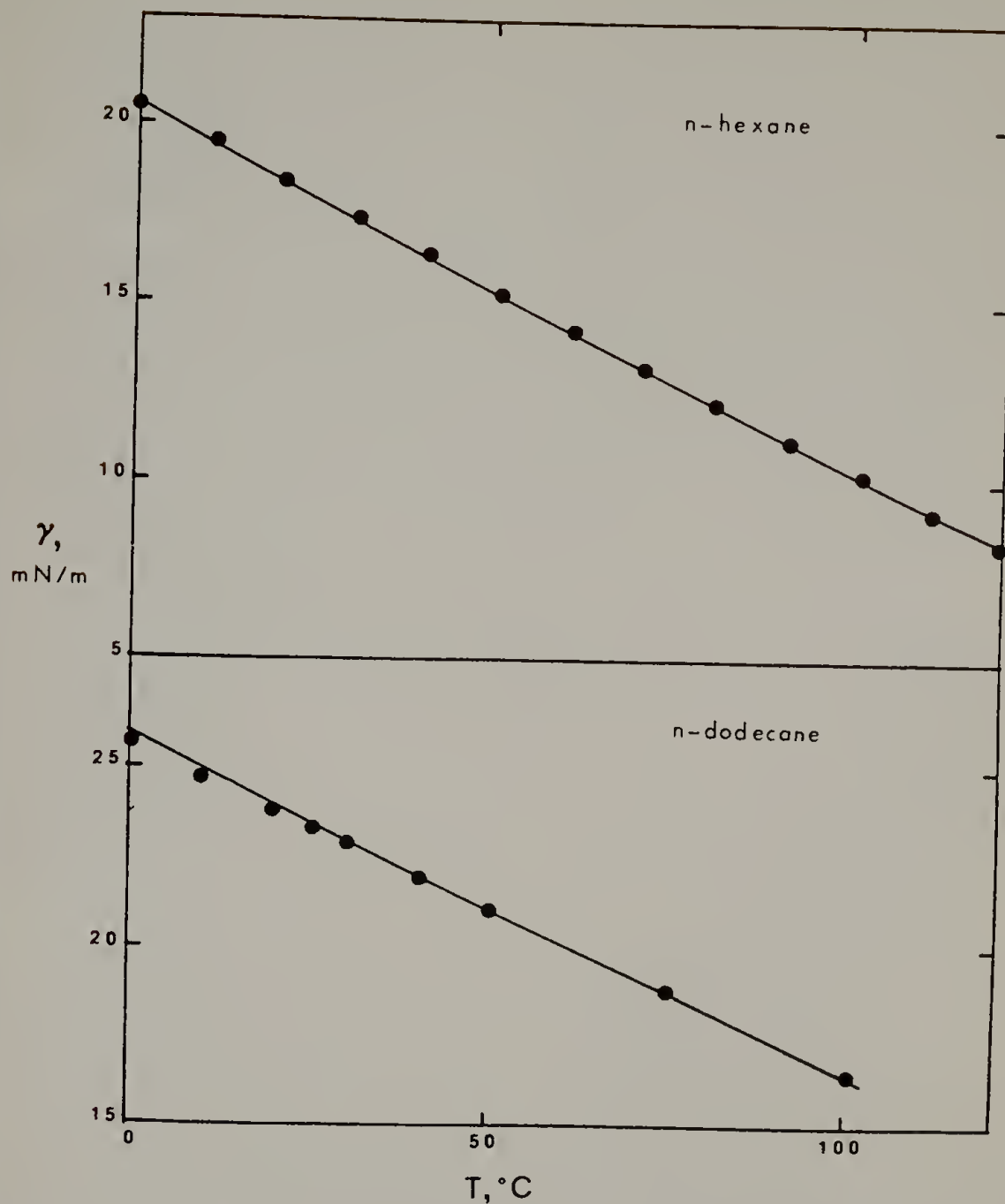


Figure 15. Comparison of experimental and theoretical tensions versus temperature for n-hexane and n-dodecane with  $\tilde{\kappa} = .61$ . Data points are from reference 70.

improvement over those resulting with the ab initio value of  $\tilde{\kappa} = .5$ . Recall that the value of .5 corresponds to  $m = 6$  for the exponent of the attractive part of the interaction potential. If  $\tilde{\kappa} = .61$ ,  $m = 5.75$ . (cf. eqs. V.7 and V.14). The value of  $m = 6$  implies that the interaction is purely due to dispersive forces. Reducing the value of  $m$  below 6 extends the tail of the potential (i.e. the range of the forces is larger than that of purely dispersive forces). The fact that a value of  $m = 5.75$  gives a satisfactory fit to the tension data appears to suggest that the interaction between these nonpolar molecules is longer-range than would be expected for pure dispersion.

When branched alkanes and other nonpolar and slightly polar molecules are included in the calculation of an average fitted value of  $\tilde{\kappa}$ , the result is  $\tilde{\kappa} = .62 \pm .05$ . In other words, the tension of nonpolar and slightly polar molecules can be described by the present theory to within about 5% using a single value of  $\tilde{\kappa}$ . Since  $\tilde{\kappa}$  scales both the surface tension and the surface entropy, this result lends further support to the basic validity of the gradient-free energy approach. Fig. 16 shows two examples of the results obtained for nonhydrocarbon liquids with  $\tilde{\kappa} = .62$ . Table 5 contains a compilation of the maximum and average errors in the range of  $.4 < T/T_c < .7$  for all low molecular liquids included in the determination of  $\tilde{\kappa} = .62$ . The values of the reduction parameter for the tension are also included. Errors were calculated using data from reference 70; the values given in parentheses were obtained from alternate sets of data.<sup>69</sup>

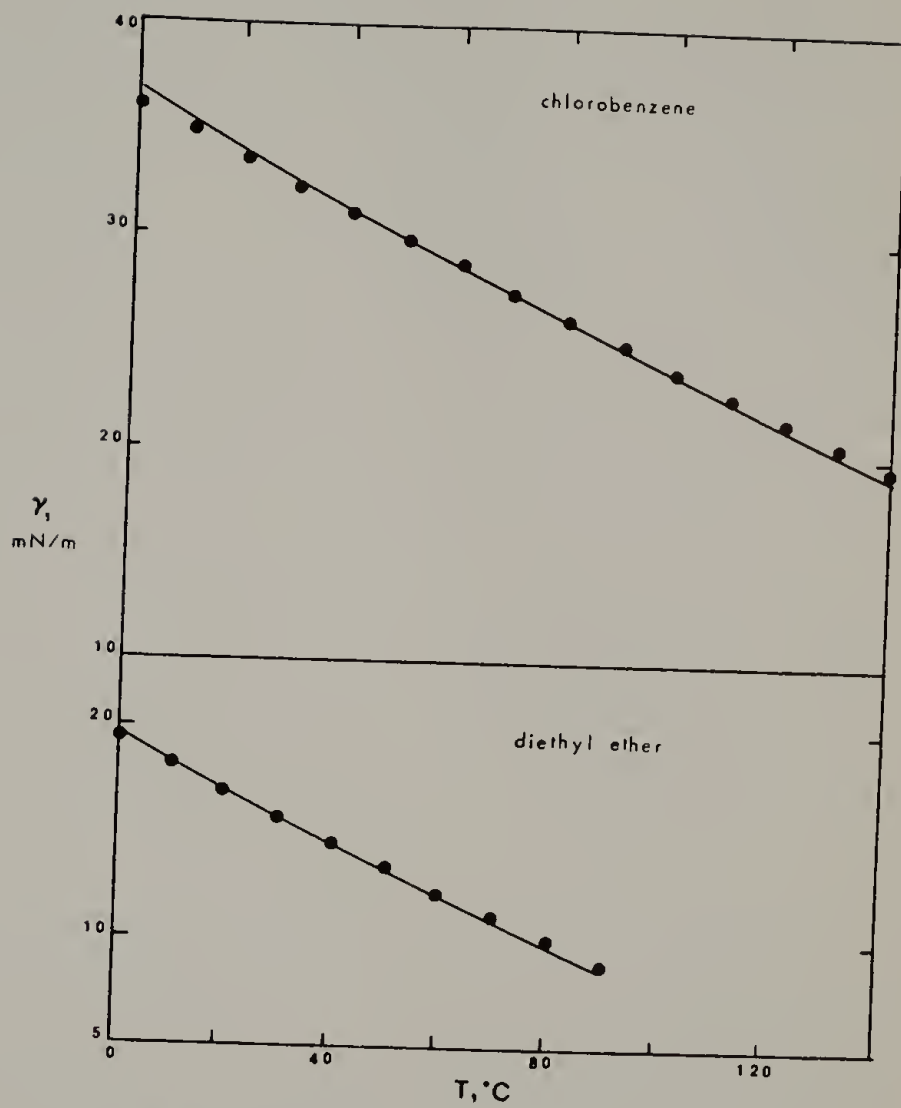


Figure 16. Comparison of experimental and theoretical tensions versus temperature for chlorobenzene and diethyl ether with  $\tilde{\kappa} = .62$ . Data points are from reference 70.



Table 5

ERRORS BETWEEN CALCULATED AND EXPERIMENTAL TENSIONS FOR LOW MOLECULAR WEIGHT LIQUIDS

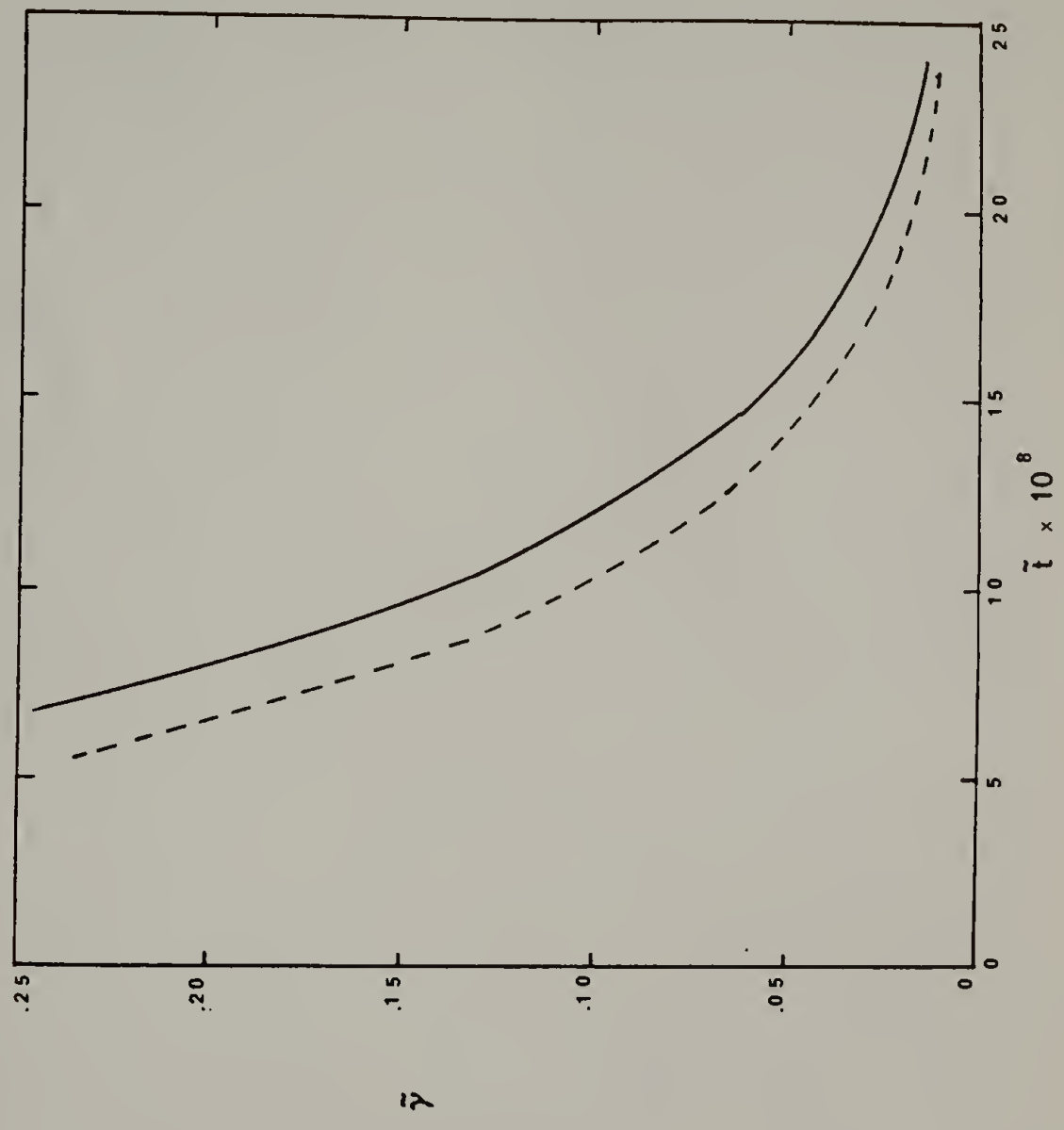
	<u>maximum % error</u>	<u>average % error</u>
methane	-2.9	-2.1
ethane	4.7	4.4
propane	3.8	3.0
n-butane	3.9	2.4
n-pentane	-2.5 (-2.4)	-1.4 (-1.8)
n-hexane	.7 (1.3)	.1 (.2)
n-heptane	-2.2 (1.3)	-1.4 (.1)
n-octane	3.4 (3.8)	1.1 (1.1)
n-nonane	1.7 (2.2)	.5 (1.1)
n-decane	1.9 (2.2)	.9 (1.3)
n-undecane	2.0 (2.4)	.9 (1.6)
n-dodecane	2.1 (2.6)	1.1 (1.8)
n-tridecane	1.7 (2.2)	.7 (1.4)
n-tetradecane	1.3 (1.7)	.6 (1.2)
n-heptadecane	.5 (-1.0)	.2 (-.8)
cyclohexane	-6.4	-4.9
isobutane	1.2	.1
isopentane	-5.6	-3.9
benzene	-4.0	-2.2
toluene	3.3	.05
o-xylene	3.9	2.7
p-xylene	4.5	3.5
m-xylene	4.1	3.2
Cl-benzene	-3.0	-.4
CCl <sub>4</sub>	-4.6	-3.5
diethyl ether	-1.9	-.6

calculated values using  $\tilde{\kappa} = .62$

The quality of the theoretical predictions for polar molecules (such as alcohols) was also examined. For a not-too-polar molecule (aniline), the maximum error in the selected temperature range was around 10% with  $\tilde{\kappa} = .62$ . However, the calculated surface entropy and thus the slope of the tension curve was seriously in error (by about 33%). For alcohols, acids, and water the errors become even more serious. In order to fit the data for such compounds a temperature dependent expression for  $\tilde{\kappa}$  would need to be used; such an expression would be unique to a particular liquid. This result is not surprising, since polar liquids are characterized by strong molecular correlations. A mean field theory is thus by definition outside the range of its validity when applied to such systems.

Since the theory gives good results for tensions of nonpolar and slightly polar systems, an examination of the predictions for such molecules related to the interfacial thickness is instructive. Various operational definitions of the interfacial thickness,  $t$ , can be made. For the present case of low molecular weight liquids, we have used the definition that the thickness is the distance between the two points at which the fluid density value reaches 99% of the density of one of the equilibrium phases. The reducing parameter for the thickness is, of course,  $v^*^{1/3}$ . Fig. 17 shows the relationship between the reduced tension and thickness as well as the effect of a change in  $\tilde{\kappa}$  for n-heptane. The temperature range corresponding to the range of  $\tilde{\gamma}$  for this figure is  $.54 < T/T_c < .95$ . The change observed upon increasing the value of  $\tilde{\kappa}$  is as expected--an interface of the same thickness will

Figure 17. Reduced tension,  $\tilde{\gamma}$ , versus reduced interfacial thickness,  $\tilde{t}$ , for n-heptane at two values of  $\tilde{\kappa}$ . The broken line represents the curve calculated with  $\tilde{\kappa} = .5$ , while the solid line corresponds to  $\tilde{\kappa} = .62$ . The reduced temperature range for which the curves are shown is  $.5 < \tilde{T}/\tilde{T}_c < .95$ .  $\tilde{T}_c$  is the reduced theoretical critical temperature.

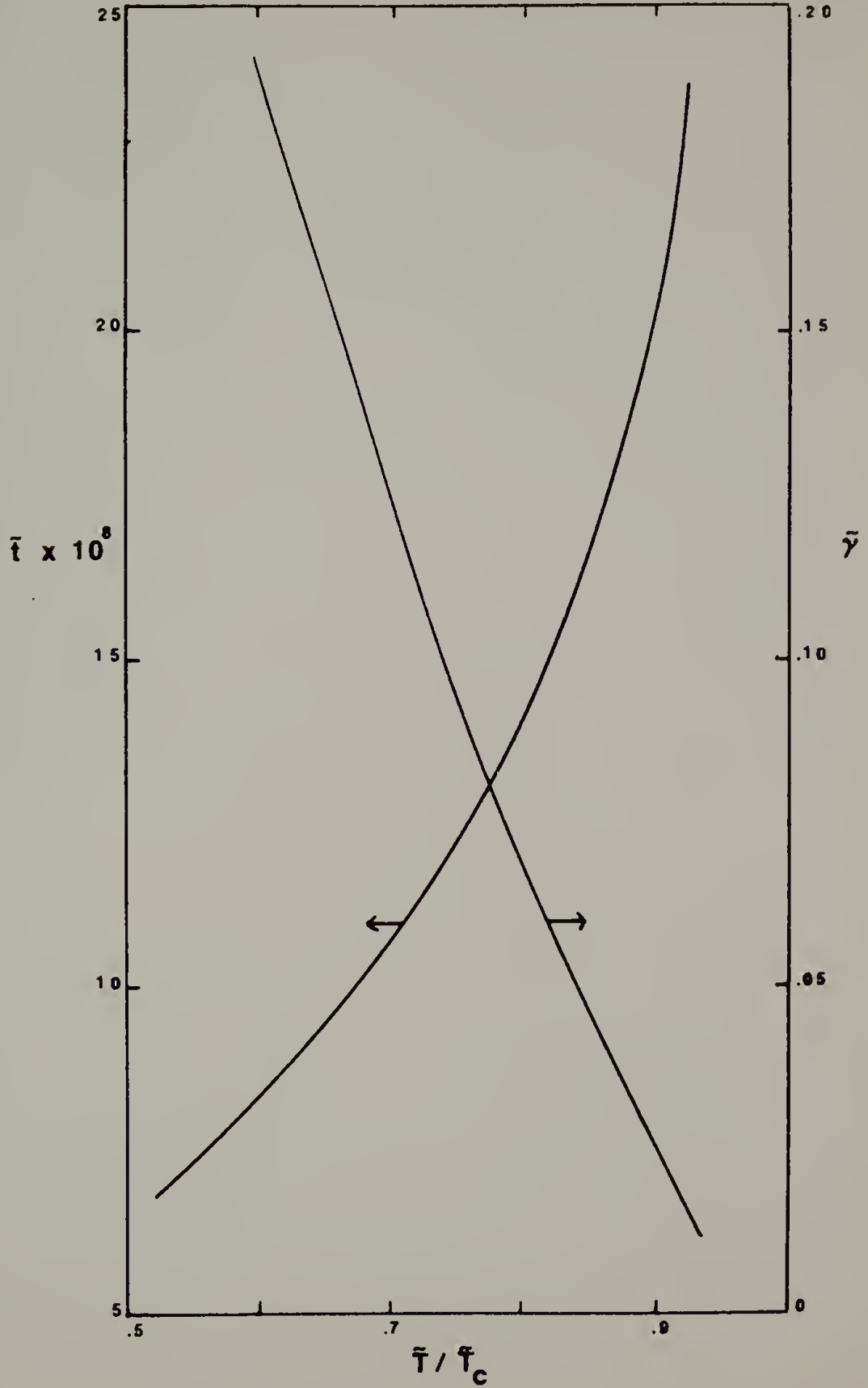


result in a higher tension if  $\tilde{\kappa}$  is larger. The actual thicknesses predicted for n-heptane are reasonable (at 20°C,  $t$  is 1.46 nm at  $\tilde{\kappa}=.5$  and 1.63 nm at  $\tilde{\kappa} = .62$ ). The change in slope of the curves in Fig. 17 also illustrates that as the thickness gets larger, the accompanying decrease in the surface tension gets smaller. This point is shown more clearly in Fig. 18, where  $\tilde{\gamma}$  and  $\tilde{t}$  have been plotted vs.  $\tilde{T}/\tilde{T}_c$  ( $\tilde{T}_c$  is the reduced theoretical critical temperature). Clearly,  $\tilde{\gamma}$  must go to zero while  $\tilde{t}$  becomes infinite at the critical temperature. The exact dependence of  $\tilde{t}$  on  $\tilde{T}/\tilde{T}_c$  is a function of the size parameter  $r$ , just as is the case for the reduced tension. In Fig. 19, the reduced thickness has been plotted vs.  $r$  for a number of molecules at the same value of  $\tilde{T}/\tilde{T}_c = .72$ . The thickness can be seen to decrease with increasing  $r$ . An analagous plot for  $\tilde{\gamma}$  would show an increase with  $r$  as mentioned earlier.

The molecular weight dependence of the interfacial tensions of n-alkanes has considerable practical significance, and has received a good deal of attention.<sup>15,16,71,72</sup> Since experimental measurements of polymer tensions are difficult, extrapolation of n-alkane data was hoped to provide a check on values for linear polyethylene. Two alternate empirical equations have been proposed to describe the molecular weight-tension relationship of homologous series and, as an extension, of polymers. Wu<sup>15</sup> proposed the use of

$$\gamma^{\frac{1}{2}} = \gamma_{\infty}^{\frac{1}{2}} - \frac{K_s}{M_n} \quad (V.20)$$

Figure 18. Reduced interfacial tension,  $\tilde{\gamma}$ , and thickness,  $\tilde{t}$ , as a function of  $\tilde{T}/\tilde{T}_c$  for n-heptane with  $\tilde{\kappa} = .62$ .  $\tilde{T}_c$  is the theoretical reduced critical temperature.



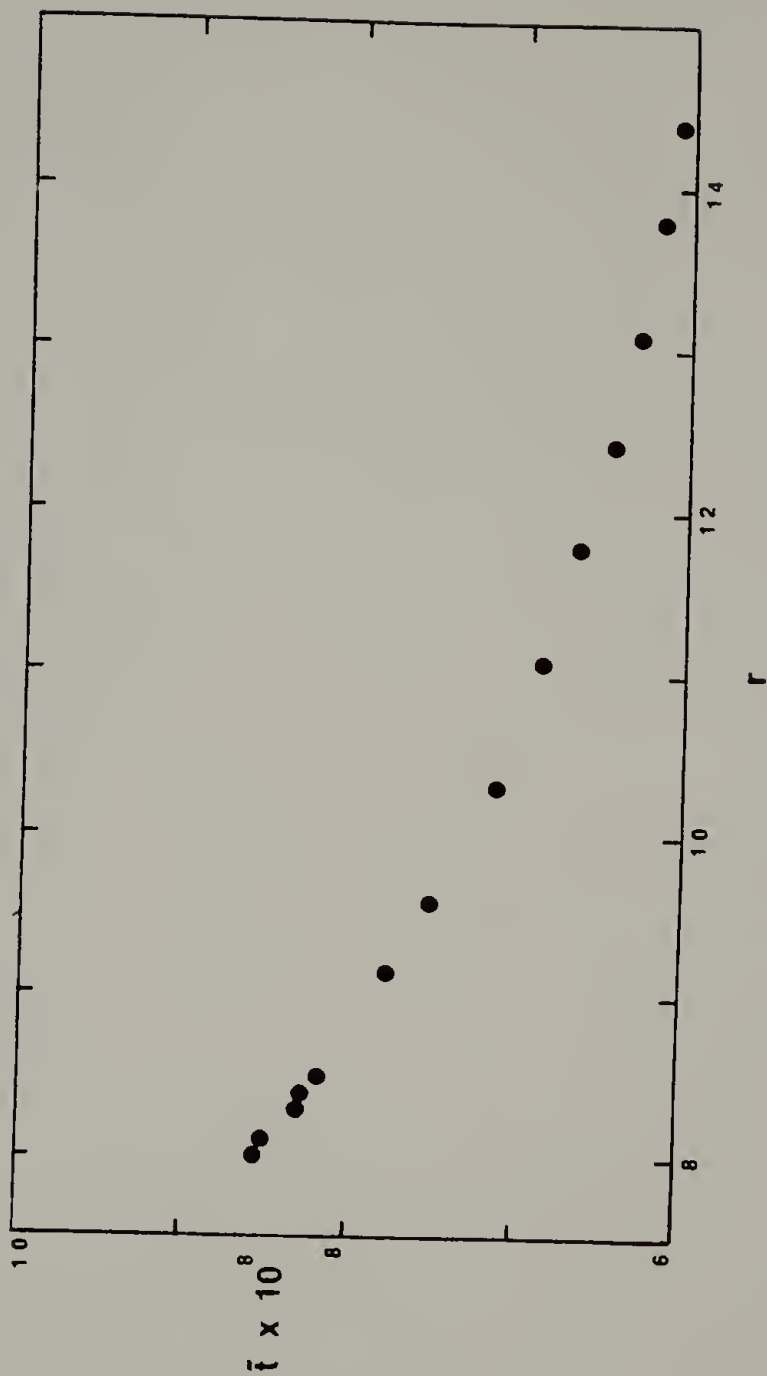


Figure 19. Reduced interfacial thickness,  $\bar{l}$ , versus the molecular size parameter,  $r$ , for several liquids at constant ratio of the reduced temperature to the reduced theoretical critical temperature. Calculated points were obtained at  $\bar{l}/\bar{l}_c = .72$  with  $\kappa = .62$ . Points shown are for n-alkanes from n-pentane to n-tetradecane and for benzene, chlorobenzene, toluene, and o-xylene.



where  $\gamma_\infty$  is the interfacial tension at infinite molecular weight,  $M_n$  is the number average molecular weight and  $K_s$  is a positive constant. LeGrand and Gaines have used<sup>71</sup>

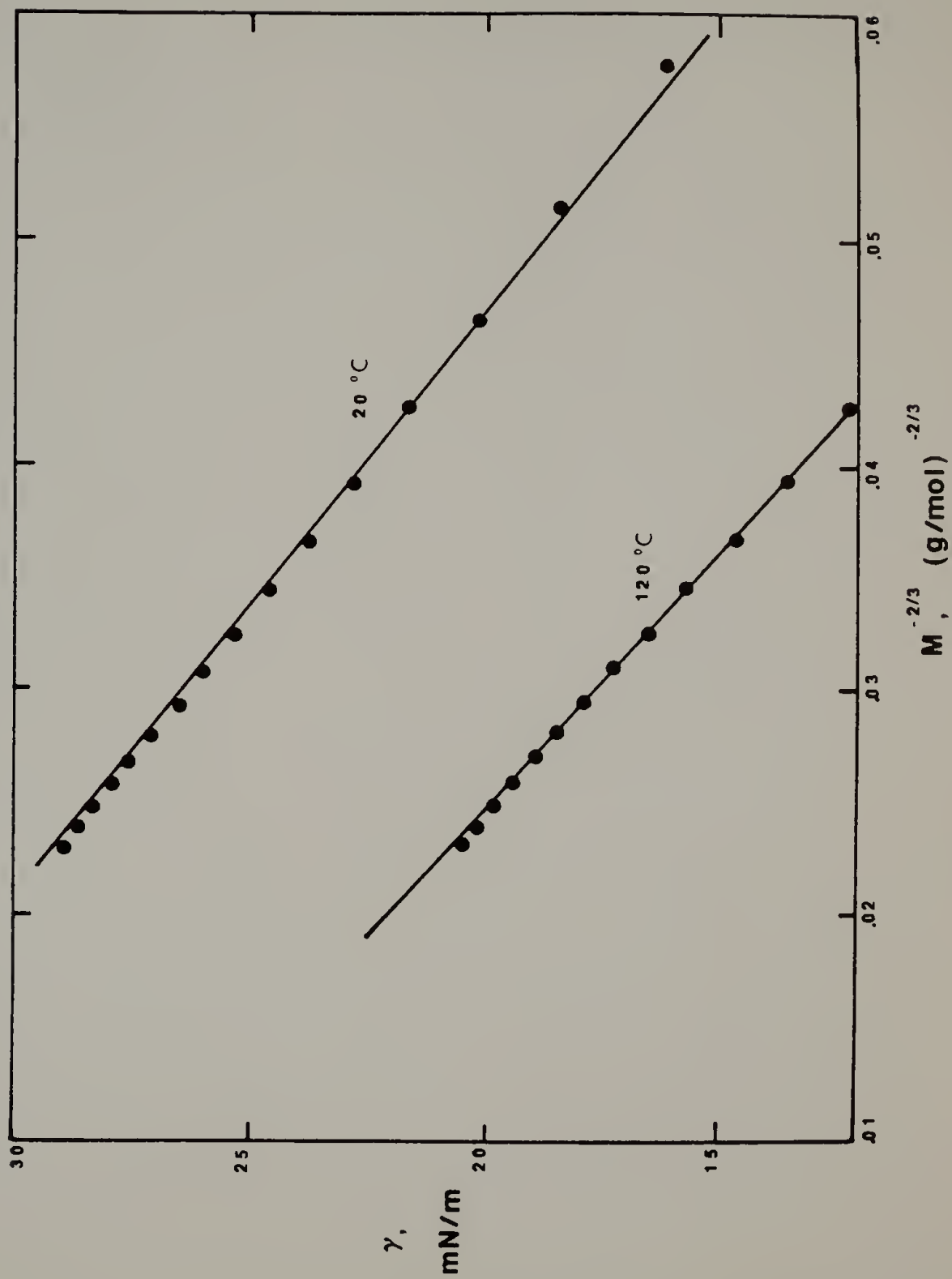
$$\gamma = \gamma_\infty - \frac{K_e}{M_n^{2/3}} \quad (\text{V.21})$$

where  $K_e$  is an empirical constant.

Equations V.20 and V.21 were fitted by linear regression to the theoretical tension values of the n-alkanes from pentane to heptadecane obtained from the present theory. At 20°C the standard deviation between eq. V.20 and our calculated tensions is .12 mN/m, while the fit of eq. V.21 to the calculated tensions yields a deviation of .11 mN/m. Similar deviations are obtained at 120°C. Thus, the two equations are indistinguishable in describing the molecular weight dependence of the interfacial tension values obtained from the present theory. Fig. 20 compares the experimental data for n-alkanes to eq. V.21, where  $\gamma_\infty$  and  $K_e$  have been obtained from the fit of this equation to our calculated values. The agreement is good at both 20 and 120°C.

The inherent molecular weight dependence of the interfacial tension, evident in Fig. 10, is directly related to the density. As  $r$  increases the liquid density increases,  $\partial \tilde{\rho}_l / \partial r)_{\tilde{T}} > 0$ , and the gas density decreases,  $\partial \tilde{\rho}_g / \partial r)_{\tilde{T}} < 0$ . An increase in the bulk density difference results in an increase in  $\Delta a$  which leads to a steeper density gradient. Thus the interfacial tension increases and the thickness decreases. The experimentally observed molecular weight

Figure 20. Molecular weight dependence of the interfacial tension for n-alkanes. Experimental points for n-pentane-n-eicosane were taken from references 70 and 72. The lines were obtained by performing a least-squares fit of Eq. V.21 to the theoretical tension values for n-pentane-n-heptadecane.



dependence is further complicated by the fact that for a homologous series such as the n-alkanes,  $\epsilon^*$  and  $v^*$  also increase with  $r$ . At constant temperature,  $T$ , the value of  $\tilde{T}$  thus decreases, as does the value of  $\gamma^*$ . A plot of  $\tilde{\gamma}$  vs.  $r$  at constant  $\tilde{T}$  would therefore only qualitatively reflect the molecular weight dependence of a series such as the n-alkanes. Fig. 21 shows the effect of the increasing value of  $\gamma^*$  for the n-alkane series from pentane to tetradecane. The values of  $\tilde{\gamma}$  and  $\gamma$  have been normalized to the n-octane values, and were calculated at a constant value of  $\tilde{T} = .58$ . Fig. 22 compares the values of  $\tilde{\gamma}$  (again normalized by the n-octane values) at constant  $\tilde{T} = .58$  to those obtained at  $T = 20^\circ\text{C}$ . For n-octane,  $20^\circ\text{C}$  corresponds to  $\tilde{T} = .58$ . Clearly, the increase in  $\gamma^*$  and the decrease in  $\tilde{T}$  both work to increase the experimentally observed molecular weight dependence, with the increase in  $\epsilon^*$  contributing the larger portion of this effect. This observation again emphasizes the importance of intermolecular interactions to interfacial phenomena.

As Fig. 10 illustrates, the present theory predicts that as  $r$  increases,  $\tilde{\gamma}$  rapidly approaches a limiting value,  $\tilde{\gamma}_\infty$ , which implies a corresponding states principle for polymer melts. In Fig. 23,  $\tilde{\gamma}_\infty$  is plotted as a function of  $\tilde{T}$  and compared with experimental data for six polymers. A value of  $\tilde{\kappa} = .55$  yields a good fit to the data. All of the data were taken between 413 K and 453 K;<sup>72,73</sup> absolute values of  $\gamma$  range from a high of 32.1 mN/m for polystyrene to a low of 12.1 mN/m for poly(dimethyl siloxane). Interfacial tension

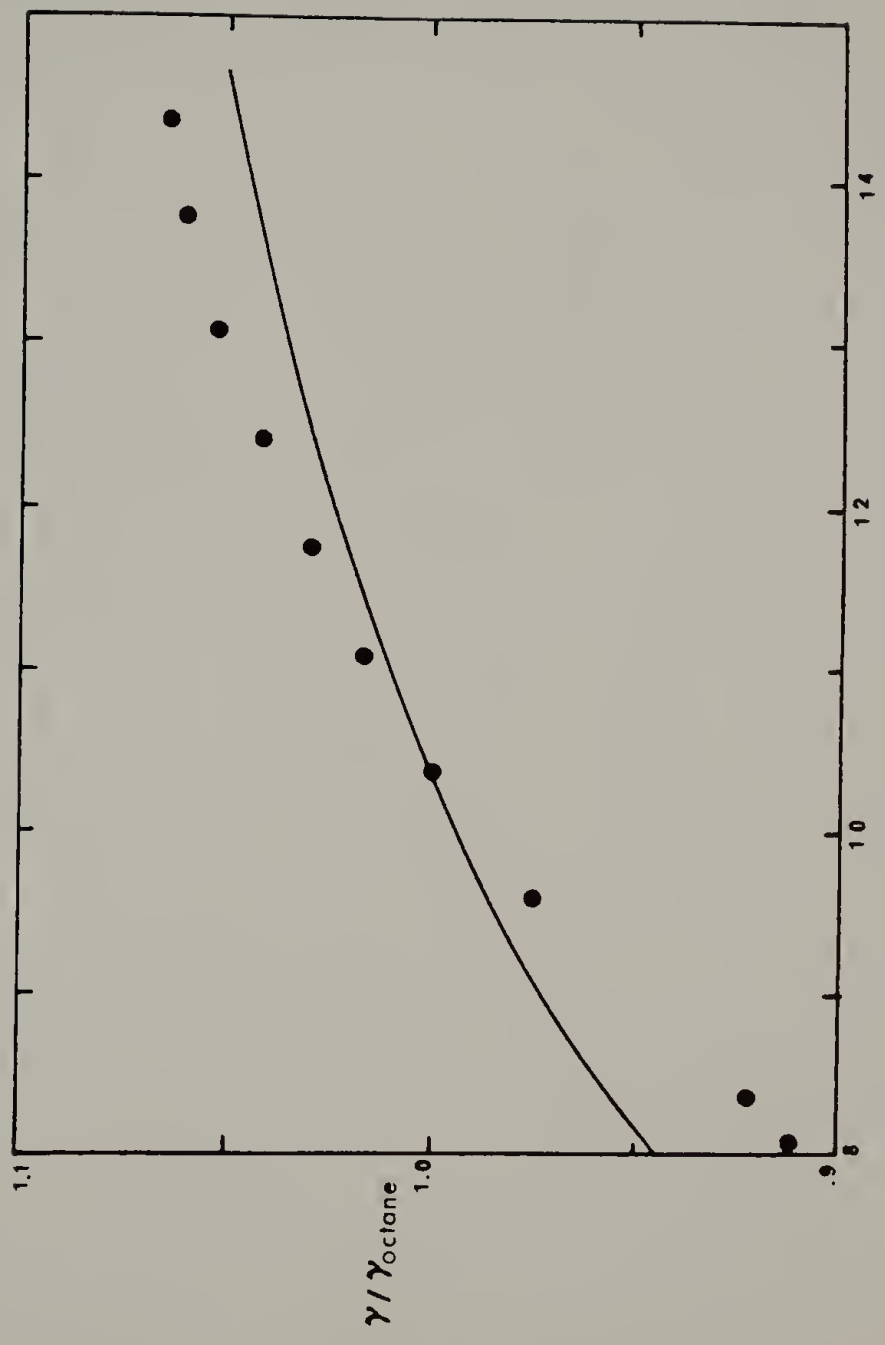


Figure 21. Effect of  $\gamma^*$  on the calculated tension for n-alkanes. The line represents the calculated reduced tensions normalized by the value for n-octane. The points show the n-octane normalized actual tensions for the n-alkanes from n-pentane to n-tetradecane. Calculations were performed at a constant reduced temperature of  $\tilde{T} = .58$ .  $r$  is the molecular size parameter.

Figure 22. Effect of  $\epsilon^*$  on the calculated tension for n-alkanes. The calculated reduced tensions of n-alkanes from n-pentane to n-tetradecane (normalized by the n-octane value) at  $\tilde{T} = .58$  are given by the solid line. The points represent reduced tensions, also normalized, at a constant temperature  $T = 20^\circ\text{C}$ .

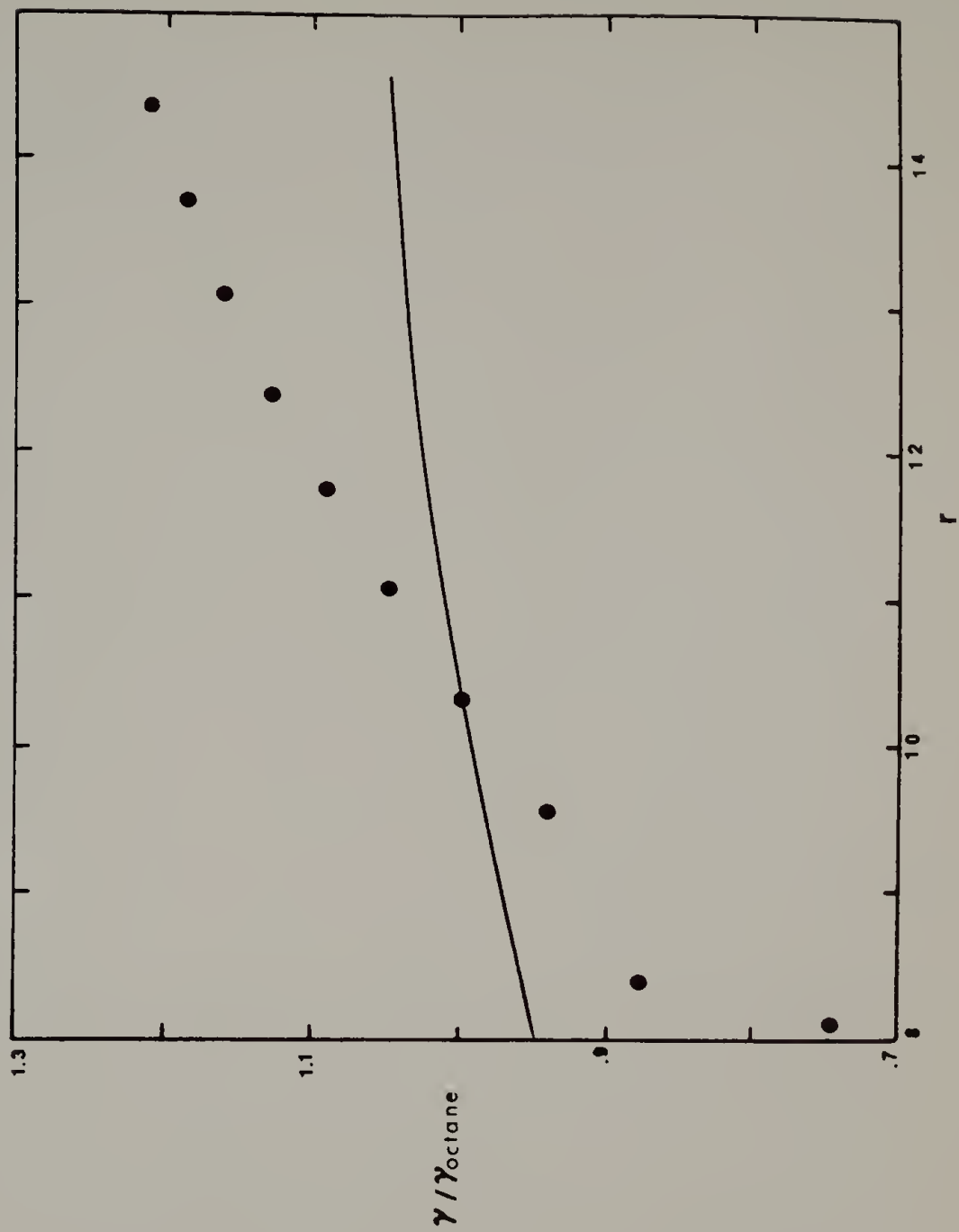
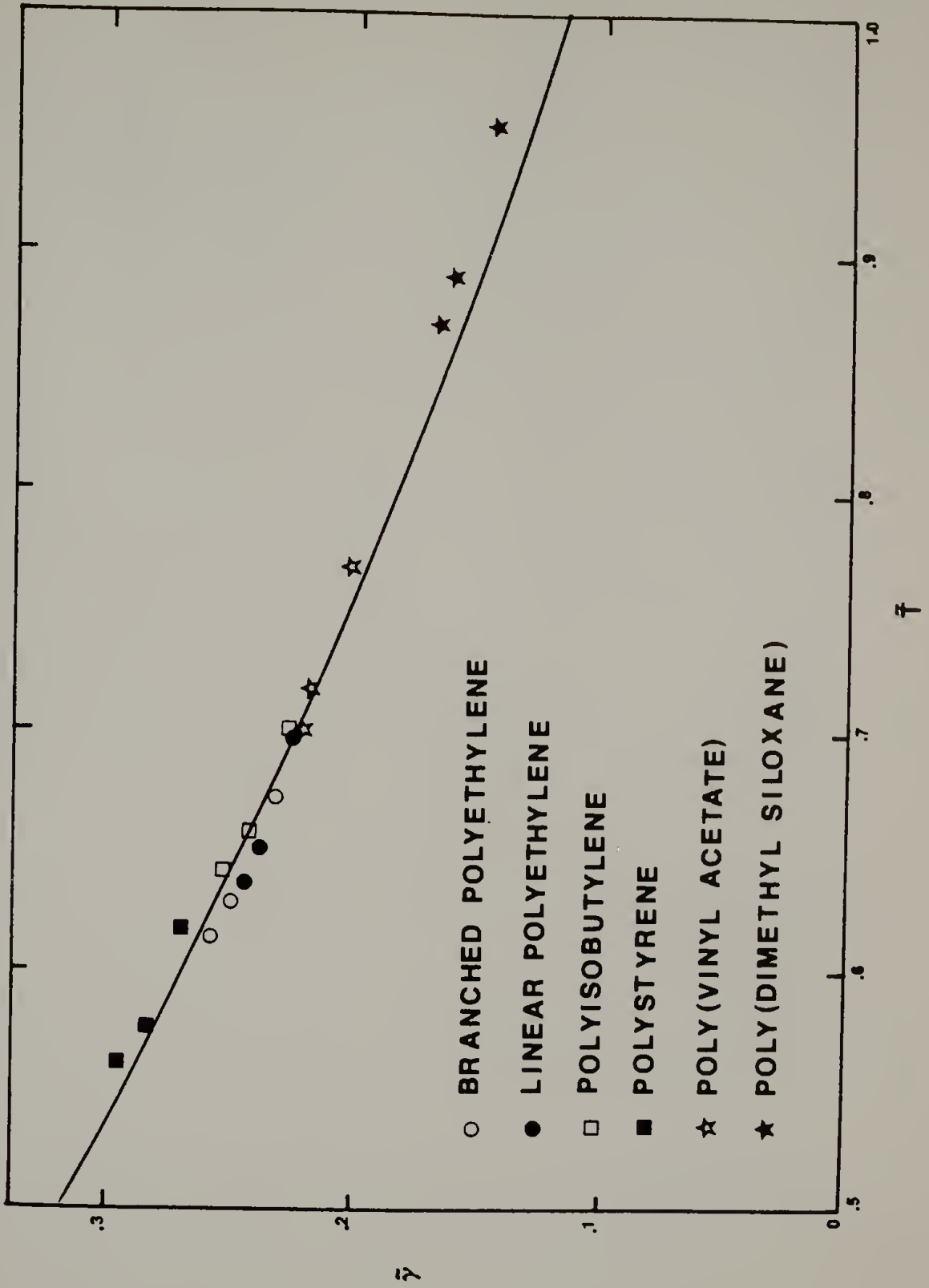


Figure 23. Reduced interfacial tension versus reduced temperature for polymers. The theoretical line was calculated using  $r = \infty$  and  $\tilde{\kappa} = .55$  and experimental values were taken from references 73 and 74.





measurements of polymer melts are difficult, due to the high viscosities of polymers and their tendency to degrade at elevated temperatures. Experimental uncertainties lie in the range of 2-5%. The maximum error between experiment and theory in Fig. 23 (using  $\tilde{\kappa} = .55$ ) is about 10%.

Figs. 24 and 25 compare the calculated tension vs. temperature curves to the experimental data for branched polyethylene, poly(vinyl acetate), polystyrene, and linear polyethylene. For polymers, the data is usually given in the literature in the form of the linear equation obtained from a least squares fit. Points in Figs. 24 and 25 were calculated from such equations, and thus do not necessarily represent the exact measured value.

As was the case for low molecular weight systems, the polar polymers which were examined (poly(methyl methacrylate), poly(n-butyl methacrylate), poly(ethylene oxide)) did not correlate well with the theory. Poly(vinyl acetate), which is included in Figs. 24 and 25, forms an exception to this observation. This polymer also exhibits rheological properties which are more like those of a nonpolar than polar polymer,<sup>74</sup> although the origin of this anomaly is not understood.

Experimentally, the surface entropy,  $-\mathrm{d}\gamma/\mathrm{d}T$ , of a polymer melt is smaller than for a similar low molecular weight liquid. This effect is qualitatively apparent in Fig. 10. The reason behind this phenomenon can again be understood in terms of density. A polymeric liquid has a smaller thermal expansion coefficient,  $\alpha$ , than a similar low molecular weight liquid; that is,  $\partial\alpha/\partial r)_{\bar{T}} < 0$ . Thus the

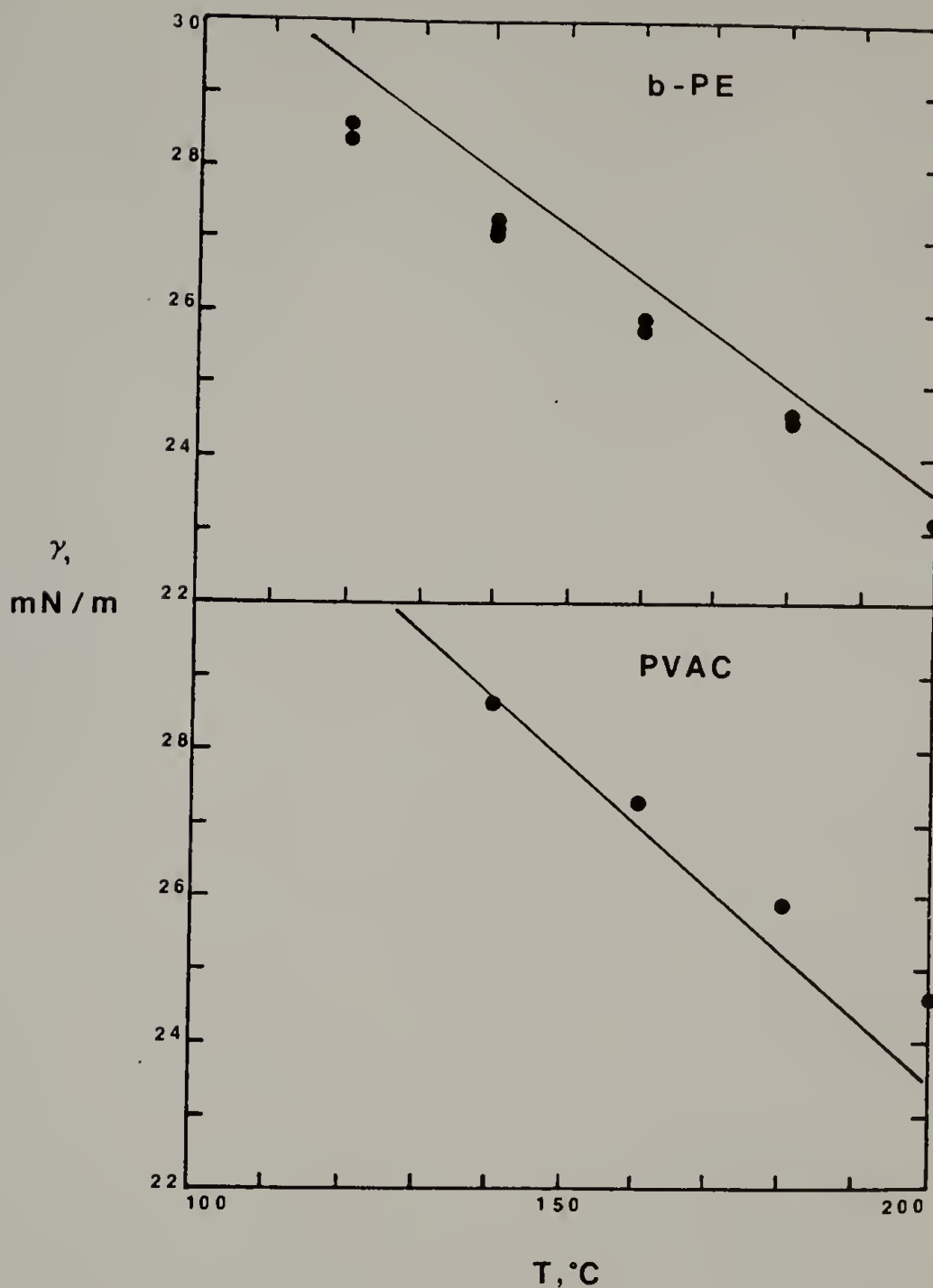


Figure 24. Interfacial tension versus temperature for branched polyethylene and poly(vinyl acetate). Theoretical lines were calculated using  $\tilde{\kappa} = .55$  and the experimental values were taken from correlations given in reference 74.

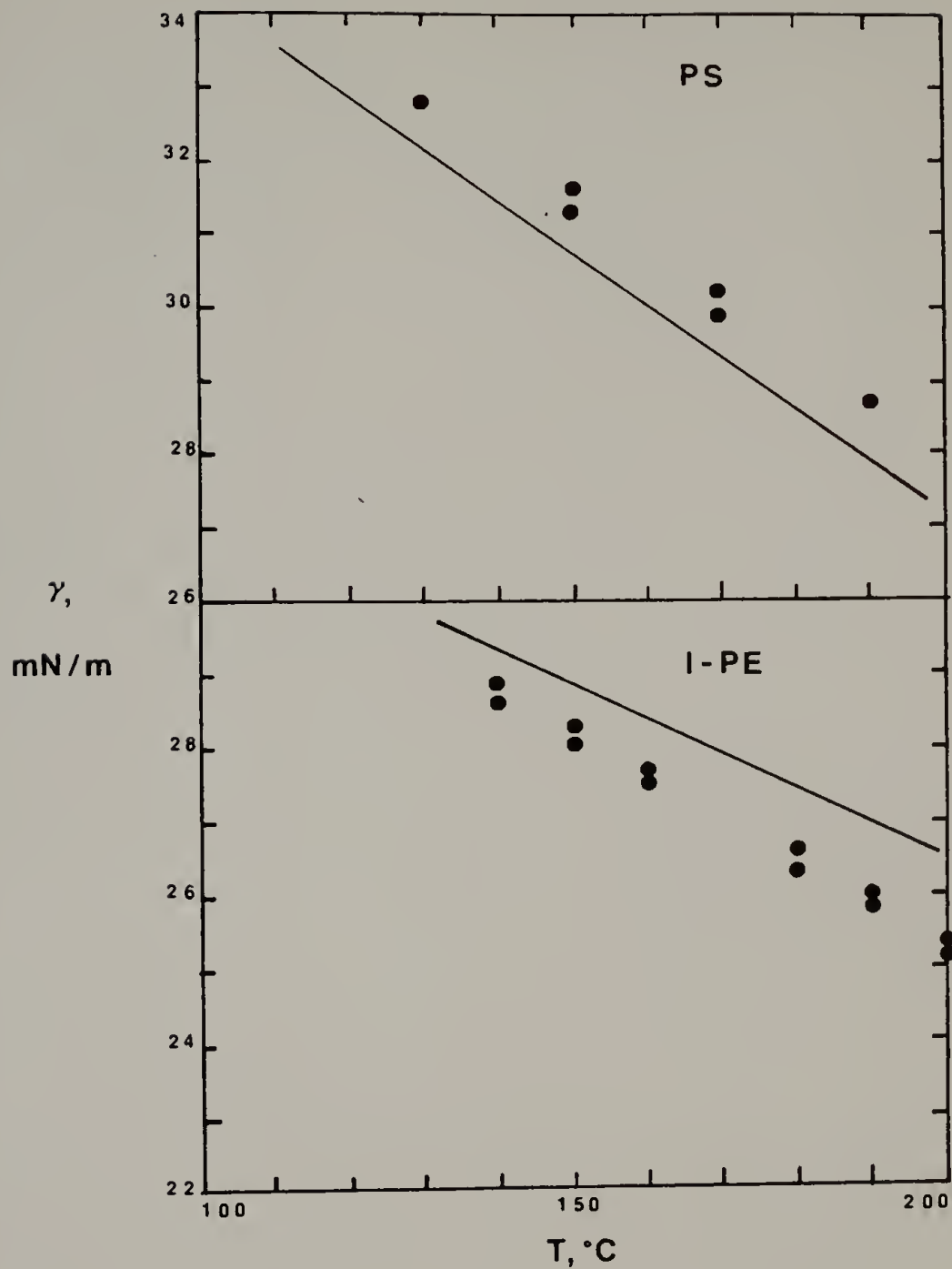


Figure 25. Interfacial tension versus temperature for polystyrene and linear polyethylene. Theoretical lines were calculated with  $\tilde{\kappa} = .55$  and experimental values were taken from correlations given in reference 74.

interfacial density gradient and tension change more slowly with temperature for a polymer liquid. There is another reason why the surface entropy should be smaller for a polymer liquid than for a low molecular weight liquid. The presence of an interface restricts the number of conformations available to a polymer molecule which should lower the surface entropy.<sup>75</sup> Since we have explicitly assumed the entropy in the inhomogeneous region to be independent of the density gradient, we have neglected this effect. As a result, the theory should overestimate  $-d\gamma/dT$  for polymers. Tables 6 and 7 show the experimental and calculated values of  $-d\gamma/dT$  for n-alkanes and polymers, respectively. Notice the greater error for polymers which points to the significance of the conformational entropy effect. Since  $\tilde{\kappa}$  scales both the tension and the surface entropy as pointed out previously, the lower value of  $\tilde{\kappa}$  required to fit the polymer data in the experimentally accessible range might be explained as arising from the neglect of the conformational entropy. Use of  $\tilde{\kappa} = .62$  to calculate polymer surface entropies results in an increase in the % difference between the calculated and experimental values of about 10%.

In order to evaluate the usefulness of the present theory for polymers further, comparison with previous methods of tension-temperature predictions is useful. Three methods, all more or less empirical, have been widely used. The oldest of these methods is based on the parachor concept first proposed for small molecules by Sugden.<sup>76</sup> The parachor concept arose from the fact that the exponent,  $p$ , in McLeod's<sup>77</sup>

Table 6  
SURFACE ENTROPY OF n-ALKANES

no. of C	calc. s.entropy mN/m-K	exp. s. entropy mN/m-K	% difference
5	.1140	.110	3.6
6	.1084	.103	5.2
7	.1070	.104	2.9
8	.1045	.096	8.9
9	.1020	.094	8.5
10	.0997	.0919	8.5
11	.0978	.0894	9.4
12	.0962	.0878	9.6
13	.0947	.0878	8.7
14	.0930	.0863	7.8
17	.0886	.0838	5.7

using  $\tilde{\kappa} = .61$

Table 7

## SURFACE ENTROPY OF POLYMERS

compound	calc. s. entropy	exp. s. entropy	% difference
	mN/m-K	mN/m-K	
-PE	0.0820	0.057	44%
b-PE	0.0729	0.067	9%
PIB	0.0725	0.066	9%
PS	0.0722	0.072	0%
PVA	0.0920	0.066	39%
PMMA	0.0914	0.076	20%
PnBMA	0.0826	0.059	40%
PEO	0.0975	0.076	28%
PDMS	0.0609	0.048	27%

$$\tilde{\kappa} = .55$$

equation

$$\gamma = \gamma_0 (\rho_l - \rho_g)^P \quad (\text{V.21})$$

is found to be close to 4 for many unassociated low molecular weight liquids.<sup>77,78</sup>  $\gamma_0$  is a constant for a given liquid. Sugden used this equation to obtain

$$P = \gamma^{\frac{1}{4}} \frac{M}{\rho_l - \rho_g} \quad (\text{V.22})$$

where  $M$  is the molecular weight, and  $P$  is a constant for the liquid which Sugden called the parachor. When this equation is applied to polymers,  $P$  and  $M$  refer to the repeat unit. An extensive tabulation of atomic parachors has been compiled by Quayle<sup>79</sup> and can be used to calculate  $P$ . The accuracy of this method is limited by the fact that the McLeod's exponent for polymers often differs significantly from 4. In this connection, Wu<sup>80</sup> has suggested that smaller values of  $p$  reflect the conformational restrictions on the polymer imposed by the interface. Table 8 compares the % error in the surface entropy predicted by the present theory to the McLeod's exponents for some polymers. The correlation between the two quantities is striking, although the result for polystyrene is puzzling.

Another method for predicting polymer interfacial tensions is based on the empirical relation between tension and solubility parameters,  $\delta_s$ , observed by Hildebrand and Scott<sup>83</sup> for low molecular weight liquids. This relationship is



Table 8  
COMPARISON OF SURFACE ENTROPY ERROR TO MacLEOD'S  
EXPONENT

<u>polymer</u>	<u>% error in surface entropy</u>	<u>MacLeod's exponent</u>	<u>reference</u>
l-PE	44	3.2	80
PVA	39	3.4	80
PDMS	27	3.6	81
PIB	9	4.1	80
PS	0	4.5	82

$$\gamma = 0.039 \delta^{2.30} V^{1/3}, \quad (\text{V.23})$$

where  $V$  is the molar volume of the molecule which is by assumption spherical. The difficulty in applying this relation to polymers arises in the choice of unit to which  $V$  refers. One approach, suggested by Siow and Patterson,<sup>16</sup> is to substitute  $RT_p^*/P_p^*$  for  $V$ , where  $T_p^*$  and  $P_p^*$  are the temperature and pressure reduction parameters of Prigogine's corresponding states theory.<sup>18</sup> This leads to

$$\gamma = (0.095 P_p^{*2/3} T_p^{*1/3}) / \tilde{V}^{2.1}, \quad (\text{V.24})$$

where  $\tilde{V}$  is the reduced volume.

Prigogine's corresponding states theory is also the basis of a third predictive method, due to Patterson and Rastogi.<sup>17</sup> These authors found the following empirical relation:

$$\gamma = k^{1/3} P_p^{*2/3} T_p^{*1/3} \tilde{\gamma} \quad (\text{V.25})$$

where  $k$  is the Boltzmann constant. The calculation makes use of the Flory equation of state<sup>84</sup> and the isobaric thermal expansion coefficient,  $\alpha$ , to calculate  $\tilde{V}$ :

$$\alpha T = (1 - \tilde{V}^{-1/3}) \left( \frac{4}{3} \tilde{V}^{-1/3} - 1 \right). \quad (\text{V.26})$$

The reduced tension can then be obtained from

$$\gamma \tilde{V}^{5/3} = 0.29 - (1 - \tilde{V}^{-1/3}) \ln \left( \frac{\tilde{V}^{1/3} - 0.5}{\tilde{V}^{1/3} - 1} \right). \quad (\text{V.27})$$

$T_p^*$  and  $P_p^*$  result from

$$T_p^* = T\tilde{V}^{-1} (1-\tilde{V}^{-1/3}) \quad (\text{V.28})$$

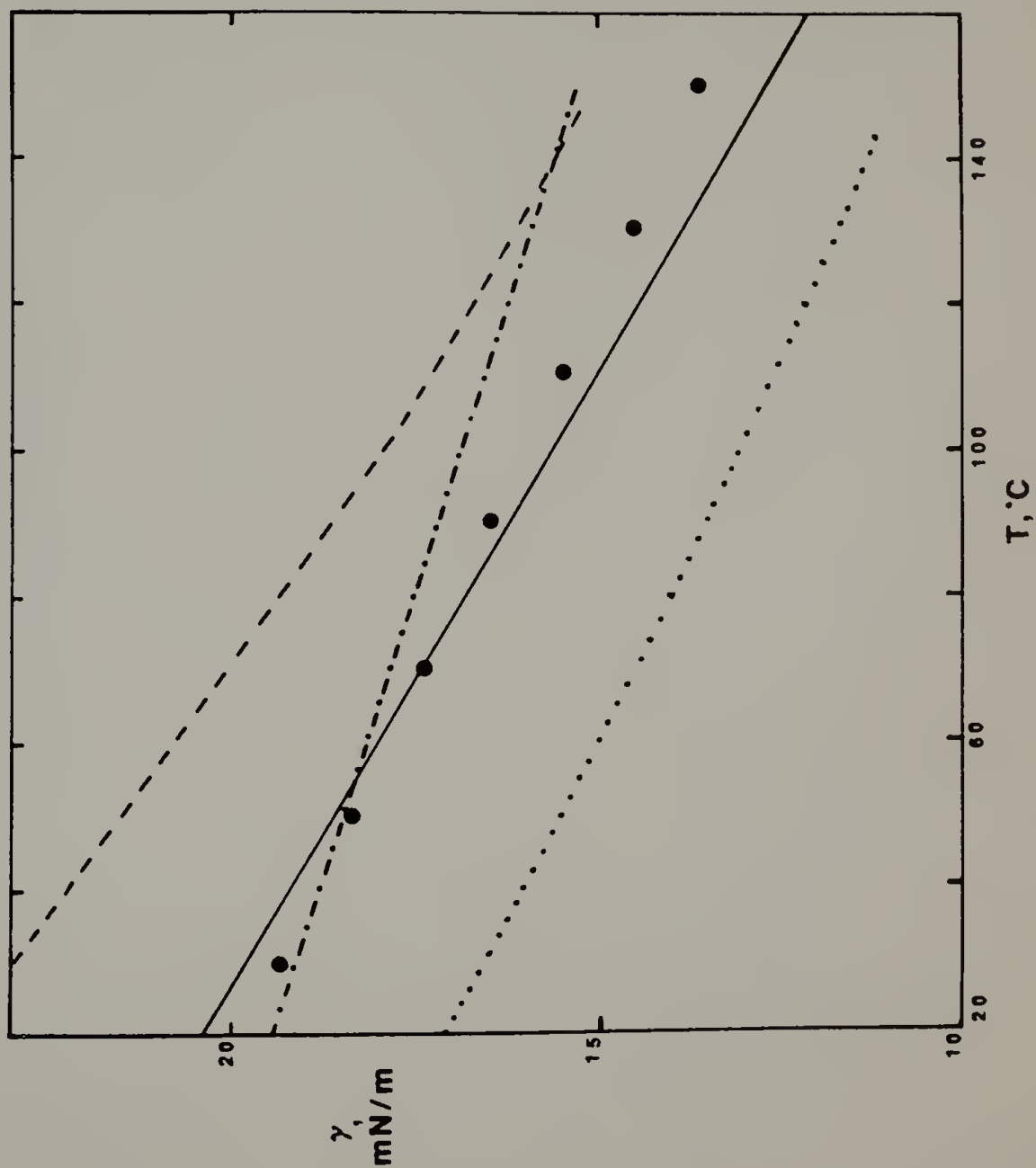
$$P_p^* = (\alpha/\beta) T\tilde{V}^2 \quad (\text{V.29})$$

where  $\beta$  is the isothermal compressibility.

Figs. 26-29 show a comparison of the results of eq. V.22, V.24, and V.25 to the experimental data and the theoretical predictions of the present theory for four different polymers. The LF-gradient theory can be seen to be generally superior to all three of the empirical correlations.

In summary, we have found that the LF-gradient theory yields a unified description of the interfacial tension of nonpolar and slightly polar pure liquids of arbitrary molecular weight. Although the theory is not applicable near the critical point, good results are obtained outside this region. Without any adjustable parameters, calculated tensions are usually 10-15% lower than experimental ones. By setting  $\tilde{\kappa}$  equal to .62 for low molecular weight liquids and .55 for polymers, much better agreement is obtained. In addition, the theory correctly predicts the molecular weight dependence of the tension for n-alkanes.

Figure 26. Comparison of the theory to empirical predictions for poly(dimethyl siloxane). The solid line represents the present theory with  $\tilde{\kappa} = .55$ , the dotted line corresponds to the parachor, the dashed line to the corresponding states theory, and the dot-dash line to solubility parameter predictions. Data for the empirical predictions was taken from reference 16, and experimental values are from reference 74.



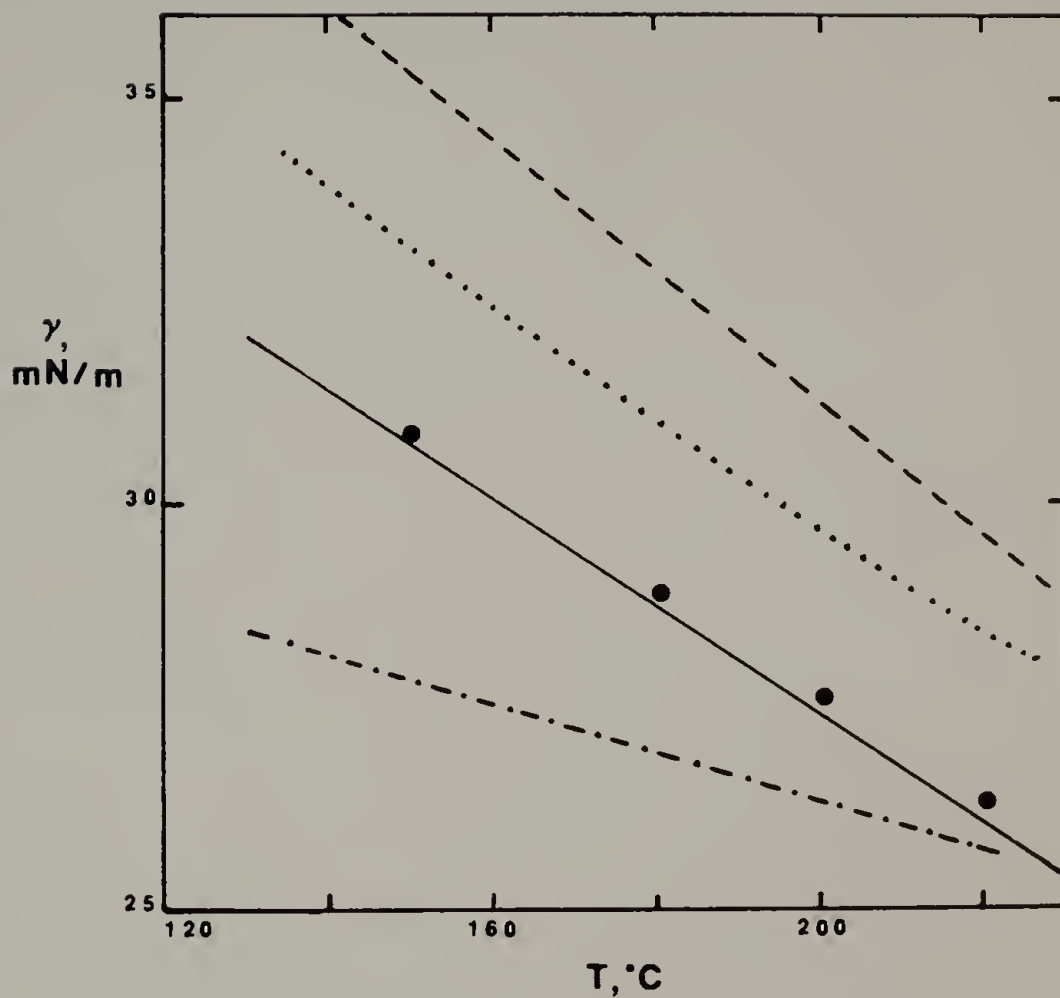


Figure 27. Comparison of the theory to empirical predictions for polystyrene. Lines and experimental points have the same significance and were taken from the same sources as for Fig. 26.

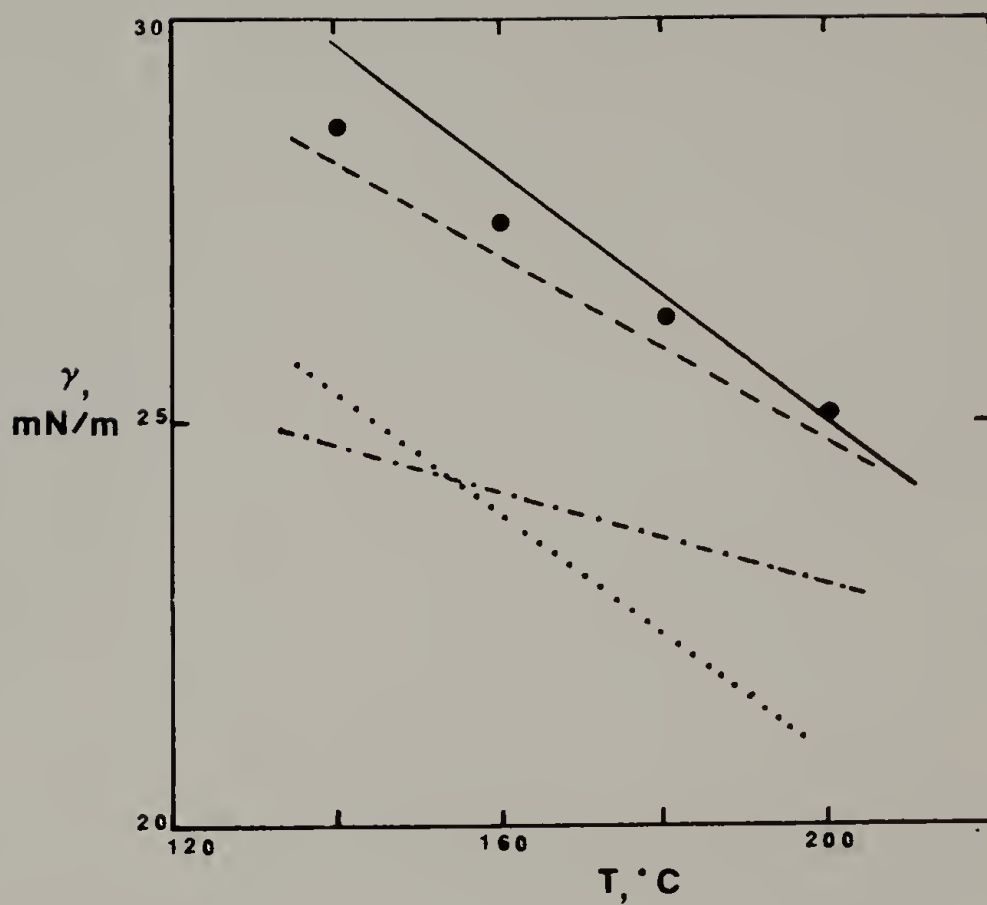


Figure 28. Comparison of the theory to empirical predictions for linear polyethylene. Lines and experimental points have the same significance and were taken from the same sources as for Fig. 26.

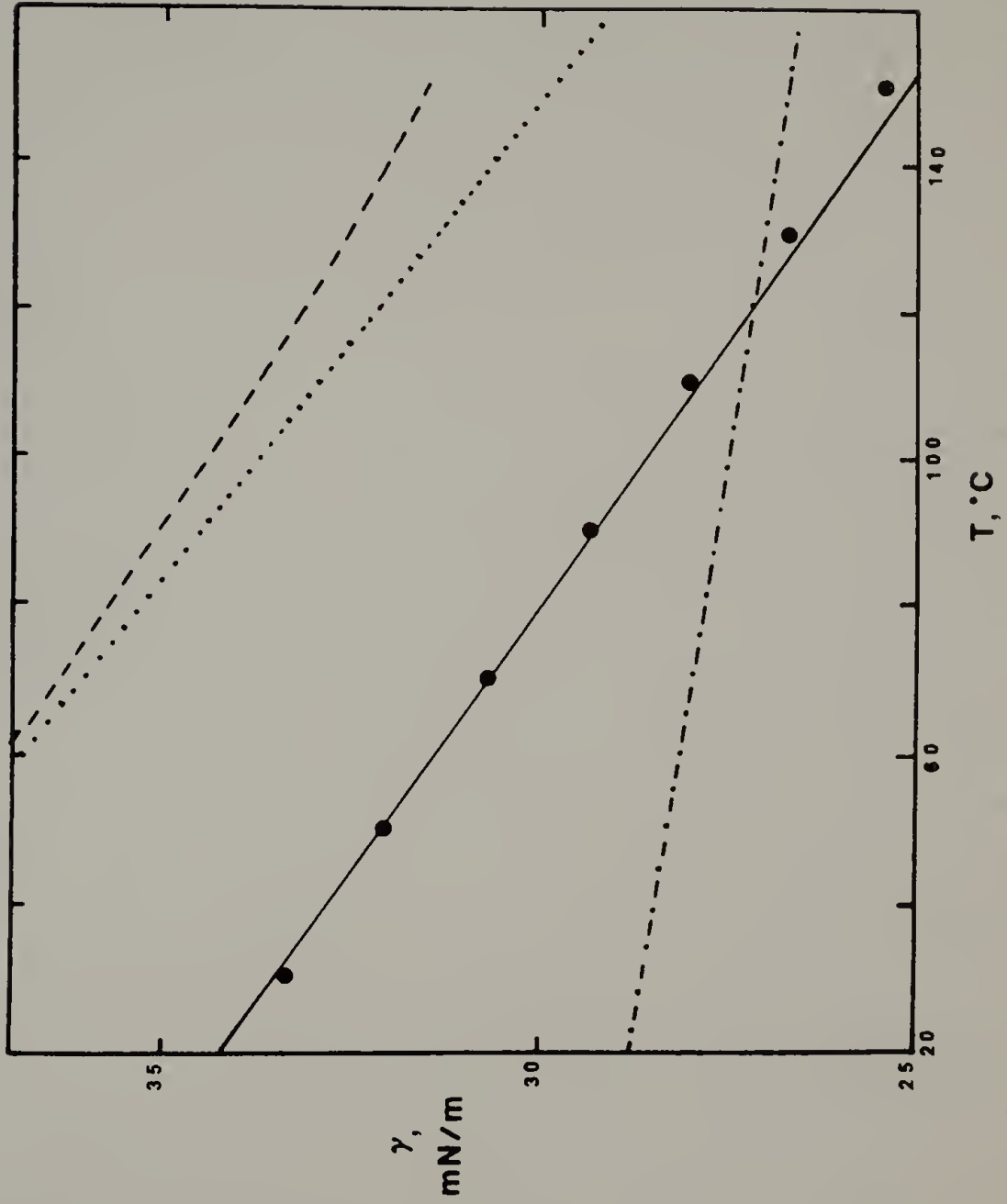


Figure 29. Comparison of the theory to empirical predictions for polyisobutylene. Lines and experimental points have the same significance and were taken from the same sources as for Fig. 26.



CHAPTER VI  
TWO-COMPONENT SYSTEMS

A. Theory

For a binary mixture, the governing equations for the interface may be written:

$$\gamma = \int_{-\infty}^{\infty} \left\{ \Delta a + \frac{1}{2} \kappa_{11} \rho_1'^2 + \kappa_{12} \rho_1' \rho_2' + \frac{1}{2} \kappa_{22} \rho_2'^2 \right\} dx \quad (\text{VI.1})$$

subject to

$$\frac{\partial \Delta a}{\partial \rho_1} - \kappa_{11} \rho_1'' - \kappa_{12} \rho_2'' = 0 \quad (\text{VI.2})$$

$$\frac{\partial \Delta a}{\partial \rho_2} - \kappa_{12} \rho_1'' - \kappa_{22} \rho_2'' = 0$$

where the following notation has been introduced

$$\kappa_{ij} \equiv \kappa_2^{ij} \quad (\text{VI.3})$$

$$\rho_i' \equiv d\rho_i/dx ; \quad \rho_i'' \equiv d^2\rho_i/dx^2 \quad (\text{VI.4})$$

We have again used

$$u_{ij}(s) = \begin{cases} \infty & s < \sigma_{ij} \\ -\epsilon_0^{ij} (\sigma_{ij}/s)^m & s > \sigma_{ij} \end{cases}$$

so that (from eq. II.13):

$$\kappa_{ij} = \frac{1}{3} \epsilon_{ij}^* \sigma_{ij}^5 \frac{(m-3)}{(m-5)} \quad (\text{VI.6})$$

Note that  $\kappa_{11}$  and  $\kappa_{22}$  are exactly equal to the pure component  $\kappa$ 's of components one and two, respectively, and can thus be expressed as

$$\kappa_{11} = 2\epsilon_{11}^* v_1^{*5/3} \tilde{\kappa}_1 ; \quad \tilde{\kappa}_1 = \frac{1}{6}(m-3)/(m-5) . \quad (\text{VI.7})$$

The cross-term,  $\kappa_{12}$ , can be evaluated using the combining rules

$$\kappa_{12} = 2\zeta(\epsilon_{11}^* \epsilon_{22}^*)^{1/2} [\frac{1}{2}(v_1^* + v_2^*)(\delta+1)]^{5/3} \tilde{\kappa}_{12} \quad (\text{VI.8})$$

where  $\tilde{\kappa}_{12}$  is assumed to obey the geometric mean:

$$\tilde{\kappa}_{12} = (\tilde{\kappa}_1 \tilde{\kappa}_2)^{1/2} . \quad (\text{VI.9})$$

Alternately,  $\kappa_{12}$  can be treated as an adjustable parameter. A useful simplification in the Euler equations can be achieved when  $\kappa_{12}$  is assumed to be given by

$$\kappa_{12} = (\kappa_{11} \kappa_{22})^{1/2} . \quad (\text{VI.10})$$

Eq. VI.2 then reduces to the algebraic form

$$\kappa_{22}^{1/2} \frac{\partial \Delta a}{\partial \rho_1} - \kappa_{11}^{1/2} \frac{\partial \Delta a}{\partial \rho_2} = 0 \quad (\text{VI.11})$$

Both methods of evaluating  $\kappa_{12}$  have been employed, with special emphasis on the latter, due to the considerable simplification afforded by eq. VI.11. For convenience in the discussion which follows, we define a parameter

$$c \equiv \kappa_{12} / (\kappa_{11} \kappa_{22})^{1/2} \quad (\text{VI.12})$$

which expresses the deviation of  $\kappa_{12}$  from the geometric mean approximation.

$c = 1$  represents the upper limit of permissible values for  $\kappa_{12}$ . This can be seen by examining the form of eq. II.29 for a binary mixture

$$\Delta a = \frac{1}{2}\kappa_{11}\rho_1'^2 + \kappa_{12}\rho_1'\rho_2' + \frac{1}{2}\kappa_{22}\rho_2'^2 \quad (\text{VI.13})$$

which leads to

$$\gamma = 2 \int_{-\infty}^{\infty} \Delta a \, dx \quad (\text{VI.14})$$

Clearly, if  $\gamma$  is to be positive,  $\Delta a$  must be positive, so that the quadratic form on the right hand side of eq. VI.12 must be positive definite. Since the  $x$ -derivatives of  $\rho_1$  and  $\rho_2$  can be either positive or negative,  $\kappa_{12} \leq (\kappa_{11}\kappa_{22})^{\frac{1}{2}}$  or equivalently  $c \leq 1$  is a necessary condition if the quadratic is to be positive definite.<sup>86</sup>

The numerical evaluation of the interfacial tension can be more easily handled by transforming the equations from  $x$ -space to  $\rho$ -space.<sup>12</sup> Such a transformation changes the limits of the integral in eq. VI.1 from infinite to finite. Eq. VI.13 can be rewritten as

$$\rho_1' = \pm \left[ \frac{2\Delta a}{\kappa_{11} + 2\kappa_{12}d\rho_2/d\rho_1 + \kappa_{22}(d\rho_2/d\rho_1)^2} \right]^{\frac{1}{2}} \quad (\text{VI.15})$$

Using this result to effect a change of variables in eq. VI.14 yields

$$\gamma = \sqrt{2} \int_{\rho_1^I}^{\rho_1^{II}} \left[ \kappa_{11} + 2\kappa_{12} \frac{d\rho_2}{d\rho_1} + \kappa_{22} \left( \frac{d\rho_2}{d\rho_1} \right)^2 \right]^{\frac{1}{2}} \Delta a^{\frac{1}{2}} d\rho_1 \quad (\text{VI.16})$$

where I and II refer to the two equilibrium phases. Eq. VI.15 can also be formally integrated to yield the interfacial tension profile

$$x - x_0 = \int_{\rho_1(x_0)}^{\rho_1(x)} [\kappa_{11} + 2\kappa_{12} d\rho_2/d\rho_1 + \kappa_{22} (d\rho_2/d\rho_1)^2]^{1/2} \Delta a^{-1/2} d\rho_1 . \quad (\text{VI.17})$$

When the geometric mean approximation is used for  $\kappa_{12}$ , eq. VI.11 is the minimization condition for eq. VI.16. If  $\kappa_{12}$  is not equal to the geometric mean, eq. VI.2 must be used which reduces in  $\rho$ -space to

$$[\kappa_{11} + 2\kappa_{12} d\rho_2/d\rho_1 + \kappa_{22} (d\rho_2/d\rho_1)^2] [\partial \Delta a / \partial \rho_2 (\kappa_{11} + \kappa_{12} d\rho_2/d\rho_1) - \frac{\partial \Delta a}{\partial \rho_1} (\kappa_{12} + \kappa_{22} d\rho_2/d\rho_1)] - d^2 \rho_2 / d\rho_1^2 [2\Delta a (\kappa_{11} \kappa_{22} - \kappa_{12}^2)] = 0 . \quad (\text{VI.18})$$

Although the equations lose their symmetry and look much more complicated in  $\rho$ -space, a great deal of computational simplicity is gained from this transformation.

Another simplification which applies only in the case where  $\kappa_{12}$  is assumed to follow the geometric mean has been employed in some cases. If one defines a variable

$$\Phi \equiv \kappa_{11}^{1/2} \rho_1 + \kappa_{22}^{1/2} \rho_2 \quad (\text{VI.19})$$

the interfacial tension relationship may be written

$$\gamma = \sqrt{2} \int_{\Phi^I}^{\Phi^{II}} \Delta a^{1/2} d\Phi \quad (\text{VI.20})$$

and solved subject to eq. VI.11. Care must be exercised in the use of this transformation, since integrating over  $\phi$  from  $\phi^I$  (i.e.  $\phi$  evaluated at  $\rho_1^I$  and  $\rho_2^I$ ) to  $\phi^{II}$  implies the assumption that  $\phi^I < \phi < \phi^{II}$ . While this is usually true for well behaved low molecular weight mixtures, there is no guarantee that a smooth profile will result when this assumption is used. The profiles must thus always be monitored simultaneously as a check on such a calculation. A detailed discussion of the numerical techniques employed to solve the interfacial problem for a binary mixture in the various approximations will be found in the numerical appendix.

For the LF theory, the number density of mers,  $\rho_i$ , was identified as

$$\rho_i \equiv \phi_i \tilde{\rho} / v^* \quad . \quad (\text{VI.21})$$

Using this definition along with

$$\Delta a = a_o - \rho_1(x) \mu_1^e - \rho_2(x) \mu_2^e - P_e \quad (\text{VI.22})$$

we obtain for the general combining rules:

$$\Delta a = \epsilon^* \tilde{\rho} / v^* \{ -\tilde{\rho} + \tilde{T} [ (\tilde{v}-1) \ln(1-\tilde{\rho}) + \frac{1}{r} \ln \tilde{\rho} + \frac{\phi_1}{r_1} \ln \phi_1 + \frac{\phi_2}{r_2} \ln \phi_2 ] \} - \tilde{\rho} \phi_1 \mu_1^e / v^* - \tilde{\rho} \phi_2 \mu_2^e / v^* - P_e \quad . \quad (\text{VI.23})$$

The  $\mu_i^e$  must be given in units of energy/mer. In addition,  $\frac{\partial \Delta a}{\partial \rho_1}$  and

$\frac{\partial \Delta a}{\partial \rho_2}$ , appear in the minimization conditions and must be evaluated.

In Chapter II, we pointed out:

$$\frac{\partial \Delta a}{\partial \rho_i} = \mu_i(\rho) - \mu_i^e. \quad (\text{VI.24})$$

$\mu_i(\rho)$  is the chemical potential per mer of a hypothetical homogeneous (equilibrium) fluid of the local density and concentration. The symbol  $\rho$  is here used to signify  $\rho_1, \rho_2, \dots, \rho_n$ . This quantity can be evaluated in two ways. The chemical potential expression can be derived directly from the local Helmholtz free energy density via

$$\left( \frac{\partial a_0}{\partial \rho_i} \right)_{\rho_j, T} = \mu_i(\rho) \quad (\text{VI.25})$$

which is then evaluated at the local mer densities. More conveniently, the pressure necessary to produce an equilibrium system of the local mer densities can be evaluated from the equation of state, and then substituted into the chemical potential obtained from the Gibbs free energy. The expressions which result from the two procedures are, of course, equivalent.  $\mu_1(\rho)$  for a binary mixture can be written:

$$\begin{aligned} \mu_1(\rho) = kT \left[ \frac{1}{r_1} \ln \phi_1 + \left( \frac{1}{r_1} - \frac{1}{r_2} \right) \phi_2 + (\tilde{v}-1) \ln(1-\tilde{\rho}) + \frac{1}{r_1} \ln \tilde{\rho} \right] \\ + \frac{\epsilon^*}{v^*} \left\{ -\tilde{\rho} - T \left[ \tilde{v} \ln(1-\tilde{\rho}) + 1 - \frac{1}{r} \right] \right\} (v_1^* + \phi_2^2 \Delta v) - \tilde{\rho} (\epsilon_{11}^* - \phi_2^2 \chi_{12}). \end{aligned} \quad (\text{VI.26})$$

$\mu_2^0$  can again be obtained by exchanging subscripts.

Eqs. VI.1 and VI.2 can thus be solved by several methods of varying complexity. For liquid-vapor systems, results obtained

with  $c = 1$  were found to differ little from those calculated with  $c < 1$ , where  $c$  was evaluated using eq. VI.8 for  $\kappa_{12}$ . For liquid-liquid systems, on the other hand, the results are very sensitive to the value of  $c$ .

#### B. Results for Liquid-Vapor Systems

As an initial assessment of the interfacial theory for binary liquid-vapor interfaces, calculations were performed using the geometric mean approximation for  $\kappa_{12}$  ( $c=1$ ), and setting  $\tilde{\kappa}$  for the pure components equal to .62. The bulk mixing parameters were set to the values given in Table 4. Figs. 30-33 compare the results of such calculations to experimental data for the systems benzene-n-hexane, cyclohexane-n-hexane, benzene-cyclohexane, and benzene-n-dodecane. The maximum error in the predicted tension is about 5% for benzene-n-hexane and benzene-cyclohexane and is less for the other two systems.

A part of the error observed for these mixtures is due to the errors in the interfacial tension predicted for the pure components with  $\tilde{\kappa} = .62$ . In order to separate out the error resulting from the mixture theory, the calculations were repeated using pure component  $\kappa$ 's which were fitted to the data. Fig. 34 illustrates the type of agreement obtained for benzene-cyclohexane under these conditions. The values of  $\tilde{\kappa}$  required were:  $\tilde{\kappa}_{\text{benzene}} = .64$  and  $\tilde{\kappa}_{\text{cyclohexane}} = .67$ . The maximum error is reduced to 2% for this system. The decrease in the maximum error for benzene-n-hexane ( $\tilde{\kappa}_{\text{benzene}} = .64$ ,  $\tilde{\kappa}_{\text{hexane}} = .62$ ) was from 5% to 4.2%, and for cyclohexane-n-hexane ( $\tilde{\kappa}_{\text{cyclohexane}} = .67$ ,  $\tilde{\kappa}_{\text{n-hexane}} = .65$ ) from 4% to 2%. For the benzene-n-dodecane system

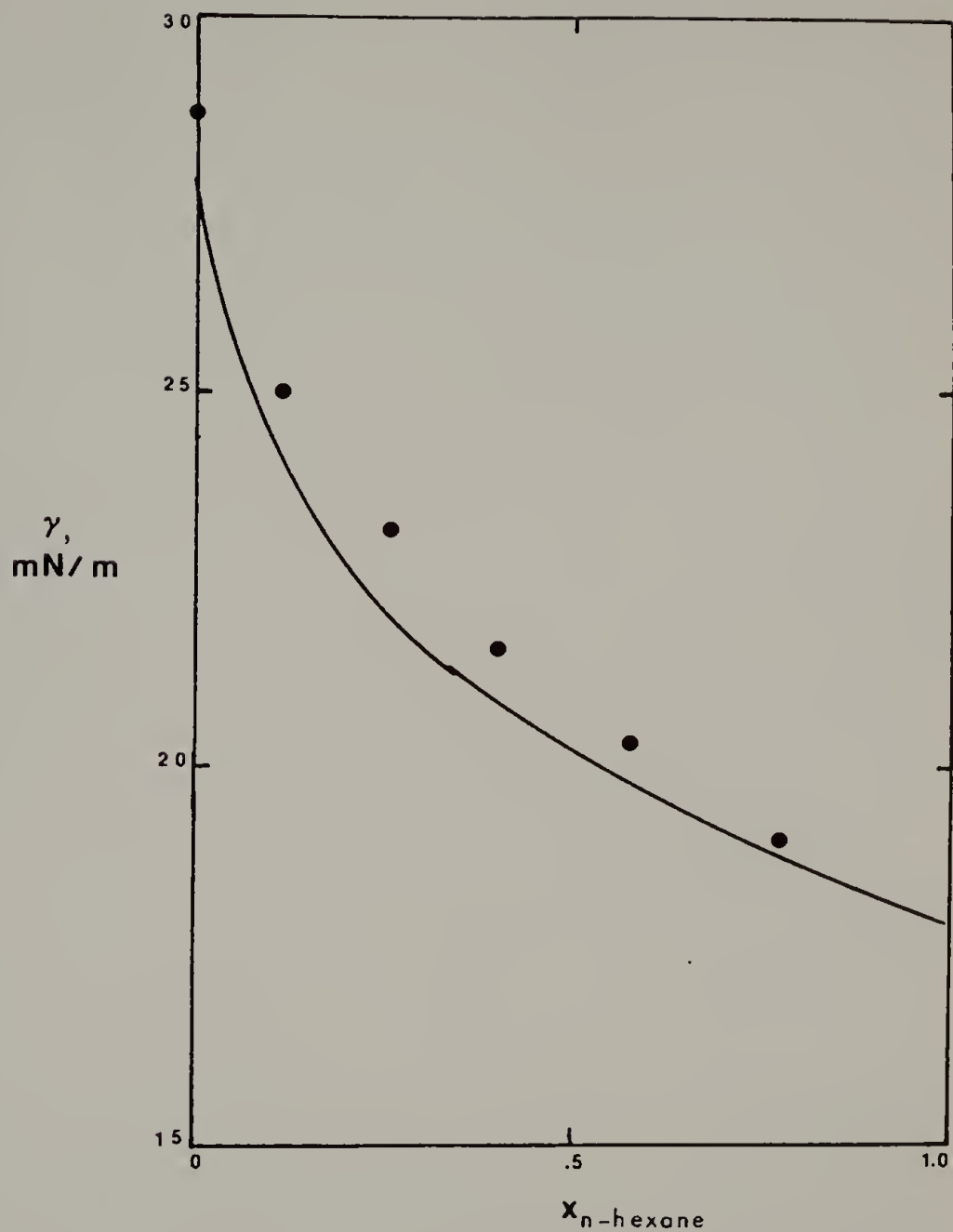


Figure 30. Interfacial tension versus mole fraction for benzene-n-hexane at 25°C. Experimental values were taken from reference 87. The theoretical line was calculated with the following parameters:  $\delta = -.0027$ ,  $\zeta = .9688$ ,  $\tilde{\kappa}_{11} = \tilde{\kappa}_{22} = .62$ , and  $c = 1$ .



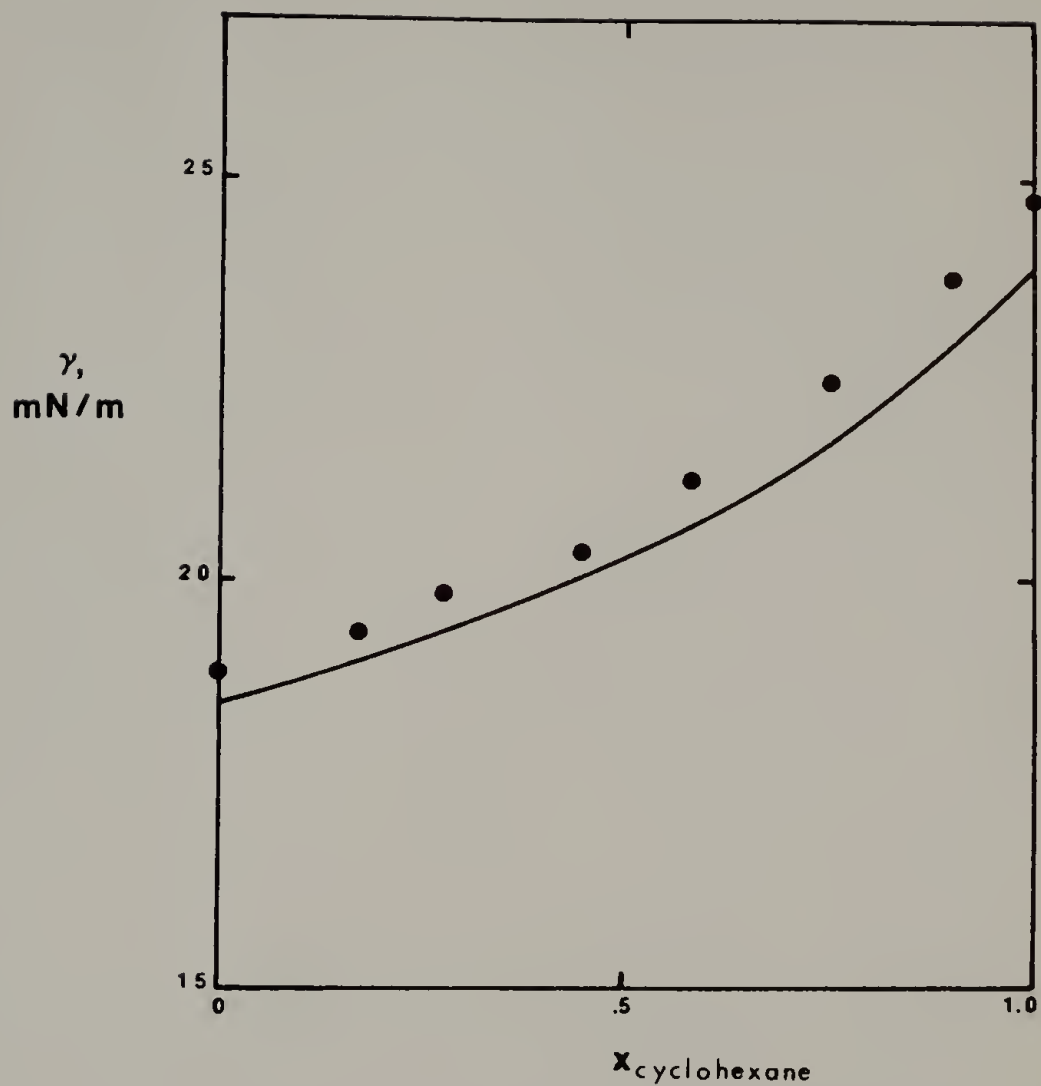


Figure 31. Interfacial tension versus mole fraction for cyclohexane-n-hexane at 20°C. Experimental values were taken from reference 88. The theoretical line was calculated with the following parameters:  $\delta = -.0041$ ,  $\zeta = .9917$ ,  $\tilde{\kappa}_{11} = \tilde{\kappa}_{22} = .62$ , and  $c = 1$ .

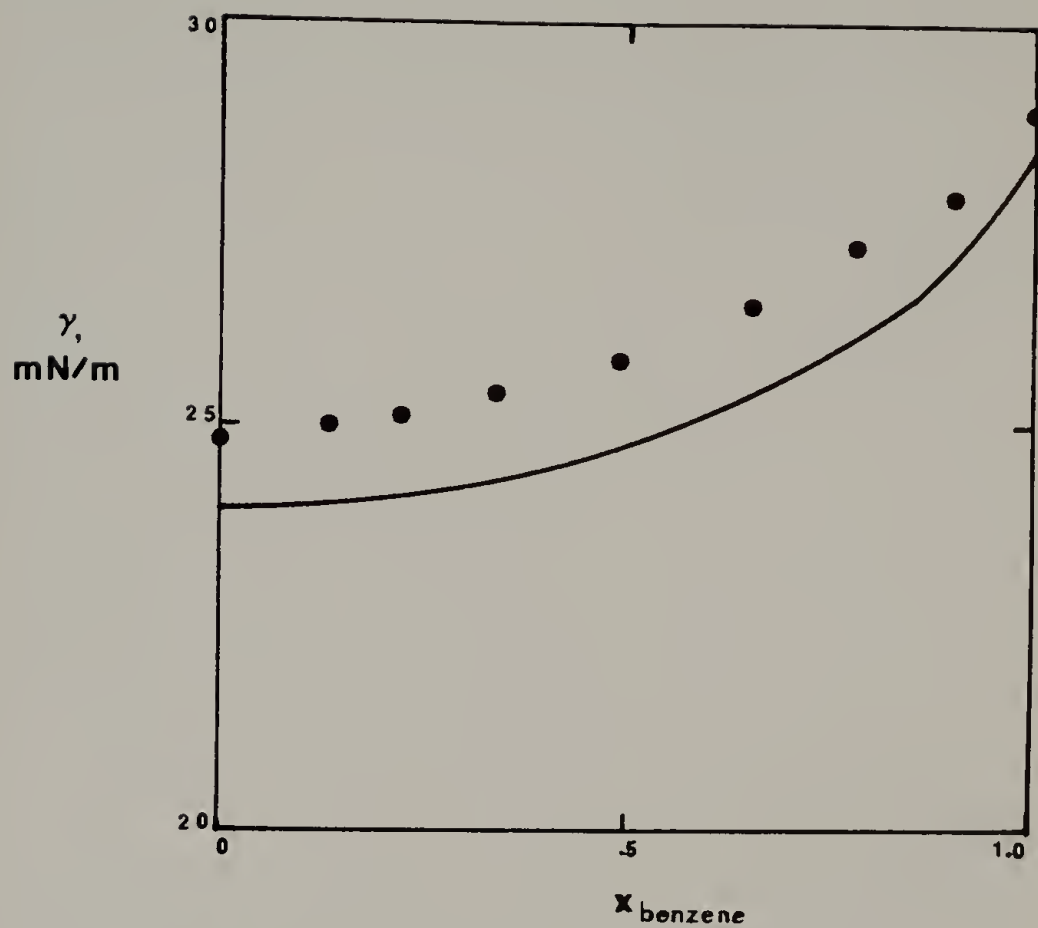


Figure 32. Interfacial tension versus mole fraction for benzene-cyclohexane at 20°C. Experimental data were taken from reference 87. The theoretical line was calculated with the following parameters:  $\delta = -.0004$ ,  $\zeta = .9635$ ,  $\tilde{\kappa}_{11} = \tilde{\kappa}_{22} = .62$ , and  $c = 1$ .

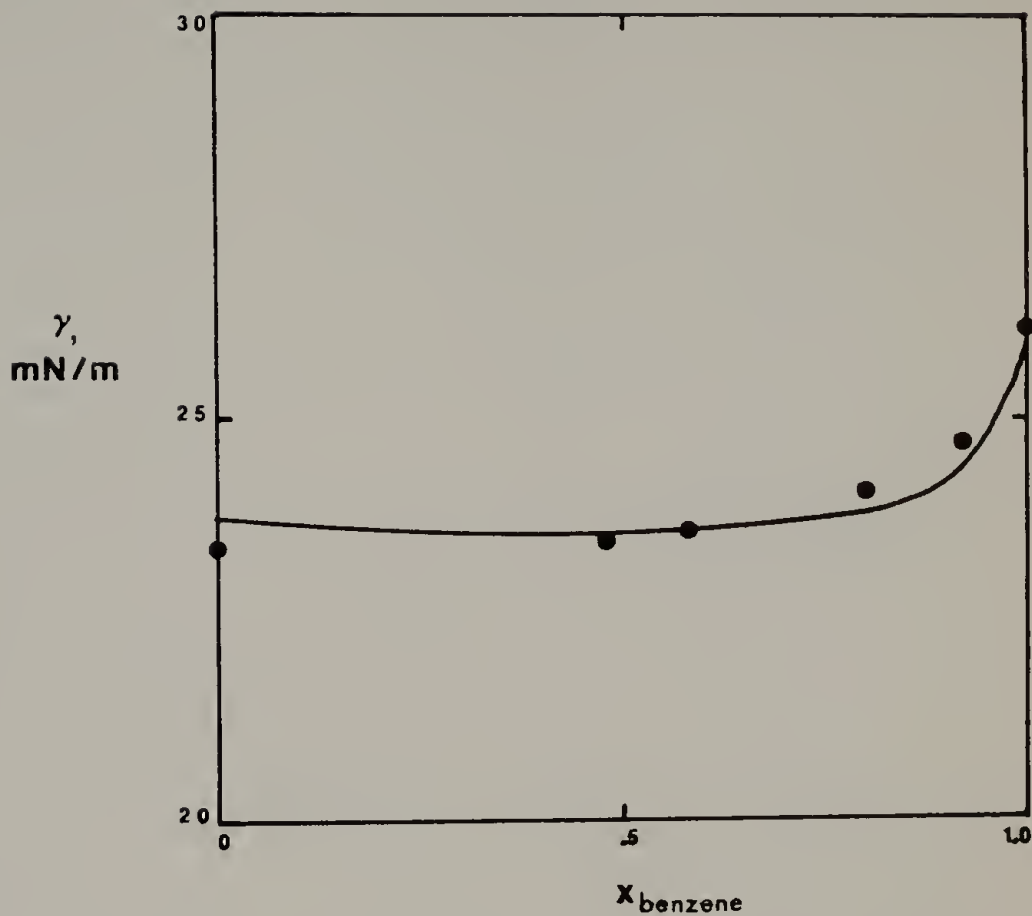


Figure 33. Interfacial tension versus mole fraction for benzene-n-dodecane at 40°C. Experimental data were taken from reference 88. The theoretical line was calculated with the following parameters:  $\delta = -.0070$ ,  $\zeta = .9521$ ,  $\tilde{\kappa}_{11} = \tilde{\kappa}_{22} = .62$ , and  $c = 1$ .

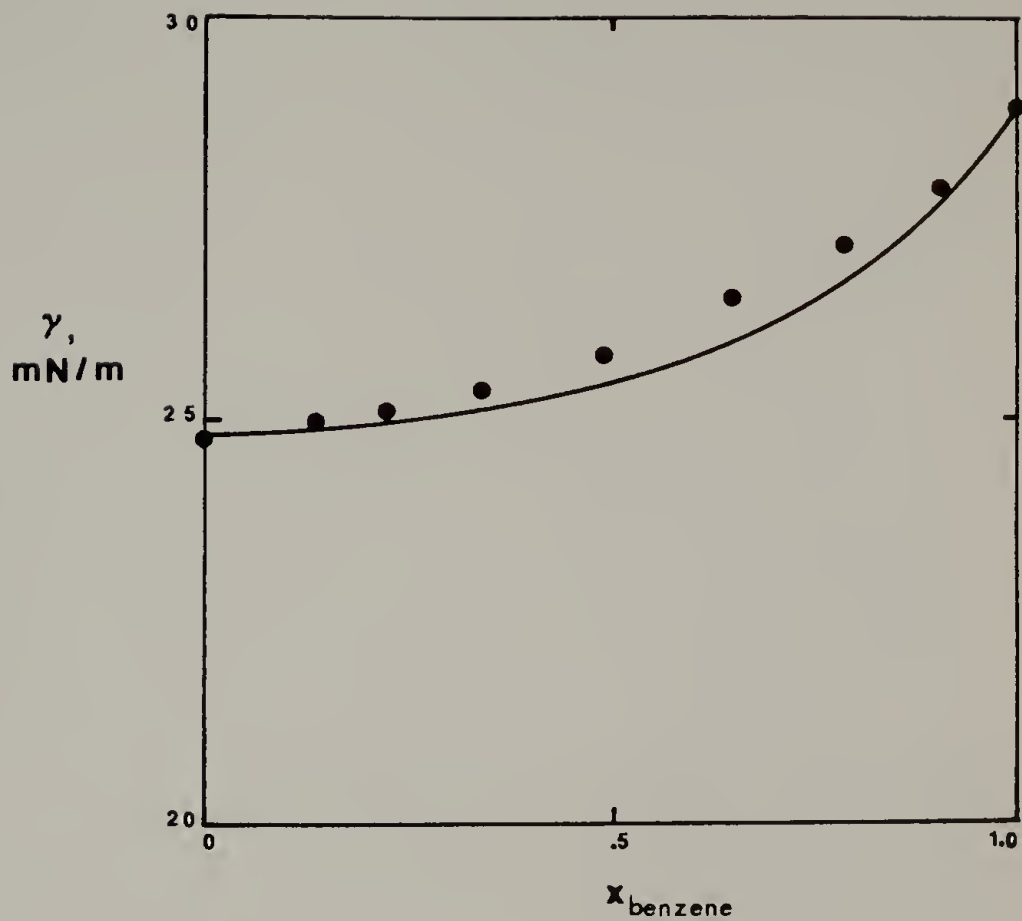


Figure 34. Interfacial tension versus mole fraction for benzene-cyclohexane at 20°C with fitted end-points. Experimental data were taken from reference 87. The theoretical line was calculated with the following parameters:  $\delta = -.0004$ ,  $\zeta = .9635$ ,  $\tilde{\kappa}_{\text{benzene}} = .64$ ,  $\tilde{\kappa}_{\text{cyclohexane}} = .67$ , and  $c = 1$ .

( $\tilde{\kappa}_{\text{benzene}} = .64$ ,  $\tilde{\kappa}_{\text{n-dodecane}} = .59$ ) the error remained about 1.5%.

Fitting the pure component  $\tilde{\kappa}$ 's introduces two adjustable parameters into a calculation which is capable of yielding predictions within 5% without adjustable parameters. If the theory were to be used to obtain a prediction of the interfacial tension's composition dependence for a nonpolar mixture, setting the  $\tilde{\kappa}$ 's equal to .62 should be adequate and simpler.

Unfortunately, the four mixtures discussed are the only ones for which both mixing data and reliable interfacial tension data could be located. We therefore investigated the effect of setting  $\zeta$  equal to its geometric mean value of 1 and  $\delta$  equal either to the arithmetic mean value of 0 or the value appropriate to the geometric mean. (If  $v_{12} = \sqrt{v_1^* v_2^*}$ , then  $\delta = [2(v_1^* v_1^*)^{\frac{1}{2}} - v_1^* - v_2^*] / (v_1^* + v_2^*)$ .) The results of such calculations for benzene and cyclohexane are shown in Table 9. The same trends are observed for the other three systems. For these nonpolar systems, the use of  $\delta = 0.0$  and  $\zeta = 1.0$  results in reasonable predictions, although somewhat less accurate than those obtained with fitted values of  $\delta$  and  $\zeta$ .

Before extending the interfacial calculations to additional systems and analyzing our results in more detail, the effect of  $c < 1$  needs to be examined. Table 10 compares the values of  $\kappa_{12}$  obtained from eq. VI.8 to the geometric mean values and also lists the  $c$  parameters appropriate to each of the four systems we have discussed. Calculations using  $c = .98$  for benzene-n-hexane and  $c = .97$  for

Table 9

INTERFACIAL TENSION OF BENZENE-CYCLOHEXANE AT 20°C FOR DIFFERENT  
VALUES OF THE MIXING PARAMETERS

$x_{\text{benzene}}$	$\gamma_{\text{exp}}$ mN/m (ref. 87)	$\gamma_{\text{calc}}$ mN/m		
		$\zeta = .9635$ $\delta = .0004$	$\zeta = 1.0$ $\delta = 0.0$	$\zeta = 1.0$ $\delta = -.0001$
.1282	25.00	24.87	25.21	25.22
.2174	25.14	24.96	25.49	25.50
.4874	25.84	25.45	26.44	26.46
.6470	26.54	25.96	27.08	27.11
.7814	27.20	26.64	27.70	27.72
.9033	27.88	27.64	28.33	28.34

$$\tilde{\kappa}_{\text{benzene}} = .64$$

$$\tilde{\kappa}_{\text{cyclohexane}} = .67$$

Table 10

COMPARISON OF THE GEOMETRIC MEAN APPROXIMATION TO EQ. VI.8.

For  $c < 1$ ,  $\kappa_{12}$  was evaluated using the mixing parameters from Table 4. Pure component  $\tilde{\kappa}$ 's were fitted to the data.

	T °C	$\tilde{\kappa}_{11}$	$\tilde{\kappa}_{22}$	c=1	c < 1	
				$\kappa_{12}$ $\frac{\text{Kcal-cm}^5}{\text{mol}^{8/3}}$	$\kappa_{12}$ $\frac{\text{Kcal-cm}^5}{\text{mol}^{8/3}}$	c
benzene-n-hexane	25	.64	.62	72.25	70.60	.98
benzene-cyclohexane	20	.64	.67	64.49	62.30	.97
cyclohexane-n-hexane	20	.67	.62	78.06	77.59	.99
benzene-n-dodecane	30	.64	.59	85.30	83.61	.98

benzene-cyclohexane were performed for a few selected compositions. These two mixtures were chosen because their  $c$  parameters showed the larger deviations from the geometric mean value of 1. The smaller values of  $c$  decreased the calculated interfacial tension slightly. At .5 mole fraction of benzene, the decrease for benzene-n-hexane was .4%, while the tension for benzene-cyclohexane decreased by about .6%.  $c=1$  thus appears to be a good approximation for the liquid-vapor interfaces of the nonpolar mixtures under investigation. Since the numerical solution of the interfacial equations with  $c < 1$  requires about twice the computational time of the solution with  $c = 1$ , the latter was used for all further liquid-vapor calculations. As we shall see later, the effect of  $c < 1$  is much more pronounced for liquid-liquid interfaces.

In the further examination of the present mixture theory's predictions, the concept of an "ideal" interfacial tension,  $\gamma_{id}$ , is useful. This quantity is defined by

$$\gamma_{id} \equiv x_1\gamma_1 + x_2\gamma_2 \quad . \quad (VI.27)$$

and represents the interfacial tension exhibited by an ideal system. Note that for the four systems discussed the tensions fall below  $\gamma_{id}$  (which can, of course, be represented as a straight line connecting the pure component tensions in a plot of  $\gamma$  vs.  $x_1$ ). Such negative deviations are associated with the preferential adsorption of the lower tension component at the interface. Fig. 35 shows the calculated interfacial profiles for benzene-n-hexane at 25°C. These profiles



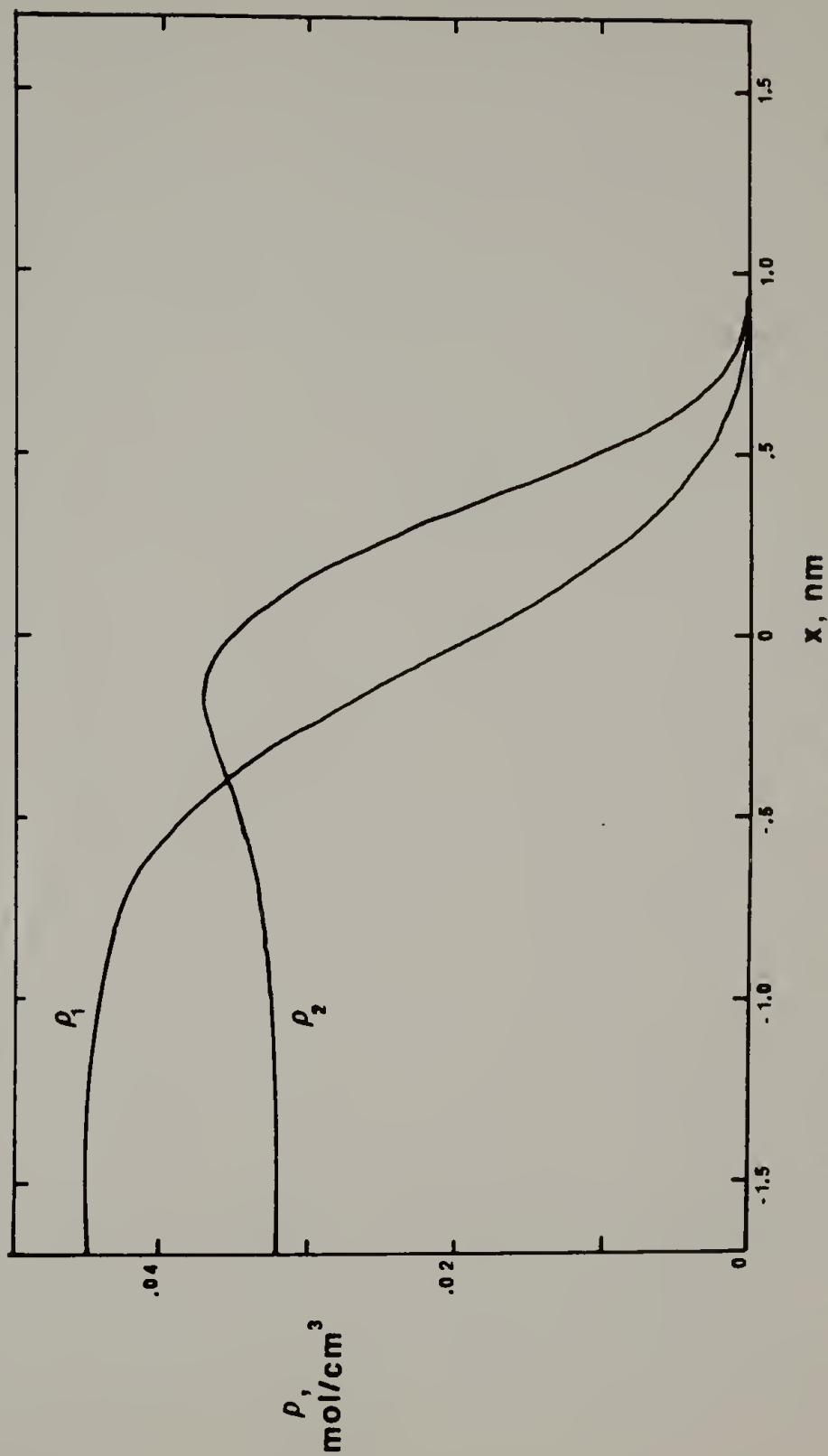


Figure 35. Interfacial profiles for benzene-n-hexane at 25°C. Component 1 is benzene. The theoretical line was calculated with a benzene mole fraction of .6 and the following values of the parameters:  $\delta = -.9927$ ,  $\zeta = .9688$ ,  $\tilde{\kappa}_{11} = .64$ , and  $c = 1$ .

clearly demonstrate the ability of the present theory to predict preferential adsorption phenomena.

Some systems, such as n-hexane-n-dodecane, exhibit a slightly positive deviation from  $\gamma_{id}$ .<sup>89</sup> Table 11 contains a comparison of the experimental and calculated excess interfacial tensions ( $\gamma - \gamma_{id}$ ) for this mixture. The theory is seen to be in qualitative agreement with experiment. Since the present theory appears capable of predicting the deviations from ideal behavior, we may use it to examine the effect of size and shape on the interfacial tension. To this end we have calculated the tensions of n-hexane with three pentanes (n-pentane, isopentane, and neopentane). The difference between n-hexane and n-pentane is essentially one of size only, while isopentane and neopentane additionally exhibit an increasing shape difference from n-hexane. Although this series of mixtures appears ideal for such an investigation, interpretation of the results is not as straightforward as might be thought. The tensions of the pure pentanes (calculated with  $\tilde{\kappa} = .62$ ) decrease from 15.72 mN/m for n-pentane to 14.28 mN/m for isopentane, and to 11.57 mN/m for neopentane at 20°C. The calculated tension at the same value of  $\tilde{\kappa}$  and temperature is 18.48 mN/m. In order to minimize the influence of tension differences we have plotted the percent deviation of the predicted values from  $\gamma_{id}$  for the three mixtures in Fig. 36. The n-hexane-n-pentane mixture again deviates positively from  $\gamma_{id}$ . The results for n-hexane with isopentane and neopentane do suggest that a greater shape

Table 11

CALCULATED AND EXPERIMENTAL EXCESS INTERFACIAL TENSIONS FOR N-HEXANE-N-DODECANE AT 30°C

$x_{\text{n-dodecane}}$	$(\gamma - \gamma_{id})_{\text{experimental}}$ mN/m (ref. 89)	$(\gamma - \gamma_{id})_{\text{calculated}}$ mN/m
.2494	.45	.11
.3859	.57	.16
.6174	.43	.17
.7297	.19	.15

$$\tilde{\kappa}_{\text{n-dodecane}} = .59 \quad \tilde{\kappa}_{\text{n-hexane}} = .62 \quad \delta = 0.0 \quad \zeta = 1.0$$

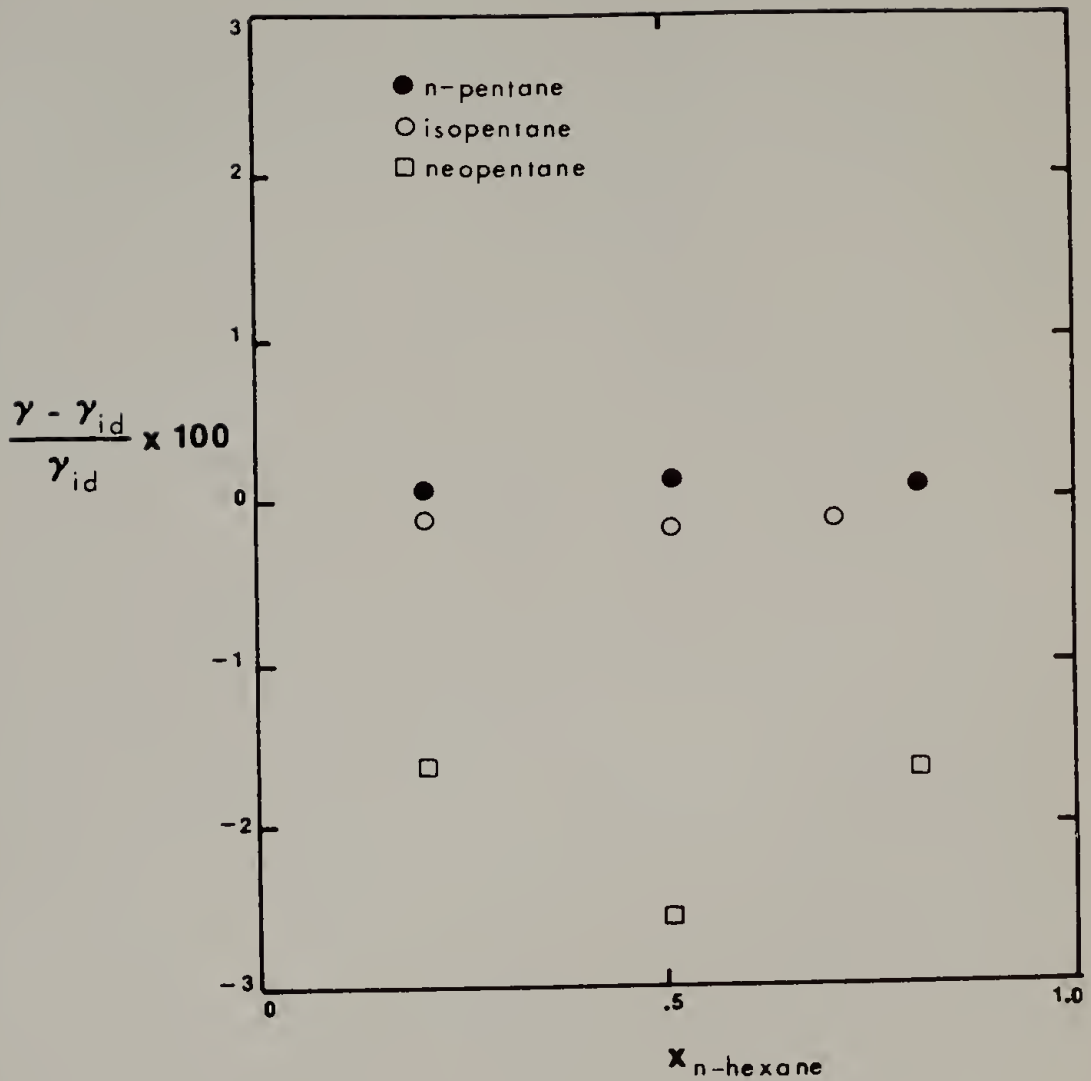


Figure 36. Excess interfacial tension of n-hexane with three pentanes. The theoretical points were calculated with the following parameters:  $\delta = 0.0$ ,  $\zeta = 1.0$ ,  $\tilde{\kappa}_{11} = \tilde{\kappa}_{22} = .62$ , and  $c = 1$ . The temperature was set to  $20^\circ\text{C}$ .

dissimilarity results in a stronger negative deviation. This idea is supported by calculations for toluene-chlorobenzene shown in Fig. 37. These molecules are of similar shape (and size) and behave nearly ideally. The curve shown in this figure was obtained using fitted mixture parameters (from Table 4) and  $\tilde{\kappa}_{11} = \tilde{\kappa}_{22} = .62$ .

The system benzene-n-dodecane exhibits an extremely negative deviation from  $\gamma_{id}$  (Fig. 33). Schmidt and Clever<sup>89</sup> attempted to explain the unusual shape of the experimental benzene-n-dodecane curve by postulating a layer of n-dodecane molecules oriented perpendicularly to the surface. They advanced a similar picture to account for the positive deviation from  $\gamma_{id}$  in n-dodecane-n-hexane mixtures. The present theory correctly predicts both the shape of the benzene-n-dodecane curve, and the positive deviation for n-dodecane-n-hexane, without invoking orientational effects. Positive deviations from  $\gamma_{id}$  are particularly puzzling, since energetic arguments cannot provide a basis for such results for nonpolar mixtures. We found, however, that the observed positive deviations for the n-dodecane-n-hexane mixture can be removed if the size difference between the molecules is taken into account. Recalling the definition of the mer fraction

$$\phi_i = r_i N_i / rN \quad (\text{VI.28})$$

we define

$$\gamma'_{id} \equiv \phi_1 \gamma_1 + \phi_2 \gamma_2 \quad (\text{VI.29})$$

and plot the experimental and theoretical values of  $\gamma$  vs.  $\phi_1$ . Fig. 38

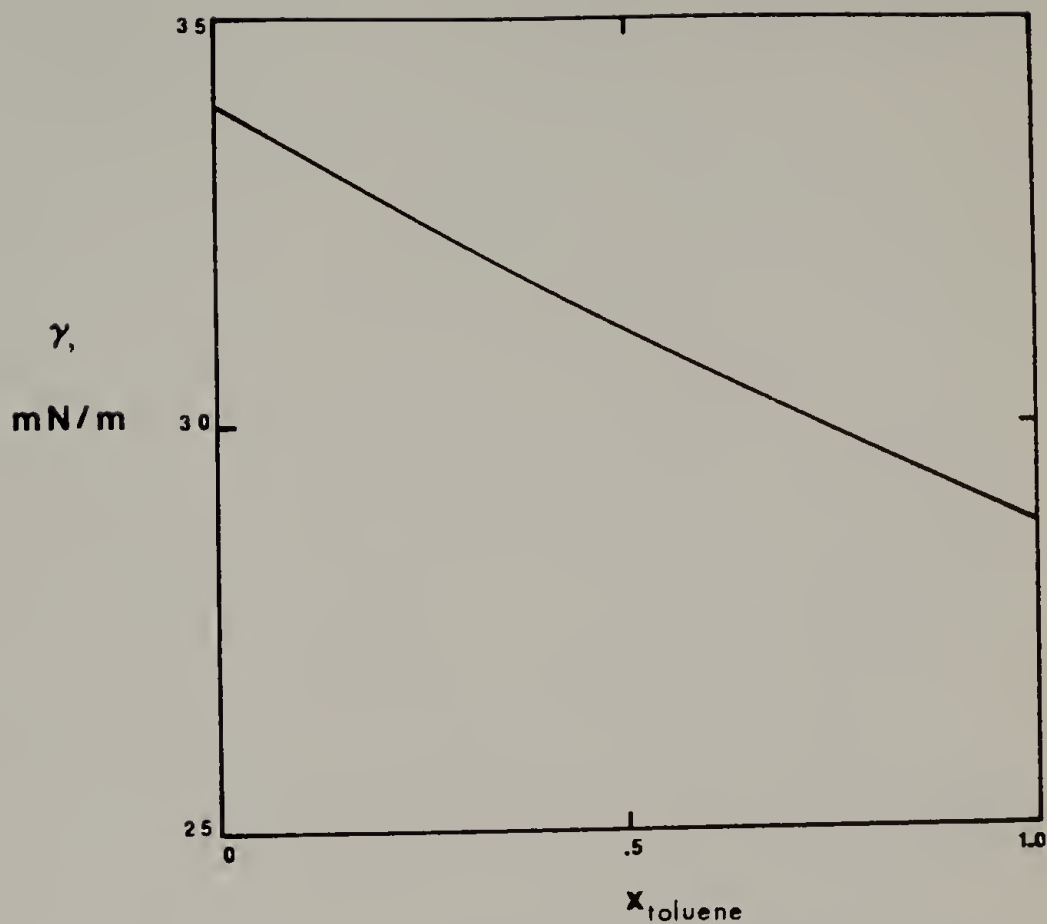


Figure 37. Interfacial tension versus mole fraction for toluene-chlorobenzene at 20°C. The theoretical line was calculated with the following parameters:  $\delta = -.0006$ ,  $\zeta = 1.0038$ ,  $\tilde{\kappa}_{11} = \tilde{\kappa}_{22} = .62$ , and  $c = 1$ .

shows this plot. The broken line represents eq. VI.29. Both the data and the calculated line now exhibit a small negative deviation from the ideal value. It thus appears that the positive deviation observed when  $\gamma_{\text{excess}}$  is evaluated in the conventional way is due to the fact that the mole fraction underestimates the contribution of the larger n-dodecane molecules. When the n-hexane-n-pentane mixture, for which we calculated a positive excess tension previously, is treated in terms of mer fractions a very small but negative excess tension results ( $\gamma_{\text{exc}} \approx -.001$  at  $\phi_{\text{n-hexane}} = .5$ ). It is interesting to note that eq. VI.29 is similar to the result of the monolayer theory for polymer solutions as originally formulated by Prigogine and Marechal.<sup>19</sup> These authors predicted

$$\gamma = v_1\gamma_1 + v_2\gamma_2 \quad (\text{VI.30})$$

where  $v$  is the volume fraction.

When the benzene-n-dodecane data are plotted in terms of mer fractions, the negative deviations from ideal behavior are somewhat less extreme, but still sizeable. Fig. 39 compares the data to the values calculated with  $\delta = -.0070$  and  $\zeta = .9521$  (solid line) and to those calculated with  $\delta = 0.0$  and  $\zeta = 1.0$  (broken line). Clearly, the theory is only able to predict the data well using the fitted mixture parameters. Thus, the present theory suggests that the unusually large negative deviations in this system are related to the relatively large deviation from ideal mixing behavior. Fig. 40 illustrates the calculated mer density profiles through the interface. The solid lines were obtained with the fitted mixing parameters, and the dotted lines with  $\delta = 0.0$  and  $\zeta = 1.0$ . When the fitted

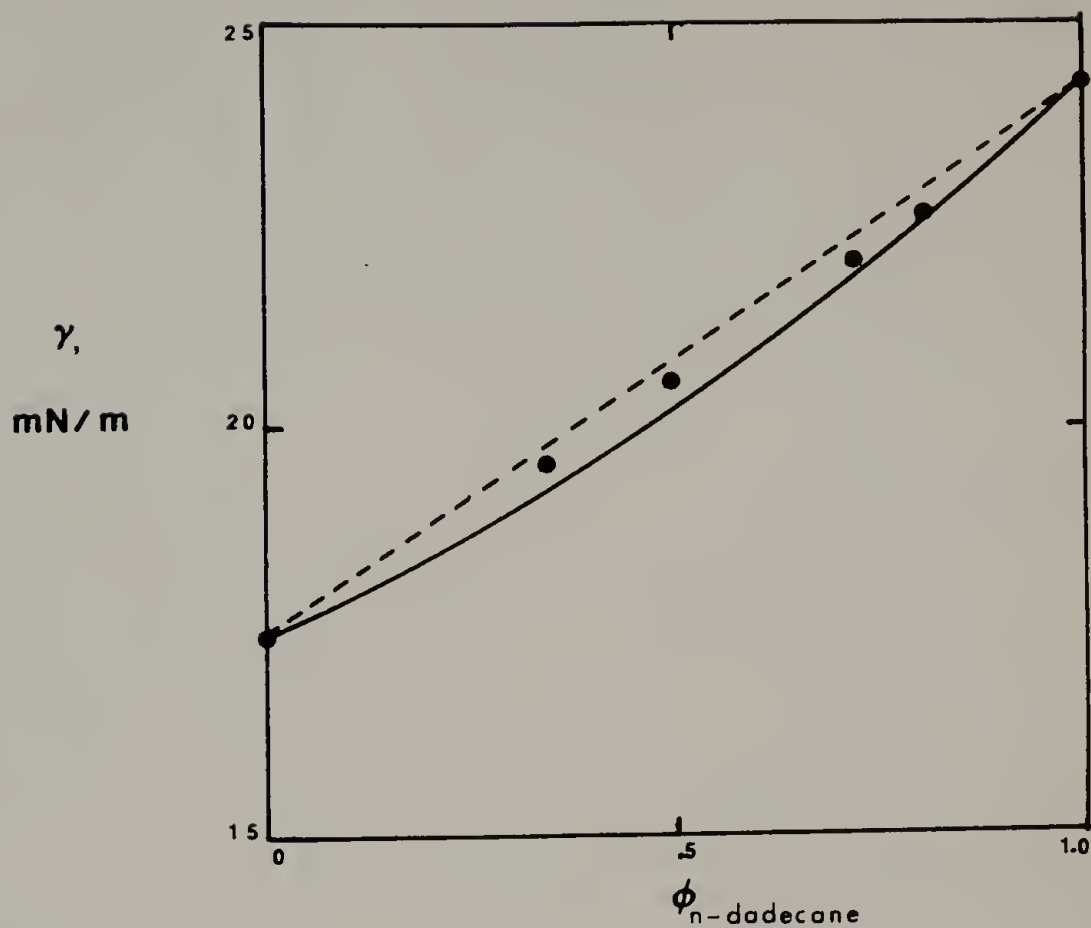


Figure 38. Interfacial tension versus mole fraction for n-dodecane-n-hexane at 30°C. Experimental data were taken from reference 89. The theoretical line was calculated with the following parameters:  $\delta = 0.0$ ,  $\zeta = 1.0$ ,  $\tilde{\kappa}_{n\text{-dodecane}} = .59$ ,  $\tilde{\kappa}_{n\text{-hexane}} = .62$ , and  $c = 1$ .



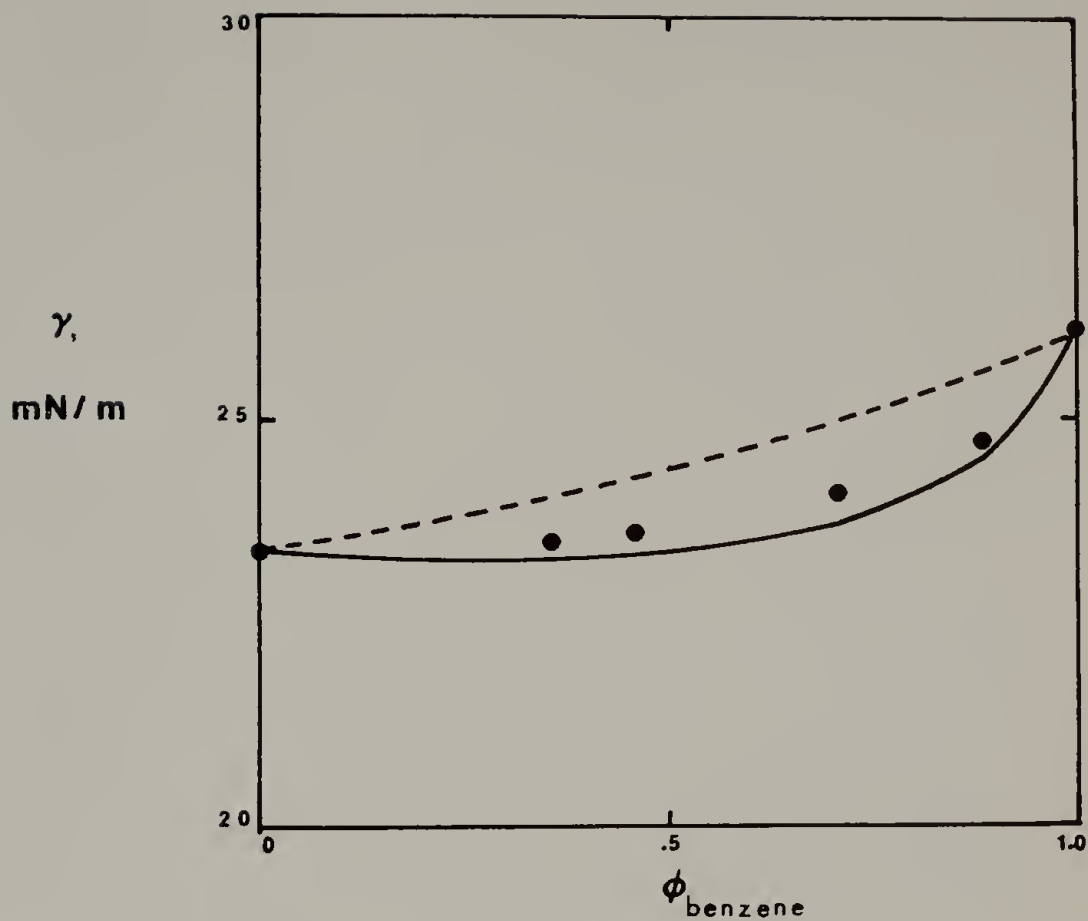


Figure 39. Interfacial tension versus mer fraction for benzene-n-dodecane at 40°C. Experimental data were taken from reference 88. The broken line was calculated with  $\delta = 0.0$  and  $\zeta = 1.0$ . The solid line was obtained from  $\delta = -.0070$  and  $\zeta = .9521$ . For both calculations,  $\tilde{\kappa}_{\text{n-dodecane}} = .59$ ,  $\tilde{\kappa}_{\text{benzene}} = .64$ , and  $c = 1$ .

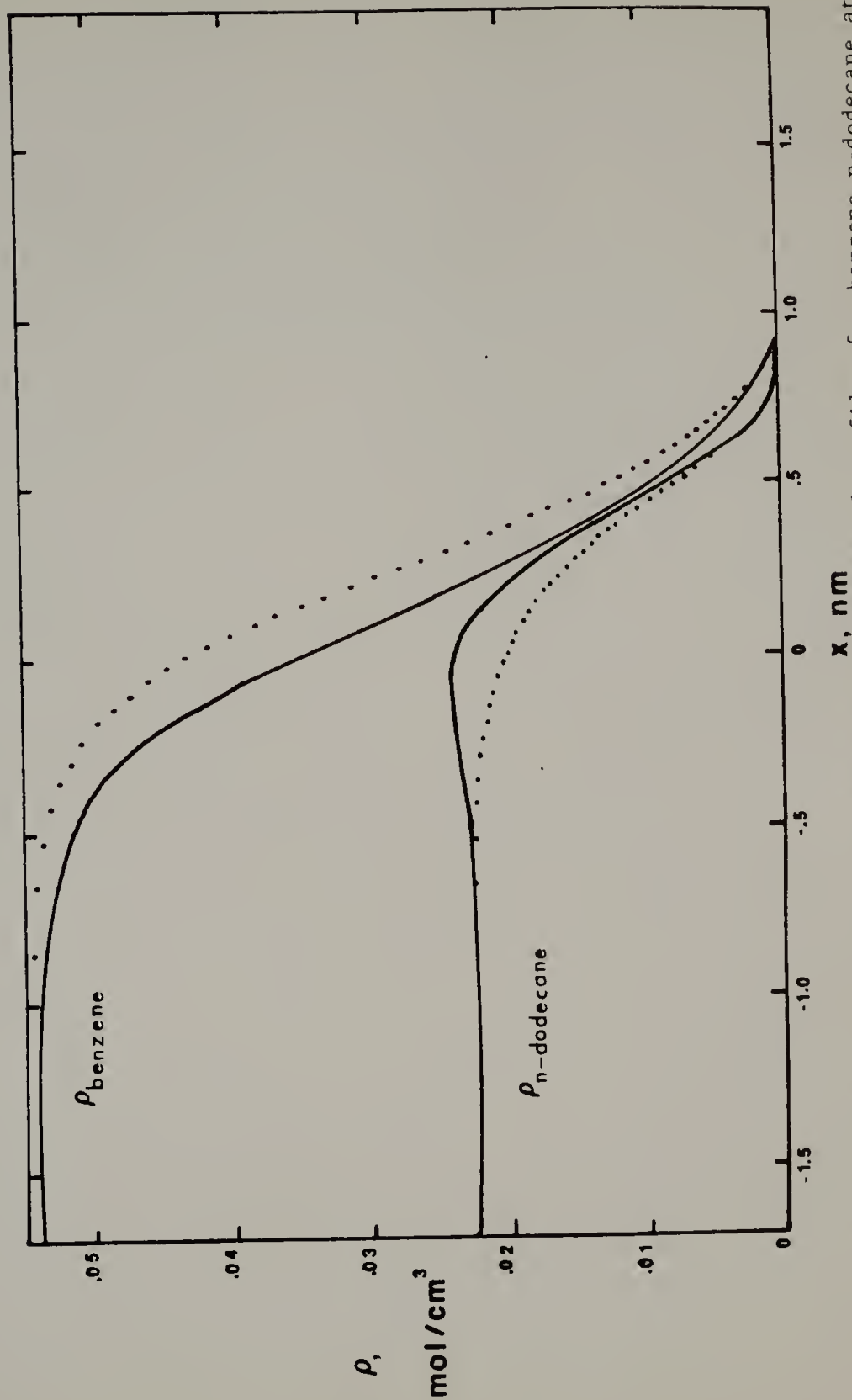


Figure 40. Effect of the mixing parameters on interfacial profiles for benzene-n-dodecane at 40°C. The mer fraction of benzene was .7. The dotted profiles correspond to  $\delta = 0.0$  and  $\zeta = 1.0$  and the solid profiles to  $\delta = -.0070$ ,  $\zeta = .9521$ . For both calculations,  $\tilde{\kappa}_{n\text{-dodecane}} = .59$ ,  $\tilde{\kappa}_{\text{benzene}} = .64$ , and  $c = 1$ .

mixing parameters are used, the interface broadens very slightly (this is not obvious in the figure). In addition, an adsorption peak appears in the n-dodecane profile. The equilibrium vapor pressure of the mixture also changes, increasing from a value of .189 atm at  $\delta = 0.0$  and  $\zeta = 1.0$  to .218 atm for the fitted parameters while the vapor composition is approximately constant at  $\phi_{\text{benzene}} = .999$ . The less favorable mixing parameters may thus lead to a lower interfacial tension, because the adsorption of the n-dodecane in the interfacial layer (where the density is decreasing) minimizes unlike contacts. At the same time, the increased vapor density reduces the density differences between the two phases. The present theory is thus able to predict the dependence of the interfacial tension-composition behavior fairly accurately for low molecular weight binary mixtures by accounting for size differences and the effect of unfavorable unlike contacts.

The interest in the liquid-vapor interfacial tension of polymer solutions derives from the experimental observation that a polymer added to a solvent of higher tension behaves like a surfactant. In other words, the polymer depresses the interfacial tension drastically at very low polymer concentrations. Figs. 41 and 42 compare the experimental data to the theoretical predictions for two systems of this type.  $\delta$  was set equal to 0.0 for these calculations. The fit obtained for the toluene-poly(dimethyl siloxane) system with  $\zeta = 1.0$  is excellent, whereas for the tetralin-poly(dimethyl siloxane)

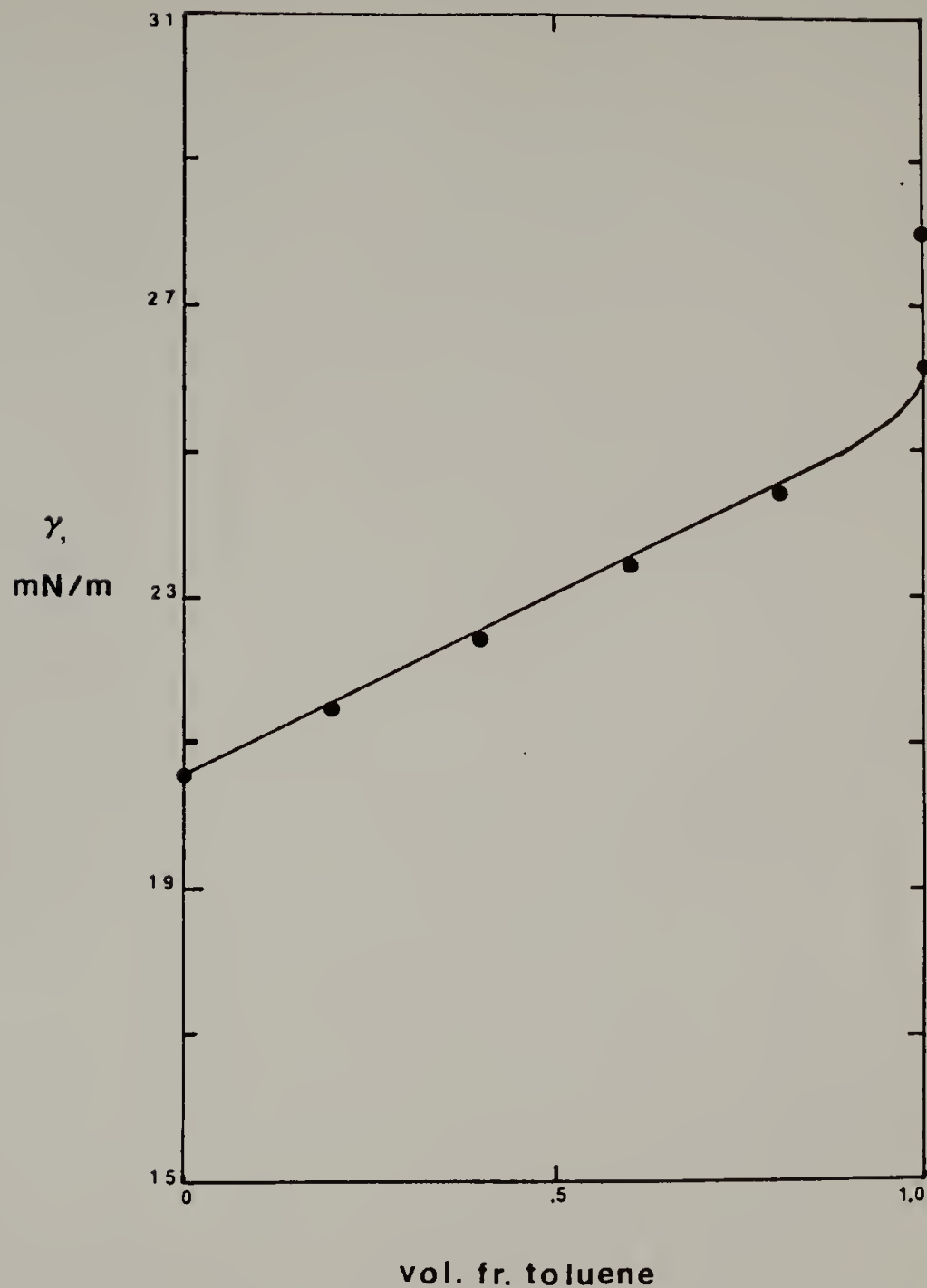


Figure 41. Interfacial tension versus volume fraction for toluene-poly(dimethyl siloxane) at 24°C. Experimental data were taken from reference 20. The theoretical line was calculated with  $\delta = 0.0$ ,  $\zeta = 1.0$ ,  $\tilde{\kappa}_{\text{toluene}} = .62$ ,  $\tilde{\kappa}_{\text{PDMS}} = .49$ , and  $c = 1$ .

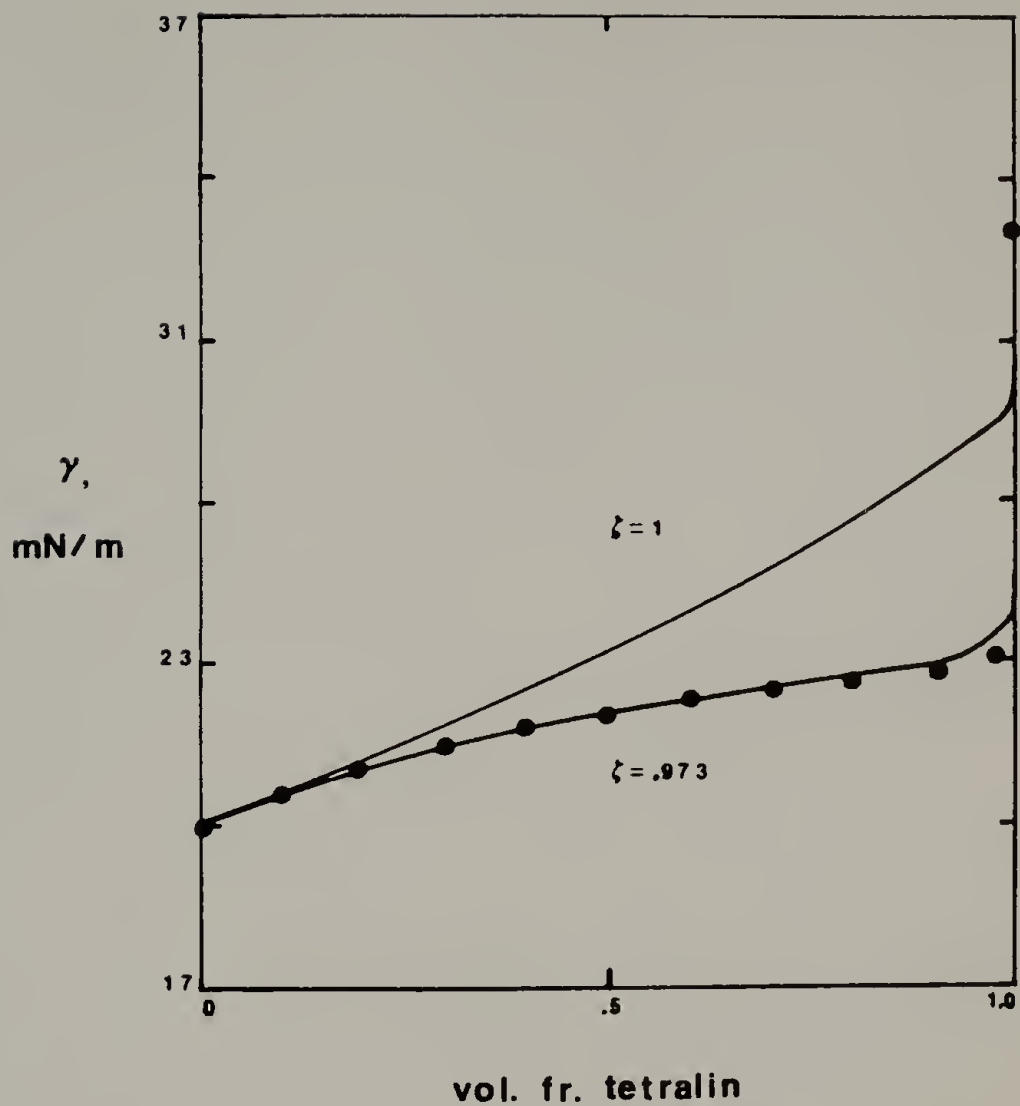


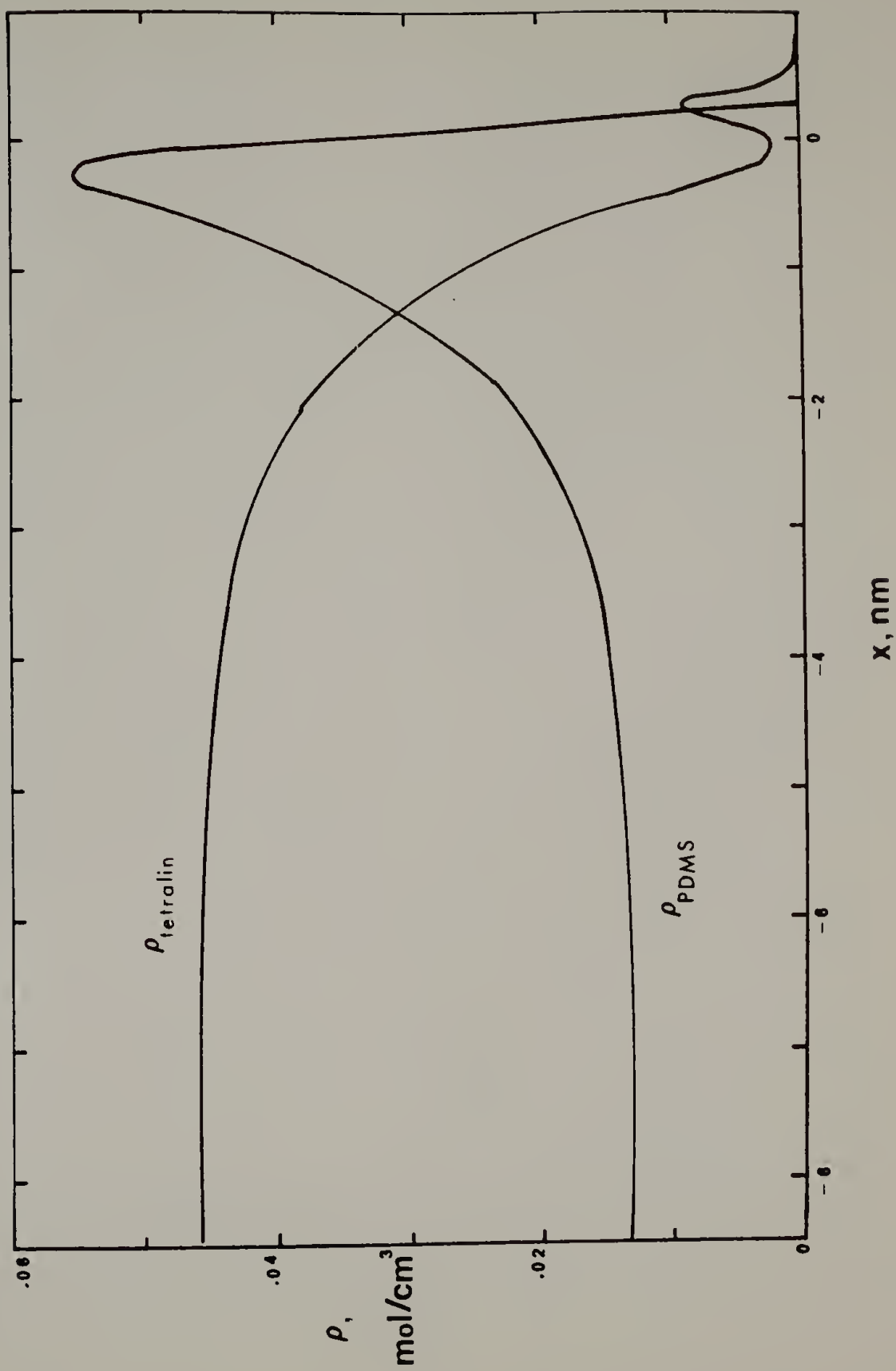
Figure 42. Interfacial tension versus volume fraction for tetralin-poly(dimethyl siloxane) at 30°C. Experimental data were taken from reference 24. The theoretical lines were calculated with  $\delta = 0.0$ ,  $\tilde{\kappa}_{\text{tetralin}} = .77$ ,  $\tilde{\kappa}_{\text{PDMS}} = .49$ , and  $c = 1$ .

system,  $\zeta = .973$  must be used in order to accurately represent the data. Equally good fits have been obtained for the same sets of data using the Gaines monolayer theory.<sup>20</sup> The values used for the monolayer theory's fitting parameter,  $\chi$ , were .106 for toluene-poly(dimethyl siloxane),<sup>20</sup> and .85 for tetralin-poly(dimethyl siloxane).<sup>24</sup> In both theories, the interaction parameter used is thus indicative of a less favorable energetic interaction for the tetralin solution.

Fig. 43 shows the calculated interfacial profiles for tetralin-poly(dimethyl siloxane) at .8 volume fraction of tetralin. For this system, we again observed an increasing adsorption peak with decreasing values of  $\zeta$  as in the benzene-n-dodecane case. In contrast to n-dodecane, the poly(dimethyl siloxane) profile exhibited an adsorption peak even at  $\zeta = 1.0$ . We also observed that the maximum in the polymer adsorption peak decreased only slightly as a function of increasing tetralin volume fraction, which is consistent with the almost flat tension curve.

Another polymer solution which we examined was polyisobutylene in n-heptane. In this case, the polymer is the higher tension component. Despite this fact, the theory predicts that the interface for this system consists of a strongly polymer-enriched region near the liquid side followed by a solvent-enriched layer which then decreases toward the vapor density. Since the profile is not monotonic in either component, we were unable to integrate the interfacial tension equation for this system. Nevertheless, the prediction of a

Figure 43. Interfacial profiles for tetralin-poly(dimethyl siloxane) at 30°C. The volume fraction of tetralin was .8. Other parameters were:  $\delta = 0.0$ ,  $\zeta = .973$ ,  $\tilde{\kappa}_{\text{tetralin}} = .77$ ,  $\tilde{\kappa}_{\text{PDMS}} = .49$ , and  $c = 1$ .





polymer-rich layer in the interface along with the results discussed above (i.e. that surface adsorption increases with decreasing  $\zeta$ ) suggest that the interface is a favorable environment for the polymer. Since the density is decreasing in the interface, polymer molecules may exhibit such strong adsorption in order to minimize polymer-solvent contacts.

The predictions of the present theory for polymer solutions are comparable in accuracy to the Gaines' monolayer approach. The conceptually unsatisfying requirement of a single surface layer containing polymers whose conformations are confined to this layer is avoided. In addition, explicit predictions for the interfacial structure can be made.

### C. Results for Liquid-Liquid Systems

Binary liquid-liquid interfaces arise in three types of systems: low molecular weight mixtures, polymer solutions, and polymer-polymer systems. Since most phase-separated low molecular weight mixtures contain highly polar components,<sup>65</sup> the work presented in this section will focus on polymer-containing systems.

Although many polymer solution phase diagrams contain partially miscible regions, the only experimental work available concentrates on the interfacial behavior near a critical solution temperature.<sup>31</sup> As shown in Chapter V, the present theory becomes unsatisfactory near a critical temperature, yielding a van der Waals' exponent of 1.5 for the dependence of the interfacial tension on  $T_c - T$ . One quantity of interest which can be examined is the structure of the interface

in such a partially miscible system. Fig. 44 shows the interfacial profiles calculated for benzene-polyisobutylene  $20^{\circ}$  below the upper critical solution temperature.  $\delta$  and  $\zeta$  were calculated from the critical temperature and composition estimated from data available in the Polymer Handbook.<sup>90</sup> The results shown were obtained with the geometric mean value of  $\tilde{\kappa}_{12}$ . For the purpose of comparison, we also calculated the interfacial profiles for cyclohexane-aniline at  $20^{\circ}\text{C}$  below the upper critical solution temperature (Fig. 45) using the geometric mean  $\tilde{\kappa}_{12}$ . Note that the cyclohexane-aniline interface is much narrower (about 3 nm) than the benzene-polyisobutylene profile (about 6 nm), since the concentration difference between the two phases is less for the polymer-containing system. The effect of using the non-geometric mean value of  $\tilde{\kappa}_{12}$  (as defined in eq. VI.8) is to broaden the profiles and simultaneously increase the interfacial tension. The interface width increases to approximately 5 nm and 10 nm for the low molecular weight system ( $c = .95$ ) and the polymer solution ( $c = .95$ ), respectively. The increase in the tension is from 0.19 mN/m to 0.33 mN/m for cyclohexane-aniline and from 0.008 mN/m to 0.15 mN/m for benzene-polyisobutylene. This increase in interfacial tension on using  $c < 1$  is the opposite of what was observed for liquid-vapor systems, where the interfacial tension decreased slightly. This fact can be understood by examining eq. VI.12. In a liquid-vapor system the overall signs of  $d\rho_1/dx$  and  $d\rho_2/dx$  are the same except for local variations. The gradient cross-term in

Figure 44. Interfacial profiles for benzene-polyisobutylene at 3°C. Benzene is component 1. The profiles were calculated with  $\delta = -.0388$ ,  $\zeta = .9765$ ,  $\tilde{\kappa}_{\text{benzene}} = .64$ ,  $\tilde{\kappa}_{\text{PIB}} = .33$ , and  $c = 1$ .

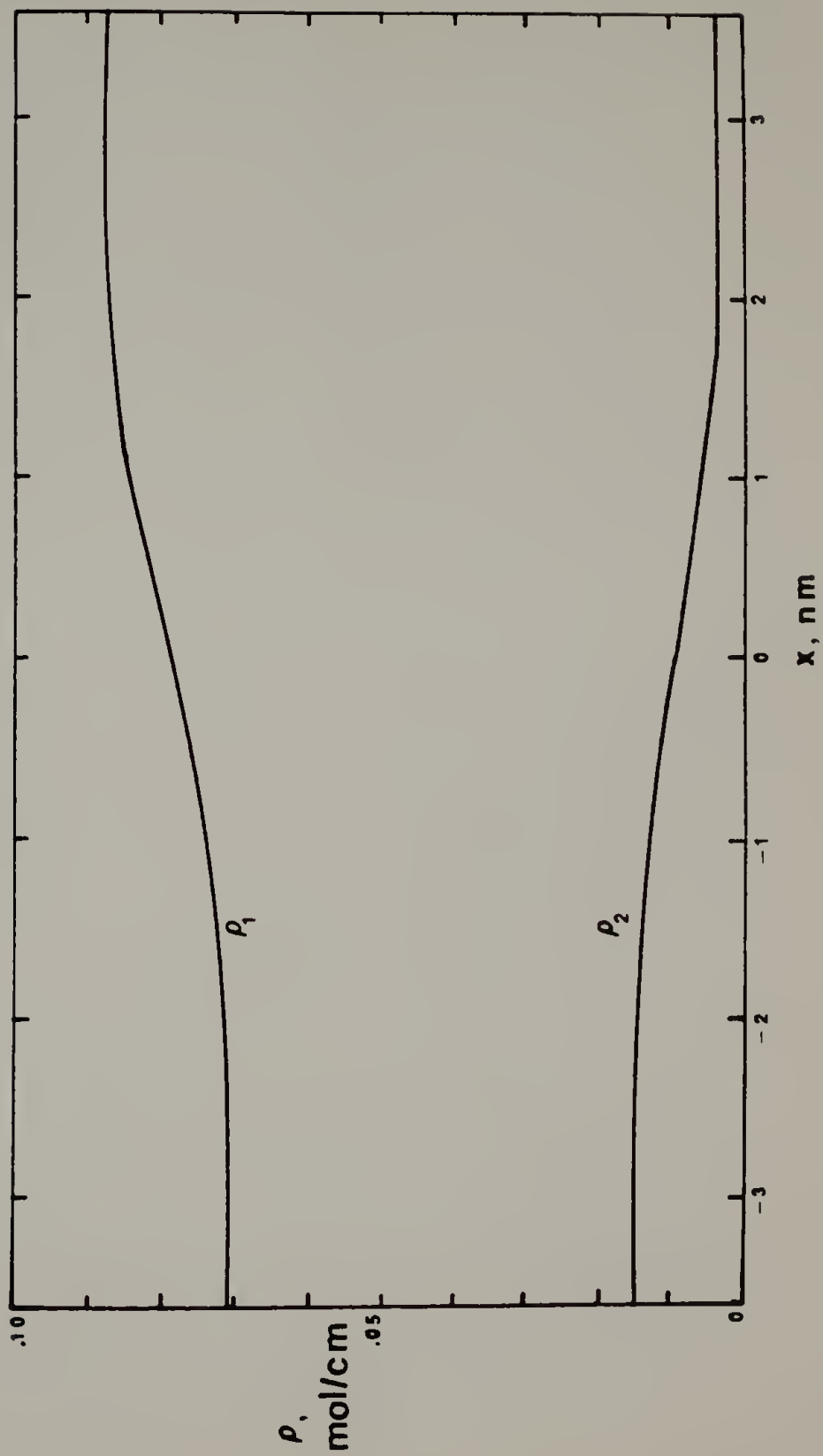
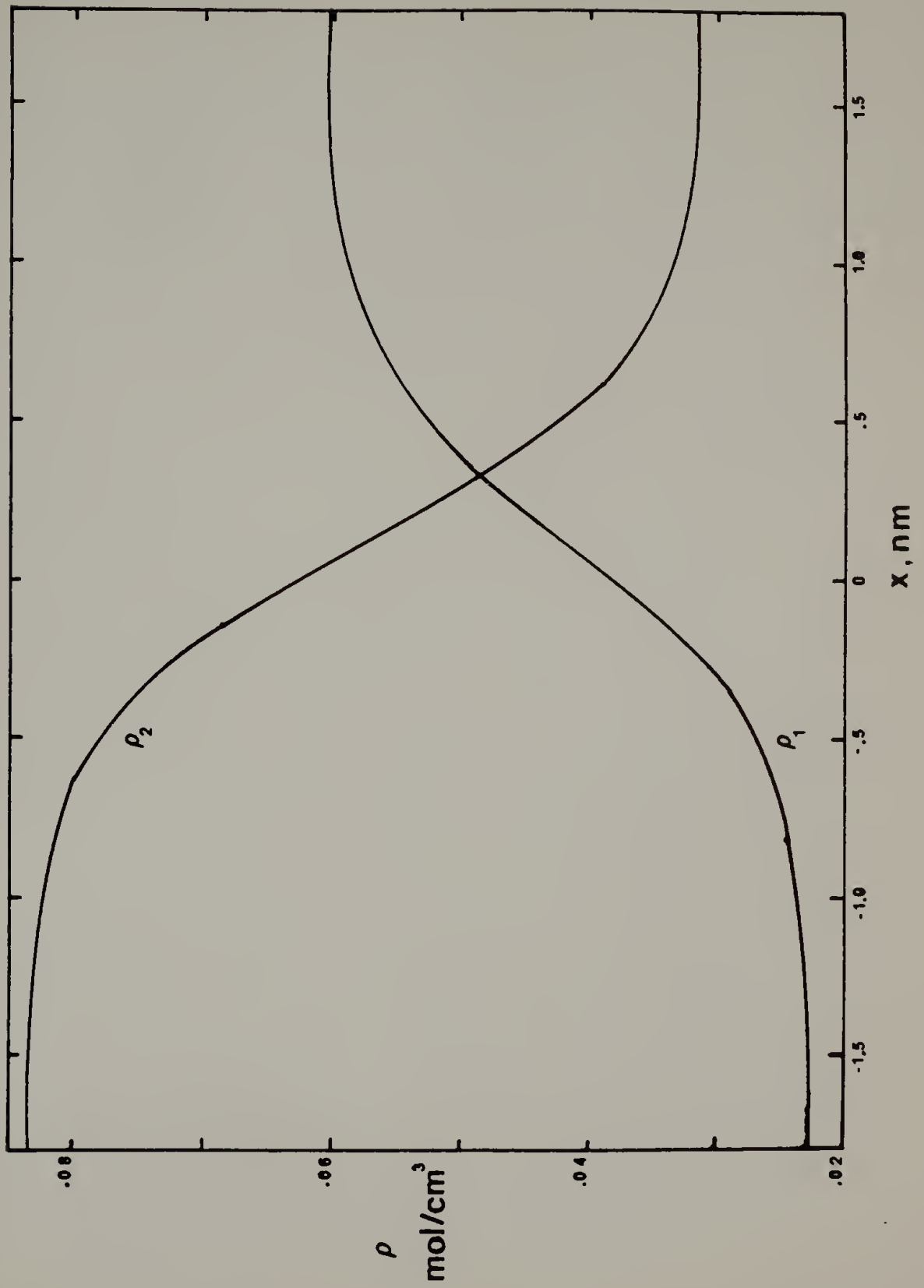


Figure 45. Interfacial profiles for cyclohexane-aniline at 9°C. Cyclohexane is component 1. The profiles were calculated with  $\delta = -.0152$ ,  $\zeta = .9598$ ,  $\tilde{\kappa}_{\text{cyclohexane}} = .66$ ,  $\tilde{\kappa}_{\text{aniline}} = .68$ , and  $c = 1$ .



eq. VI.12 is therefore generally positive. Thus decreasing  $\kappa_{12}$  decreases  $\Delta a$  and lowers the tension. For a liquid-liquid system, on the other hand,  $d\rho_1/dx$  and  $d\rho_2/dx$  carry opposite signs and the cross-term is negative. A decrease in  $\kappa_{12}$  can then increase  $\Delta a$  and the interfacial tension, provided that the density gradients do not change drastically.

Unlike for phase-separated polymer solutions, a reasonable amount of interfacial tension data is available for polymer-polymer systems.<sup>73,74</sup> However, a new difficulty arises in treating these systems. The theoretical phase diagrams are extremely sensitive to small changes in the values of the mixing parameters. Polymer-polymer interaction parameters are, however, extremely difficult to measure experimentally, and reliable data are scarce.<sup>91</sup> Due to the high sensitivity of the phase behavior,  $\delta = 0.0$  and  $\zeta = 1.0$  do not represent a good approximation for these systems. At low pressures (such as atmospheric pressure),  $\delta = 0.0$  and  $\zeta = 1.0$  leads to the prediction of complete miscibility for polyethylene with polystyrene at high molecular weights. The predictions of the interfacial theory can thus at present only be examined as a function of the parameters.

The results of the calculations for polymer interfaces will also be seen to be very sensitive to the value of  $\kappa_{12}$ . For this reason,  $\delta$  was set to the appropriate geometric mean value. In that case,  $c$  is equal to  $\zeta$ , thus allowing a more straightforward comparison of the effect of  $\kappa_{12}$  as a function of  $\zeta$ .

Fig. 46 illustrates the molecular weight dependence of the tension and interfacial thickness predicted by the theory. The curves were calculated for polyethylene-polystyrene with  $\zeta = .98$ ,  $r_1 = r_2$ , and  $c = .98$ . The thickness was here defined as:

$$t \equiv \left( dx/d\bar{\rho}_1 \right)_{\bar{\rho}_1 = \frac{1}{2}} \quad (\text{VI.28})$$

where  $\bar{\rho}_1$  is the mer density of component one reduced by the equilibrium value of  $\rho_1$  in the phase in which component one dominates. As  $r$  decreases, mixing becomes more favorable until at some critical value of  $r$  (in this case  $\sim 100$ ) the system becomes completely miscible. Consequently, the thickness must go to infinity and the tension must go to zero with decreasing  $r$ . The rapid change in both quantities as  $r$  exceeds the critical value, followed by an asymptotic dependence at large  $r$  is qualitatively in agreement with Roe's lattice theory.<sup>33</sup> If the value of  $\zeta$  is decreased, the critical  $r$  decreases, and the asymptotic values of the thickness and tension decrease and increase, respectively.

For a more detailed evaluation of the theory, we calculated the tensions for several systems at both  $c=1$  and  $c=\zeta$  as a function of  $\zeta$ . Fitted values of the pure component  $\tilde{\kappa}$ 's were used. The  $r$  values were obtained from the average molecular weights of experimental samples. The choice of  $r$  is very important. The phase diagrams for these polymer-polymer systems have an hour-glass shape, schematically shown in Fig. 47. If we increase the  $r$  value of component one while holding



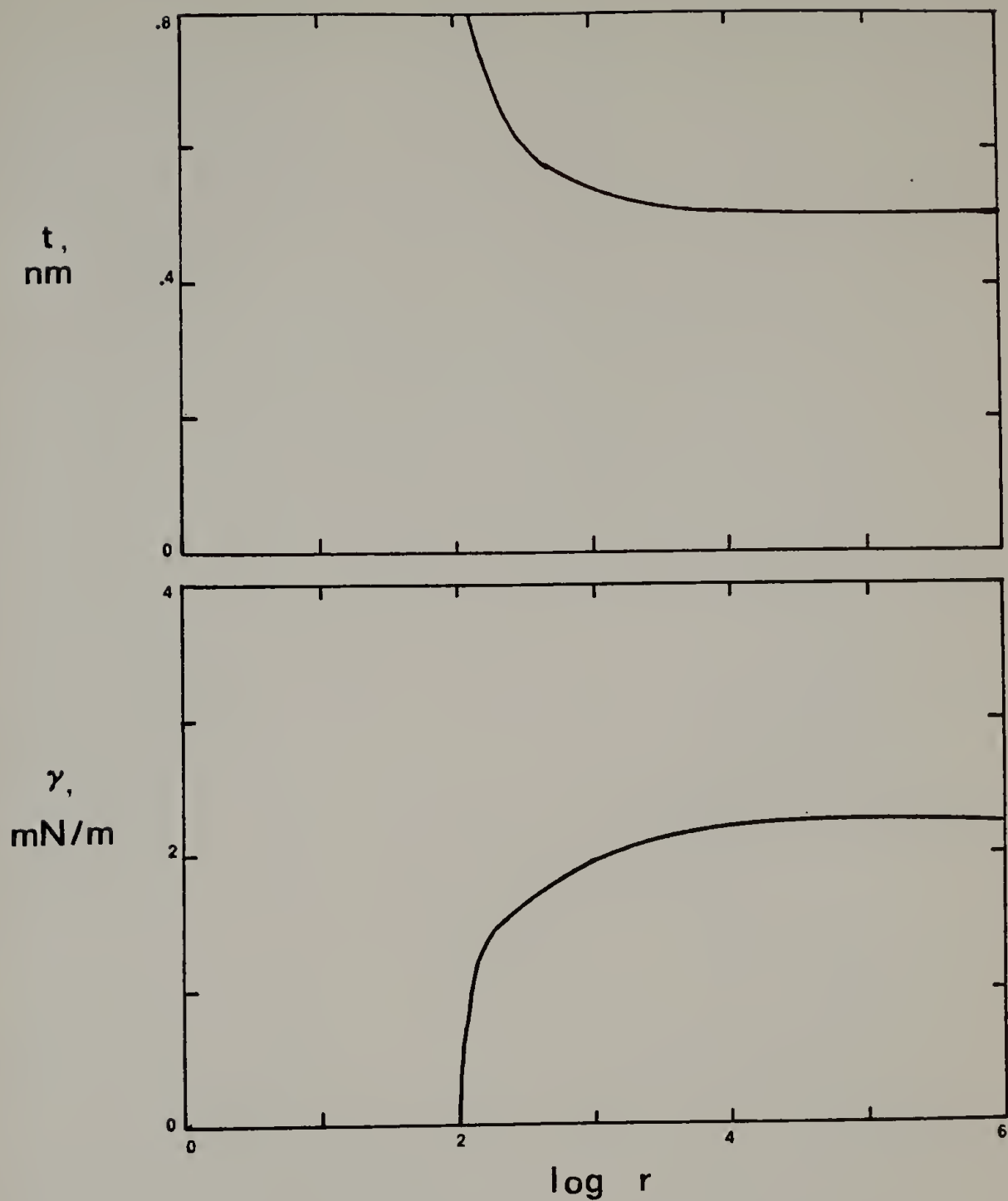


Figure 46. Interfacial tension and thickness as a function of molecular weight for linear polyethylene-polystyrene at 140°C. The curves were calculated with  $\delta = -.0110$ ,  $\zeta = .98$ ,  $\tilde{\kappa}_{\ell\text{-PE}} = .52$ ,  $\tilde{\kappa}_{\text{PS}} = .57$ , and  $c = .98$ .

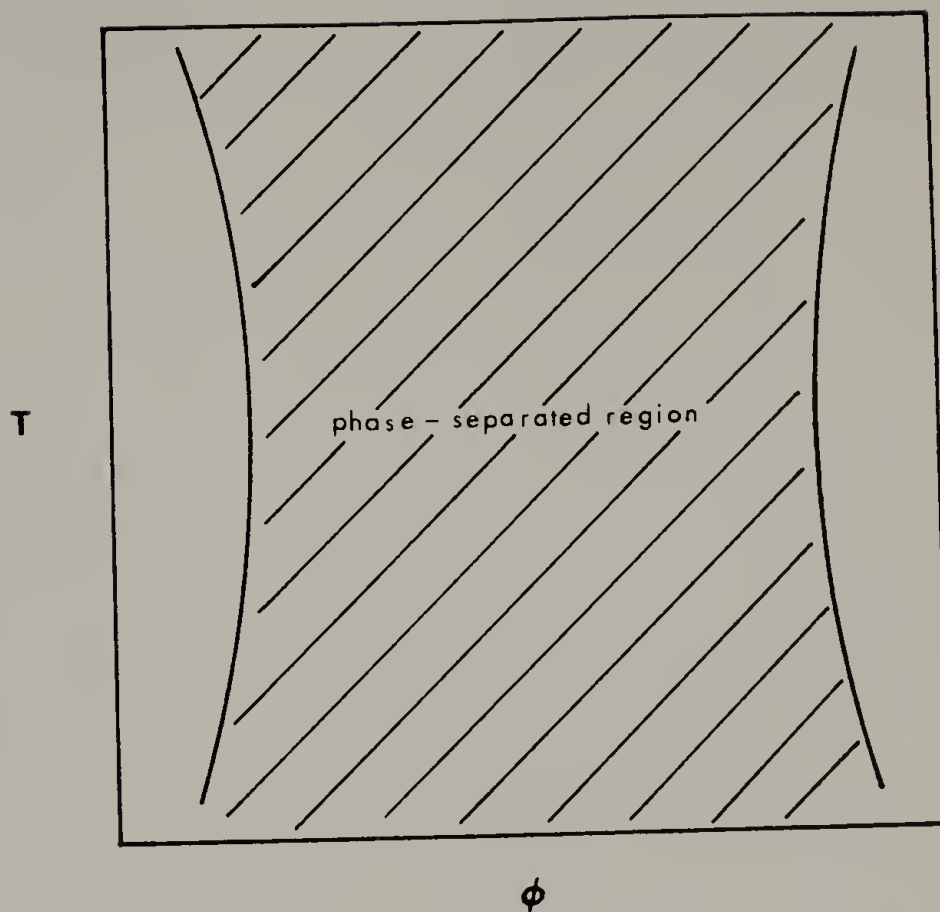


Figure 47. Schematic representation of a common polymer-polymer temperature-composition diagram.

that of the other component constant, the limits of miscibility move to lower values of  $\phi_1$ . Such a change in the phase equilibrium changes the calculated tension.

Figs. 48-51 show the dependence of  $\gamma$  on  $\zeta$  at the two different values of  $\kappa_{12}$  for four different systems. The difference between geometric mean and non-geometric mean results is striking. The inadequacy of the geometric mean results becomes obvious when we examine the predicted interfacial thickness. As  $\zeta$  decreases, the interaction between the components becomes more unfavorable, and each phase contains less of the minor component. This should lead to an increase in tension and simultaneous decrease in thickness. In Fig. 52 we have plotted the thickness as a function of  $\zeta$  for polyethylene-polystyrene. The shape of the geometric mean curve seems aphysical. The increase in thickness as  $\zeta$  decreases may be a response to the increasing severity of the geometric mean approximation.

The values of  $\zeta$  required to fit the experimental tension using  $c = \zeta$  at 140°C, as well as the calculated thicknesses, are given for three systems in Table 12. For comparison, we have also listed thicknesses predicted by the theory of Helfand and Sapse.<sup>34</sup> The present theory predicts surprisingly sharp interfaces for the systems investigated. Polyethylene-polystyrene is not included in Table 12 because, for the  $\delta$  and  $r$  values used in our calculation, no solution to the interfacial equations exists below  $\zeta = .98$  for this system. At this value of  $\zeta$ , the predicted tension is well below the experimental value of 5.9 mN/m.<sup>15</sup>

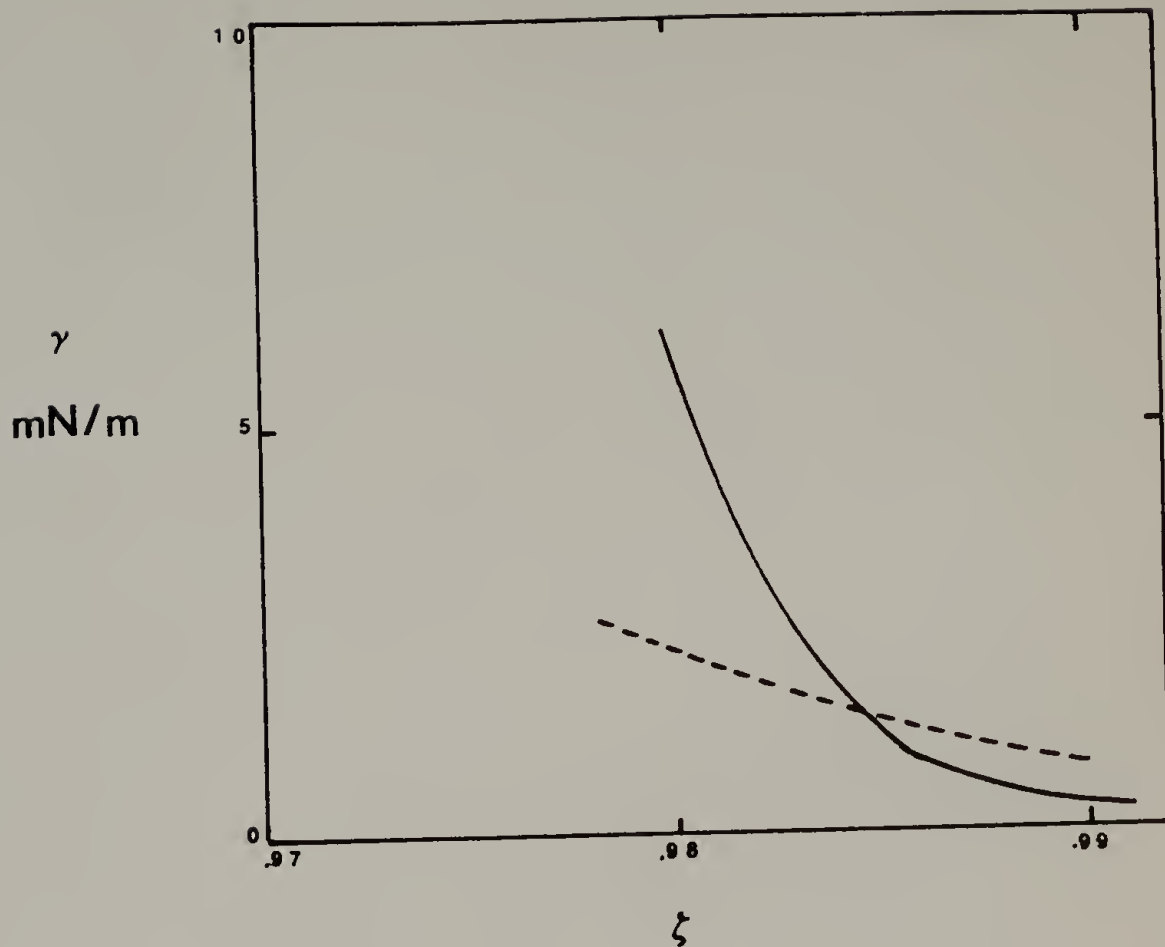


Figure 48. Dependence of the interfacial tension on the mixing parameter  $\zeta$  for linear polyethylene-polystyrene at 140°C. The curves were calculated with  $\delta = -.0110$ ,  $\tilde{\kappa}_{\ell\text{-PE}} = .52$ ,  $\tilde{\kappa}_{\text{PS}} = .57$ ,  $r_{\ell\text{-PE}} = 5845$ , and  $r_{\text{PS}} = 2331$ . The solid line corresponds to  $c = 1$ , and the broken line to  $c = \zeta$ .

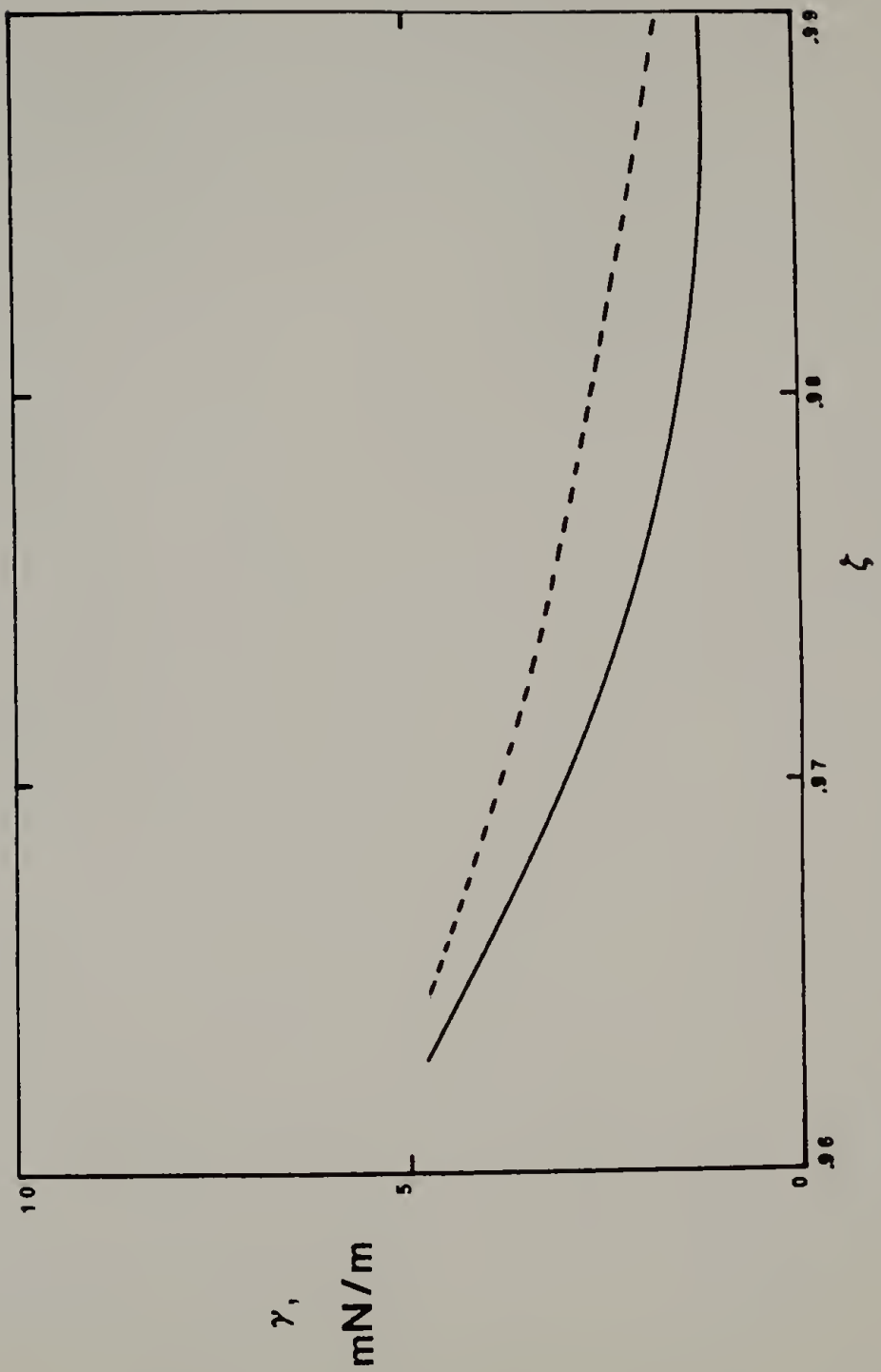


Figure 49. Dependence of the interfacial tension on the mixing parameter  $\zeta$  for poly(dimethylsiloxane)-polyisobutylene at 140°C. The curves were calculated with  $\delta = -.0025$ ,  $\tilde{\kappa}_{PDMS} = .60$ ,  $\tilde{\kappa}_{PIB} = .56$ ,  $r_{PDMS} = 3500$ , and  $r_{PIB} = 184$ . The solid line corresponds to  $c = 1$ , and the broken line to  $c = \zeta$ .

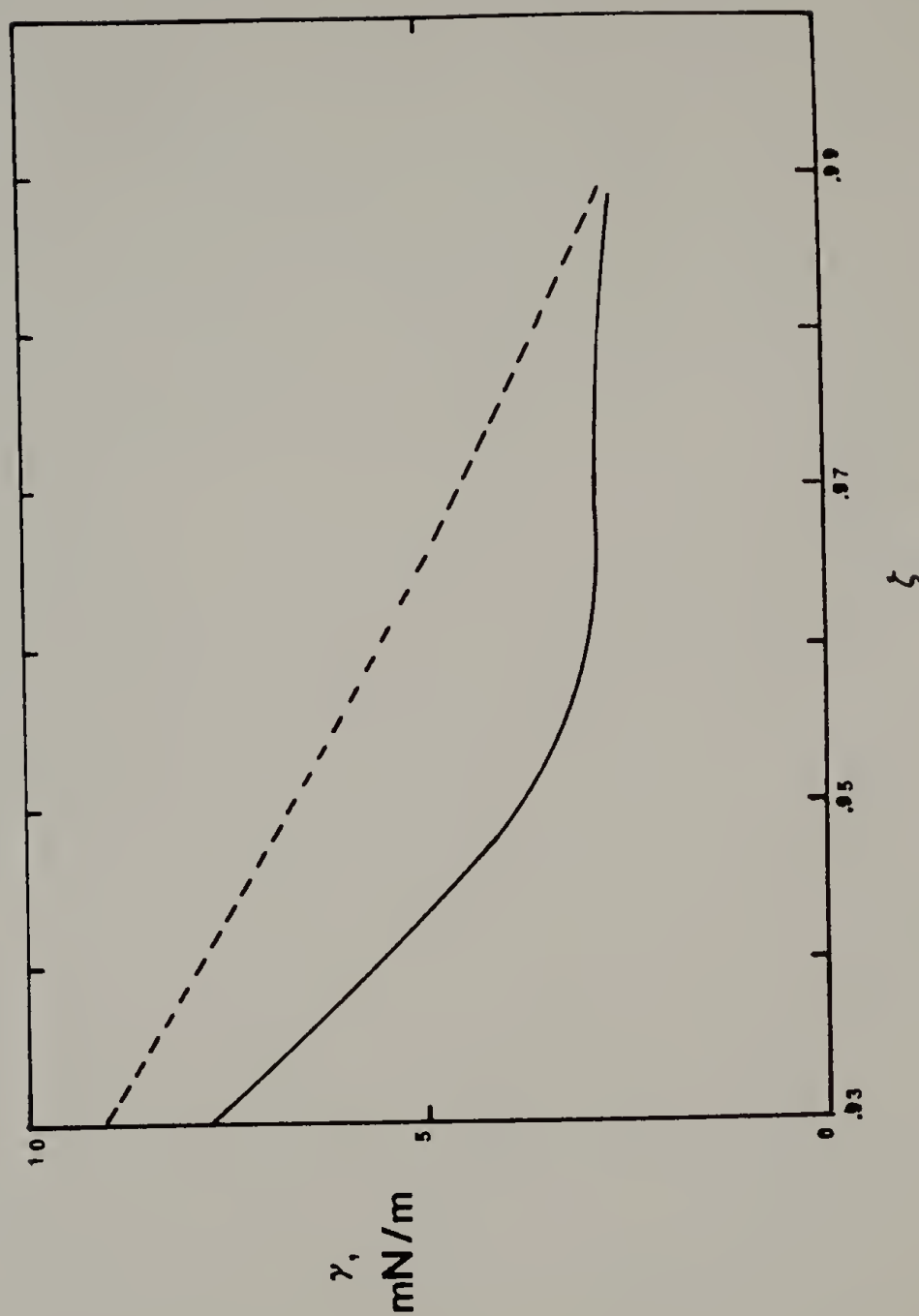


Figure 50. Dependence of the interfacial tension on the mixing parameter  $\zeta$  for poly(dimethyl siloxane)-polystyrene at 140°C. The curves were calculated with  $\delta = -.0087$ ,  $\tilde{\kappa}_{\text{PDMS}} = .60$ ,  $\tilde{\kappa}_{\text{PS}} = .57$ ,  $r_{\text{PDMS}} = 3500$ , and  $r_{\text{PS}} = 2331$ . The solid line corresponds to  $c = 1$ , and the broken line to  $c = \zeta$ .

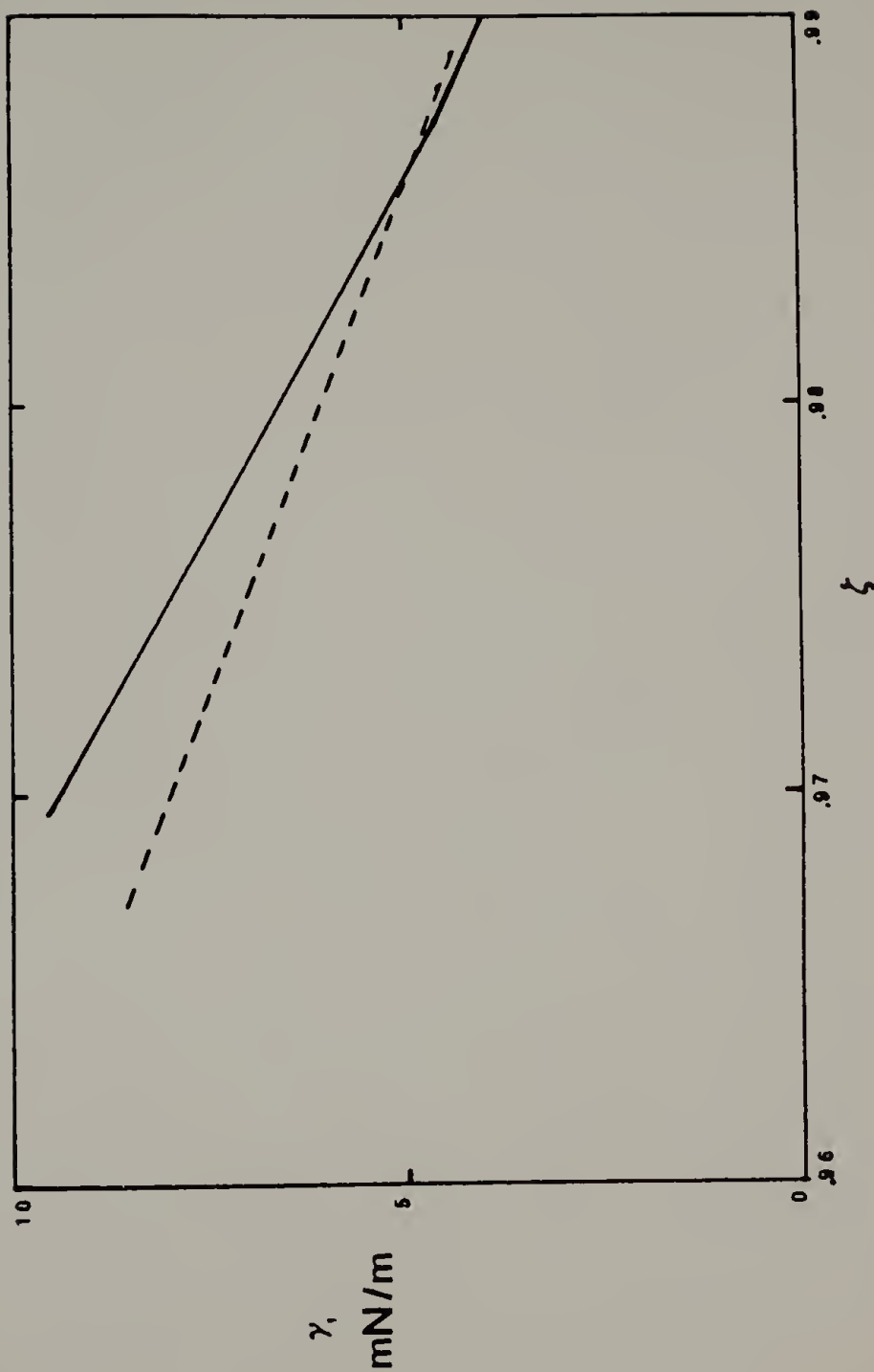


Figure 51. Dependence of the interfacial tension on the mixing parameter  $\zeta$  for poly(dimethylsiloxane)-poly(vinyl acetate) at 140°C. The curves were calculated with  $\delta = -0.0117$ ,  $\tilde{\kappa}_{\text{PDMS}} = .60$ ,  $\tilde{\kappa}_{\text{PVAc}} = .55$ ,  $r_{\text{PDMS}} = 3500$ , and  $r_{\text{PVAc}} = 889$ . The solid line corresponds to  $c = 1$ , and the broken line to  $c = \zeta$ .

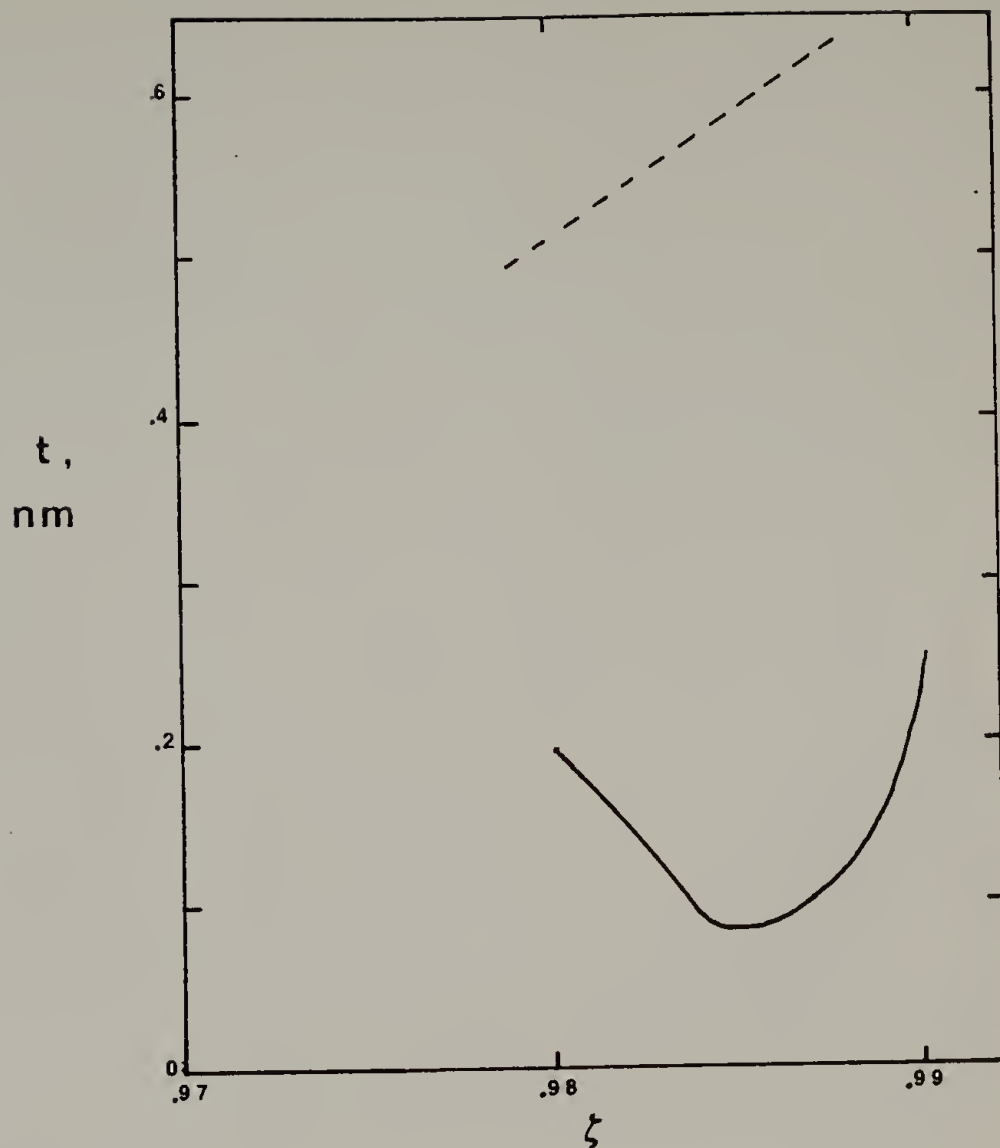


Figure 52. Dependence of the interfacial thickness on the mixing parameter  $\zeta$  for linear polyethylene-polystyrene at 140°C. The parameters are the same ones listed for Fig. 48. The solid line corresponds to  $c = 1$ , and the broken line to  $c = \zeta$ .



Table 12

THICKNESS AND  $\zeta$  FOR SOME POLYMER SYSTEMS. Values of  $\zeta$  were chosen to fit the experimental data at 140°C given in reference 74. Thicknesses predicted by Helfand and Sapse<sup>34</sup> are included for comparison.

	$\gamma_{\text{exp}}$ mN/m	$\zeta$	$\tau$ (this theory) nm	$\tau$ (Helfand & Sapse) nm
PDMS/PS	6.1	.954	.38	1.1
PDMS/PIB	4.2	.968	.35	---
PDMS/PVAC	7.4	.974	.34	.8

When we calculated the interfacial tensions of the systems in Table 12 at higher temperatures, we obtained the result that the tension increases with increasing temperature. Experimentally, of course, the tension is known to decrease. This result again serves to emphasize the importance of properly predicting the phase diagram. For the systems studied,  $140^{\circ}\text{C}$  lies in the upper portion of the phase diagram illustrated in Fig. 47. As the temperature is increased, the equilibrium phases again contain decreasing amounts of the minor component. Thus the phases become more unlike which leads to the prediction of increasing tensions with increasing temperatures.

A complete assessment of the theory for polymer-polymer systems is not possible at this time, because of the lack of mixing data. Endless variations can be produced in the phase diagrams, by adjusting  $\delta$ ,  $\zeta$  and  $r$ . One interesting point raised by this theory is the possibility of obtaining a positive  $d\gamma/dT$ . Even if the phase diagram dictated such a result, the conformational surface entropy, which we have neglected, might outweigh the phase equilibrium considerations.

## CHAPTER VI

### SUMMARY

The objective of the work presented in this dissertation was the development of a unified interfacial theory for arbitrary molecular weight systems. This problem was approached by combining the lattice fluid model with the gradient approximation to the free energy minimization for inhomogeneous systems. Due to the nature of the lattice fluid model, the resulting interfacial theory is expected to be applicable to nonpolar and slightly polar molecules away from the critical point. For such systems, good results can be obtained.

For single component liquid-vapor interfaces, only one new parameter,  $\kappa$ , arises in the interfacial theory.  $\kappa$  results from the gradient approximation, and scales the contribution of the density gradient to the total free energy of the inhomogeneous system. The value of  $\kappa$  depends solely on the choice of the intermolecular interaction potential, which implies that the depth and range of the energetic interactions are crucial to interfacial phenomena. In a liquid-vapor system, the density is assumed to change continuously from the liquid density to the vapor density, passing through thermodynamically unstable intermediate densities. The density gradient, scaled by  $\kappa$ , can be interpreted as a mechanical response needed to maintain a constant chemical potential throughout the system. The constant chemical potential requirement can be met by steeper

density profiles as the value of  $\kappa$  decreases. Molecules whose interaction energy is zero would exhibit a step-function density profile.

When we select the traditional power of 6 (corresponding to purely dispersive forces) to express the range of the interaction potential's attractive tail, we find that we consistently underestimate the tensions of low molecular weight liquids by about 10%. For polymers, the error in the range of 100–200°C is about 15%. Replacing the a priori power of 6 by 5.76 (which increases the range of the potential and simultaneously  $\kappa$ ), reduces the error to 5% for low molecular weight liquids over a wide range of temperature. The fact that a constant value of this energetic parameter yields relatively small errors for a range of nonpolar and slightly polar liquids supports the basic validity of the gradient formalism. The error for polymers can be reduced to about 10% by replacing 6 with 5.87. The theory also correctly predicts the molecular weight dependence of the interfacial tension for n-alkanes.

For the formulation of the present theory, we have neglected to account for the restrictions on polymer conformations which should arise at an interface. This leads us to underestimate the surface entropy for macromolecular systems. Nevertheless, our results for polymer tensions as a function of temperature appear to be more accurate than those obtained with various empirical correlations.

The ability of the theory to predict liquid-vapor interfacial tensions is, on the whole, very good. Comparable results have been obtained for low molecular weight liquids through a combination of the

gradient approximation with the Peng-Robinson equation of state.<sup>12</sup> This equation is an empirical modification of the van der Waals' equation. The lattice fluid equation of state describes the PVT behavior of low molecular weight liquids as accurately as the Peng-Robinson equation. The fact that both equations lead to good tension predictions suggests that PVT properties are very important in interfacial phenomena. In other words, a molecular model which hopes to describe inhomogeneous systems must be able to predict bulk densities well. This idea is further supported by the experimental observation that the tension for a given system decreases as the density difference between the phases decreases.

For binary systems, the equilibrium phases differ in both density and concentration. Since bulk properties are again expected to be important, we have examined the combining rules applied to the lattice fluid model in some detail. The set which was selected for use with the interfacial theory is quite general, and gives good results for binary miscible systems. Two mixing parameters are required for best results, but for nonpolar mixtures reasonable results can be obtained without fitted parameters.

The interfacial theory for binary mixtures contains three gradient scaling parameters:  $\kappa_{11}$ ,  $\kappa_{12}$ , and  $\kappa_{22}$ .  $\kappa_{11}$  and  $\kappa_{22}$  correspond to the pure component scaling parameters, and are thus known from the pure component theory. The cross-term,  $\kappa_{12}$ , is determined by the intermolecular interaction potential of the unlike molecules. We have treated  $\kappa_{12}$  in two ways. For liquid-vapor

systems we found that good predictions of the interfacial tension as a function of composition were obtained with  $\kappa_{12}$  set equal to the geometric mean of  $\kappa_{11}$  and  $\kappa_{22}$ . Alternately, and more consistently, we can evaluate  $\kappa_{12}$  using the lattice fluid combining rules. The geometric mean was found to be the maximum permissible value of  $\kappa_{12}$ . For liquid-liquid interfaces, the geometric mean approximation for  $\kappa_{12}$  appears to be inadequate. Since the occurrence of phase-separation unequivocally indicates that mixing is unfavorable, one would expect the unlike interaction potential to be weaker than the geometric mean of the like potentials.

The following form of the interfacial tension equation

$$\gamma = \int_{-\infty}^{\infty} [\kappa_{11} (d\rho_1/dx)^2 + 2\kappa_{12} (d\rho_1/dx)(d\rho_2/dx) + \kappa_{22} (d\rho_2/dx)^2] dx \quad (\text{VII.1})$$

illustrates further the effect of the unlike interaction potential on  $\gamma$ . Decreasing  $\kappa_{12}$  from its geometric mean value should decrease the tension if  $d\rho_1/dx$  and  $d\rho_2/dx$  are of the same sign, and increase  $\gamma$  if they are of opposite signs, unless the change in  $\kappa_{12}$  causes a considerable simultaneous change in the profiles. In liquid-vapor systems, the components' density gradients are basically of the same sign except for local variations due to preferential adsorption. Weaker unlike interactions should thus lead to a decrease in the tension. In liquid-liquid interfaces, the density gradients are of opposite signs, so that a smaller  $\kappa_{12}$  may lead to a higher tension.

The present theory is able to describe the liquid-vapor inter-

facial tension's composition dependence of nonpolar miscible mixtures to within 5% for the systems examined. Preferential adsorption of the lower tension component, which minimizes the total interfacial tension, is predicted. By properly accounting for size differences and unfavorable unlike contacts, the theory is able to reproduce behavior which has previously been attributed to ordered surface layers. Results obtained for polymer solutions are comparable to those obtained with the Gaines monolayer theory.<sup>20</sup> The present theory has the advantage of providing additional insight into the interfacial region. Profiles obtained for polymer solutions and low molecular weight mixtures show that preferential adsorption increases as mixing becomes more unfavorable. Since the tension difference between the two components is not affected by the mixing behavior, the tendency toward surface adsorption cannot solely depend on this difference. Since the interfacial region is a region of decreasing density, the enhancement of the preferential adsorption may arise in order to minimize unlike interactions.

The predictions of the theory for liquid-liquid interfaces depend sensitively on the phase diagram. While this is not surprising, it represents a drawback for polymer-polymer calculations. For such systems, the data necessary for determining the mixing parameters are unavailable. Results are thus confined to a qualitative examination of the theory. One general result of both the theory and experiment is that polymer-polymer interfacial tensions are quite small compared to pure component values. This is true despite the pronounced immis-

cibility of most polymer pairs. The reason small values of the tension result can be understood by again examining eq. VII.1. As mentioned previously, for liquid-liquid interfaces  $d\rho_1/dx$  and  $d\rho_2/dx$  are of opposite signs. The gradient cross-term is thus negative. If all three  $\kappa$ 's were equal, and the profiles were symmetric, the terms in the integrand would cancel. The interfacial tension between similar molecules will thus be relatively small, and will increase with increasing difference in the  $\kappa$ 's and in the chemical potentials which determine the profiles. Polymer pairs, because of their small mixing entropy, exhibit almost complete immiscibility even at slightly unfavorable interspecies interaction energies. The contribution of the gradient cross-term thus remains quite large leading to small interfacial tension values.

Several areas for future research suggest themselves as extensions of this work. The present theory's limitations lie in two primary areas: the restrictions to nonpolar and slightly polar systems, and the neglect of surface entropy terms arising from the effect of an interface on macromolecular conformations. The first of these limitations is a result of the bulk fluid model. We chose the lattice fluid model, because more rigorous approaches to polyatomic fluids are precluded by the lack of information on pair distribution functions. For polar molecules, the same problem is further compounded by the difficulty of constructing even approximate models. Progress



in this area is thus likely to be slow.

Work on including the conformational restrictions at an interface should be fairly straightforward, once an expression for the segment density in the bulk lattice model has been derived. This kind of derivation is difficult, but preliminary results for a single chain in a vacuum are encouraging.<sup>92</sup>

Another obvious extension of the theory is to carry out the generalization to ternary mixtures. While such an extension would involve no new theoretical concepts, the numerical problems in calculating phase equilibria are formidable. The primary gain expected from the application of the theory to ternary mixtures is insight into the interfacial structure. In addition, one could use both the binary and ternary forms of the theory to examine approximately the effect of polydispersity on polymer tensions.

## BIBLIOGRAPHY

1. J. W. Gibbs, "Collected Works," vol. I, Longmans, Green, New York, 1906.
2. J. D. van der Waals, *Z. Phys. Chem.*, 13, 657, 1894.
3. J. W. Cahn and J. E. Hilliard, *J. Chem. Phys.*, 28, 258, 1958.
4. B. Widom, *ibid.*, 43, 3892, 1965.
5. S. Fisk and B. Widom, *ibid.*, 50, 3219, 1969.
6. B. McCoy and H. T. Davis, *Phys. Rev. A*, submitted for publication.
7. F. F. Abraham, *J. Chem. Phys.*, 63, 157, 1975.
8. A. M. Yang, P. D. Fleming III, and J. H. Gibbs, *J. Chem. Phys.*, 65, 7, 1976.
9. V. Bongiorno, L. E. Scriven, and H. T. Davis, *J. Coll. Int. Sci.*, 57, 462, 1976.
10. V. Bongiorno and H. T. Davis, *Phys. Rev. A*, 12, 2213, 1975.
11. B. S. Carey, L. E. Scriven, and H. T. Davis, *AIChE J.*, 24, 1076, 1978.
12. B. S. Carey, Ph. D. Thesis, University of Minnesota, 1979.
13. J. A. Barker and D. Henderson, *Rev. Mod. Phys.*, 48, 587, 1976.
14. P. J. Flory, "Principles of Polymer Chemistry," Cornell University Press, Ithaca, N.Y., 1953.
15. S. Wu in "Polymer Blends," vol. I., D. R. Paul and S. Newman, eds., pp. 244-295, Academic Press, N.Y., 1978.
16. K. S. Siow and D. Patterson, *Macromolecules*, 4, 26, 1971.
17. D. Patterson and A. K. Rastogi, *J. Phys. Chem.*, 74, 1067, 1970.
18. I. Prigogine (with A. Belleman and V. Mathot), "The Molecular Theory of Solutions," North-Holland Publishing Co., Amsterdam and Interscience, N.Y., 1957, Chapter 16.
19. I. Prigogine and J. Marechal, *J. Colloid Sci.*, 7, 122, 1952.
20. G. L. Gaines, Jr., *J. Phys. Chem.*, 73, 3143, 1969.

21. R. J. Roe, *J. Chem. Phys.*, 60, 4192, 1974.
22. E. Helfand, *Macromolecules*, 9, 307, 1976.
23. G. L. Gaines, Jr., *J. Pol. Sci., A-2*, 7, 1379, 1969.
24. K. S. Siow and D. Patterson, *J. Phys. Chem.*, 77, 356, 1973.
25. T. A. Weber and E. Helfand, *Macromolecules*, 9, 311, 1976.
26. A. Vrij, *J. Pol. Sci., A-2*, 6, 1919, 1968.
27. P. Debye, *J. Chem. Phys.*, 31, 680, 1959.
28. A. Vrij and G. J. Roeberson, *J. Pol. Sci., Pol. Phys.*, 15, 109, 1977.
29. R. Koningsveld, L. A. Kleintjens, and A. R. Shultz, *J. Pol. Sci., A-2*, 8, 1261, 1970.
30. T. Nose, *Polymer J.*, 8, 1261, 1970.
31. T. Nose and T. V. Tan, *J. Pol. Sci., Pol. Lett.*, 14, 705, 1976.
32. E. Helfand, *J. Chem. Phys.*, 63, 2192, 1975.
33. R. J. Roe, *ibid.*, 62, 490, 1975.
34. E. Helfand and A. M. Sapse, *ibid.*, 62, 1327, 1975.
35. H. W. Kammer, *Faserforschung und Textiltechnik*, 29, 459, 1978.
36. I. C. Sanchez and R. H. Lacombe, *J. Phys. Chem.*, 80, 2352, 1976.
37. I. C. Sanchez and R. H. Lacombe, *ibid.*, 80, 2568, 1976.
38. I. C. Sanchez and R. H. Lacombe, *J. Pol. Sci., Pol. Lett.*, 15, 71, 1977.
39. I. C. Sanchez and R. H. Lacombe, *Macromolecules*, 11, 1145, 1978.
40. J. G. Kirkwood and F. P. Buff, *J. Chem. Phys.*, 17, 338, 1949.
41. B. S. Carey, L. E. Scriven, and H. T. Davis, *J. Chem. Phys.*, 69, 5040, 1978.
42. C. I. Poser and I. C. Sanchez, *J. Coll. and Int. Sci.*, 69, 539, 1979.

43. R. H. Lacombe, Report to the Materials Research Laboratory at the University of Massachusetts, unpublished.
44. R. P. Rastogi, J. Nath, and J. Misra, *J. Phys. Chem.*, 71, 1277, 1967.
45. V. T. Lam, P. Picker, D. Patterson, P. Tandrede, *J. Chem. Soc., Faraday 2*, 70, 1465, 1974.
46. M. Diaz Peña and C. Menduina, *J. Chem. Thermo.*, 6, 1097, 1974.
47. T. G. Bissell, G. E. Okafor, A. C. Williamson, *J. Chem. Thermo.*, 3, 393, 1971.
48. A. E. P. Watson, T. A. McLure, J. E. Bennett, and G. C. Benson, *J. Phys. Chem.*, 69, 2753, 1965.
49. S.-S. Chen and Bruno J. Trvolinski, *J. Chem. Soc., Faraday 2*, 70, 1133, 1974.
50. B. S. Harsted and E. S. Thomson, *J. Chem. Thermo.*, 6, 549, 1974.
51. T. M. Letcher, *ibid.*, 7, 205, 1975.
52. M. Diaz Peña and J. N. Delgado, *ibid.*, 7, 201, 1975.
53. K. Y. Hsu and H. L. Clever, *J. Chem. Thermo.*, 7, 435, 1975.
54. S. Murakami, V. T. Lam, G. C. Benson, *J. Chem. Thermo.*, 1, 397, 1969.
55. R. K. Nigam, P. P. Singh, and N. N. Maini, *Indian J. Chem.*, 8, 908, 1970.
56. R. K. Nigam and P. P. Singh, *Trans. Far. Soc.*, 65, 950, 1969.
57. T. M. Letcher, *J. Chem. Thermo.*, 4, 159, 1972.
58. T. M. Letcher and J. W. Bayles, *J. Chem. Eng. Data*, 16, 266, 1971.
59. J. M. Berryman and E. L. Heric, *Can. J. Chem.*, 50, 2799, 1972.
60. C. D. Wedlake and F. A. L. Dullien, *J. Chem. Eng. Data*, 19, 229, 1967.
61. R. P. Rastogi, J. Nath, and J. Misra, *J. Phys. Chem.*, 71, 2524, 1967.

62. V. T. Lam, S. Murakami, and G. C. Benson, *J. Chem. Thermo.*, 2, 17, 1970.
63. J. Gómez-Ibáñez and C. T. Liu, *J. Phys. Chem.*, 65, 2148, 1961.
64. K. R. Harris and P. J. Dunlop, *J. Chem. Thermo.*, 2, 805, 1970.
65. J. Timmermans, "Physico-Chemical Constants of Binary Systems in Concentrated Solutions," vol. I, Interscience, New York, N.Y., 1959.
66. K. U. Co, J. J. Kozak, and K. D. Luks, *J. Chem. Phys.*, 66, 1002, 1977.
67. S. Toxvaerd, *J. Chem. Phys.*, 55, 3116, 1971.
68. R. C. Reid, T. K. Sherwood, and J. M. Prausnitz, "The Properties of Gases and Liquids," McGraw-Hill, N.Y., 1977.
69. J. Timmermans, "Physico-Chemical Constants of Pure Organic Compounds," American Elsevier, New York, vol. I, 1950 and vol. II, 1965.
70. N. B. Vargaftik, "Tables on the Thermophysical Properties of Liquids and Gases," John Wiley & Sons, New York, 2nd Ed., 1975.
71. D. G. LeGrand and G. L. Gaines, Jr., *J. Coll. and Int. Sci.*, 31, 162, 1969.
72. F. D. Rossini, "Selected Values of Properties of Hydrocarbons and Related Compounds," American Petroleum Research Institute, Research Project 44, Carnegie Press, 1953.
73. G. L. Gaines, Jr., *Pol. Eng. & Sci.*, 12, 1, 1972.
74. S. Wu, *J. Macromol. Sci.*, C10, 1, 1974.
75. R. S. Porter, private communication.
76. R. J. Roe, *J. Phys. Chem.*, 64, 2809, 1965.
77. S. Sugden, *J. Chem. Soc.*, 125, 32, 1924.
78. D. B. McLeod, *Trans. Far. Soc.*, 19, 38, 1923.
79. F. J. Wright, *J. Appl. Chem.*, 11, 193, 1961.
80. O. R. Quayle, *Chem. Rev.*, 53, 439, 1953.

81. S. Wu, *J. Coll. Int. Sci.*, 31, 153, 1969.
82. R. J. Roe, *ibid.*, 31, 228, 1969.
83. S. Wu, *J. Phys. Chem.*, 74, 632, 1970.
84. J. H. Hildebrand and R. L. Scott, "Solubility of Nonelectrolytes," Reinhold Publishing Corp., New York, N.Y., 1950.
85. P. J. Flory, R. A. Orwoll, and A. Vrij, *J. American Chem. Soc.*, 86, 3515, 1964.
86. R. Bellman, "Introduction to Matrix Analysis," McGraw-Hill, New York, N.Y., 1970.
87. K. Ridgway and P. A. Butler, *J. Chem. Eng. Data*, 12, 509, 1967.
88. R. L. Schmidt, J. C. Randall, and H. L. Clever, *J. Phys. Chem.*, 70, 3912, 1966.
89. R. L. Schmidt and H. L. Clever, *J. Coll. and Int. Sci.*, 26, 19, 1968.
90. "Polymer Handbook," J. Brandrup and E. H. Immergut, eds., 2nd edition, Wiley-Interscience, New York, N.Y., 1975.
91. E. Helfand, *Macromolecules*, 11, 682, 1978.
92. I. C. Sanchez, *in press*, *Macromolecules*, 12, 1979.
93. J. A. Nelder and R. Mead, *Comp. J.*, 7, 308, 1964.
94. R. P. Brent, "Algorithms for Minimization Without Derivatives," Prentice-Hall, Englewood Cliffs, N.J., 1973.

APPEND IX

## NUMERICAL TECHNIQUES

### A. Binary Phase Equilibria

The equations which govern any two-component two-phase equilibrium can be written:

$$\mu_1^{\text{I}}(T, P, \phi_1^{\text{I}}) - \mu_1^{\text{II}}(T, P, \phi_1^{\text{II}}) = 0 \quad (\text{A.1})$$

$$\mu_2^{\text{I}}(T, P, \phi_1^{\text{I}}) - \mu_2^{\text{II}}(T, P, \phi_1^{\text{II}}) = 0 \quad . \quad (\text{A.2})$$

For the case of liquid-vapor equilibrium these equations have been solved for the equilibrium vapor pressure and the vapor composition at a fixed liquid composition and temperature. Note that in this calculation the reducing parameters in the vapor phase are functions of the composition, as is  $\tilde{p}$  via the equation of state.  $\tilde{p}$  is also a function of the pressure in both phases. The numerical method employed was a simplex function minimization method first described by Nelder and Mead.<sup>93</sup> A good initial guess for the simplex iteration is to set the vapor composition equal to the liquid composition and the vapor pressure to the average of the two pure component vapor pressures. The convergence criteria were selected such that the sum of the residuals of eqs. A.1 and 2 did not exceed  $.5 \times 10^{-11}$  kcal/mole. The number of iterations required to produce convergence was about 120. The iterative procedure was carried out on the natural logarithms of the variables to prevent the occurrence of negative values.

For the case of liquid-vapor equilibria in polymer solutions,



the vapor concentration of polymer is negligible and was set equal to zero. Eq. A.1 was then solved for the vapor pressure. The pressure is bounded by 0 and the critical pressure of the mixture evaluated from

$$\bar{P}_c = (2r \ln(1 + 1/\sqrt{r}) + \frac{1}{2} - r)/(1 + \sqrt{r})^2 . \quad (\text{A.3})$$

These bounds were further refined using a bisectioning search routine to find two values of the pressure between which eq. A.1 changes sign. A function-solving routine due to R. Brent<sup>94</sup> was then applied to find the vapor pressure.

For the case of liquid-liquid equilibria, the simplex algorithm mentioned above can also be applied if the variables are properly chosen. When we fix the pressure and temperature and try to solve for the compositions in the two phases, this algorithm returns the trivial result of equal compositions. The problem can, however, be posed in different terms. We can specify the pressure and the composition difference between the phases and solve for the temperature and the composition in one phase. For the initial guess, any temperature below the critical temperature will serve. For the phase I composition, one half minus half of the specified difference was found to be effective. While this method is successful for determining the binodal curve, one obviously cannot use it easily to determine the compositions at a desired temperature.

For this reason, we alternately solved eqs. A.1 and A.2 for liquid-liquid systems by using a Newton-Raphson iteration on the two

composition variables at a fixed temperature and pressure. This algorithm was found to be very efficient, however, a problem arises for liquid-liquid systems whose phases contain only a very small amount of one of the components. The chemical potentials contain  $\ln \phi_j$  terms. When  $\phi_j$  is a number close to 0, the Newton-Raphson routine often produces negative values of  $\phi_j$  in the course of iteration. For two components, this problem can be dealt with by introducing four additional variables

$$Y1 = \ln \phi_1^I \quad (\text{A.4})$$

$$Y2 = \ln \phi_1^{II} \quad (\text{A.5})$$

$$Y3 = \ln (1 - \phi_1^I) \quad (\text{A.6})$$

$$Y4 = \ln (1 - \phi_1^{II}) \quad (\text{A.7})$$

along with four equations

$$e^{Y1} - \phi_1^I = 0 \quad (\text{A.8})$$

$$e^{Y2} - \phi_1^{II} = 0 \quad (\text{A.9})$$

$$e^{Y3} - 1 + \phi_1^I = 0 \quad (\text{A.10})$$

$$e^{Y4} - 1 + \phi_1^{II} = 0 \quad (\text{A.11})$$

Using this six variable Newton-Raphson algorithm, we can calculate mer fractions as low as  $10^{-22}$  without difficulty. The Newton-Raphson method uses the partial derivatives of the equations with respect to each variable in the iteration. For this particular application, numerical evaluation of these derivatives via the definition

$$\frac{\partial F}{\partial x} = \{F(x + \frac{1}{2}\Delta x) - F(x - \frac{1}{2}\Delta x)\} / \Delta x \quad (\text{A.12})$$

with  $\Delta x = \text{xx}10^{-6}$  gave adequate results.

### B. Interfacial Tensions

The interfacial equations to be evaluated for pure components are

$$\tilde{\gamma} = 2 \sqrt{\kappa} \int_{\tilde{\rho}_0}^{\tilde{\rho}_l} \frac{1}{\sqrt{\Delta \tilde{a}}} d\tilde{\rho} \quad (\text{A.13})$$

and

$$\tilde{x} - \tilde{x}_0 = \sqrt{\kappa} \int_{\tilde{\rho}_0}^{\tilde{\rho}_g} \frac{1}{\sqrt{\Delta \tilde{a}}} d\tilde{\rho} \quad (\text{A.14})$$

The integrations were performed using the Gauss-Legendre formula. Since this formula assumes an interval of integration from 0 to 1, the above integrals were normalized to this interval. The number of points,  $N$ , used in the integration varied from 100 to 198. Increasing  $N$  beyond 100 increases the value of the integral only very slightly in the sixth significant figure. For the integration of eq. A.14,  $\tilde{x}_0$  and  $\tilde{\rho}_0$  were arbitrarily set equal to zero and  $\frac{1}{2}(\tilde{\rho}_g + \tilde{\rho}_l)$ , respectively. Note that we cannot calculate the value of  $\tilde{x}$  when  $\tilde{\rho}$  is equal to  $\tilde{\rho}_g$  or  $\tilde{\rho}_l$ , since those values of  $\tilde{\rho}$  result in  $\Delta \tilde{a} = 0$ .

Several different types of calculations were used to evaluate tensions and profiles for binary mixtures. When the geometric mean approximation for  $\kappa_{12}$  is applied, the governing equation can be written in terms of a variable,  $\Phi$ , defined by

$$\Phi = \sqrt{\kappa_{11}} \rho_1 + \sqrt{\kappa_{22}} \rho_2 \quad (\text{A.15})$$

The interfacial equations are then given by

$$\gamma = \sqrt{2} \int_{\Phi}^{\text{II}} \frac{1}{\sqrt{\Delta \tilde{a}}} d\Phi \quad (\text{A.16})$$

and

$$x - x_0 = \int_{\phi_0}^{\phi} \sqrt{2\Delta a} \, d\phi. \quad (\text{A.17})$$

These equations are subject to the equilibrium condition

$$\sqrt{\kappa_{11}} \frac{\partial \Delta a}{\partial \rho_1} - \sqrt{\kappa_{22}} \frac{\partial \Delta a}{\partial \rho_2} = 0. \quad (\text{A.18})$$

The integrations are here again carried out using the Gauss-Legendre formulas. At each point in the numerical integration,  $\Delta a$  must, of course, be evaluated. This is accomplished by rewriting  $\rho_2$  in eq. A.18 as

$$\rho_2 = (\phi - \sqrt{\kappa_{11}} \rho_1) / \sqrt{\kappa_{22}} \quad (\text{A.19})$$

and subsequently solving eq. A.18 for  $\rho_1$ . Since  $\Delta a$  and  $\frac{\partial \Delta a}{\partial \rho_j}$  are more conveniently written in terms of  $\phi_1$  and  $\tilde{\rho}$ , the following transformations are useful:

$$\phi_1 = \frac{\rho_1}{(\rho_1 + \rho_2)} \quad (\text{A.20})$$

$$\tilde{\rho} = \rho_1 v_1^* + \rho_2 v_2^* + \Delta v \rho_1 \rho_2 / (\rho_1 + \rho_2). \quad (\text{A.21})$$

$\tilde{\rho}$ , by definition, must lie between 0 and 1. Eq. A.19 can be substituted into eq. A.21, which results in a quadratic in  $\rho_1$ . Lower and upper bounds on  $\rho_1$  at a given  $\phi$  are obtained by requiring the quadratic to be equal to one. The condition  $\rho_1 > 0$  serves as a lower bound if the quadratic condition yields a negative lower bound.

Once the bounds have been located, a bisecting search routine is used to refine them further by locating two values of  $\rho_1$  between which eq. A.19 changes sign. This step is necessary because eq. A.19 contains  $\ln(1-\tilde{\rho})$  terms, and thus cannot be evaluated at the bounds obtained analytically. Finally, the function-solving routine mentioned earlier<sup>94</sup> locates the value of  $\rho_1$  which satisfies eq. A.19 for the desired value of  $\Phi$ .

Alternately, the geometric mean problem can be treated using the form

$$\gamma = \sqrt{2} \int_{\rho_1^I}^{\rho_1^{II}} [\kappa_{11} + 2\kappa_{12} d\rho_2/d\rho_1 + \kappa_{22} (d\rho_2/d\rho_1)^2]^{\frac{1}{2}} \Delta a^{\frac{1}{2}} d\rho_1 \quad (\text{A.22})$$

and

$$x - x_0 = \int_{\rho_1(x_0)}^{\rho_1(x)} [\kappa_{11} + 2\kappa_{12} d\rho_2/d\rho_1 + \kappa_{22} (d\rho_2/d\rho_1)^2]^{\frac{1}{2}} \Delta a^{-\frac{1}{2}} d\rho_1. \quad (\text{A.23})$$

subject to eq. A.19. If the density profile of component one is monotonic, we can write  $m$  simultaneous equations for A.19:

$$\sum_{i=1}^m \sqrt{\kappa_{i1}} \frac{\partial \Delta a}{\partial \rho_1} (\rho_1^i, \rho_2^i) + \sqrt{\kappa_{22}} \frac{\partial \Delta a}{\partial \rho_2} (\rho_1^i, \rho_2^i) = \sum_{i=1}^m F_i = 0 \quad (\text{A.24})$$

where

$$\rho_1^i = \rho_1^{i-1} + (\rho_1^{II} - \rho_1^I) / m. \quad (\text{A.25})$$

The equations defined by eq. A.24 can then be solved for the  $\rho_2^i$  by using the  $m$ -dimensional form of the Newton-Raphson algorithm. The initial guess for the  $\rho_2^i$  was defined analogously to eq. A.25.

In this case, the partial derivative required for the iterative procedure was evaluated analytically. Using eq. VI.23, we can write

$$\frac{\partial F_i}{\partial \rho_2} = \sqrt{\kappa_{11}} \frac{\partial \mu_1}{\partial \rho_2} (\rho_1^i, \rho_2^i) + \sqrt{\kappa_{22}} \frac{\partial \mu_2}{\partial \rho_2} (\rho_1^i, \rho_2^i) . \quad (\text{A.26})$$

If we treat  $\phi_2$  as a function of  $\phi_1$ ,

$$\frac{\partial \mu_1}{\partial \rho_2} = \left. \frac{\partial \mu_1}{\partial \tilde{\rho}} \right)_{\phi_1} \frac{\partial \tilde{\rho}}{\partial \rho_2} + \left. \frac{\partial \mu_1}{\partial \phi_1} \right)_{\tilde{\rho}} \frac{\partial \phi_1}{\partial \rho_2} \quad (\text{A.27})$$

and

$$\frac{\partial \mu_2}{\partial \rho_2} = \left. \frac{\partial \mu_2}{\partial \tilde{\rho}} \right)_{\phi_1} \frac{\partial \tilde{\rho}}{\partial \rho_2} + \left. \frac{\partial \mu_2}{\partial \phi_1} \right)_{\tilde{\rho}} \frac{\partial \phi_1}{\partial \rho_2} . \quad (\text{A.28})$$

Now,

$$\frac{\partial \tilde{\rho}}{\partial \rho_2} = v_2^* + \phi_1^2 \Delta v \quad (\text{A.29})$$

and

$$\frac{\partial \phi_1}{\partial \rho_2} = -v^* \phi_1 \tilde{v} . \quad (\text{A.30})$$

The other derivatives are given by:

$$\begin{aligned} \left. \frac{\partial \mu_1}{\partial \tilde{\rho}} \right)_{\phi_1} = & -\epsilon_{11}^* + X_{12} \phi_2^2 - \tilde{v} k T [\tilde{v} \ln(1-\tilde{\rho}) + \tilde{\rho}^2 + \frac{1}{r_1}] + \\ & \{-\epsilon^* + \tilde{v} k T [\tilde{v} \ln(1-\tilde{\rho}) + \frac{1}{1-\tilde{\rho}}]\} \left( \frac{v_1^* + \phi_2^2 \Delta v}{v^*} \right) \end{aligned} \quad (\text{A.31})$$

$$\begin{aligned}
\frac{\partial \mu_1}{\partial \phi_1} \Big|_{\tilde{\rho}} &= kT \left( \frac{1}{r_1 \phi_1} + \frac{1}{r_2} - \frac{1}{r_1} \right) - \tilde{\rho} \left( 2\phi_2 X_{12} - \frac{dX_{12}}{d\phi_1} \phi_2^2 \right) + \\
&\quad \left\{ -\tilde{\rho} \frac{d\epsilon^*}{d\phi_1} + kT \left( \frac{1}{r_1} - \frac{1}{r_2} \right) \right\} \left( \frac{v_1^* + \phi_2^2 \Delta v}{v^*} \right) + \\
\epsilon^* \left\{ \tilde{\rho} + \tilde{T} \left[ \tilde{v} \ln(1-\tilde{\rho}) + 1 - \frac{1}{r} \right] \right\} &\left( \frac{v_1^* + \phi_2^2 \Delta v}{v^{*2}} \frac{dv^*}{d\phi_1} + \frac{2\phi_2 \Delta v}{v^*} \right).
\end{aligned}
\tag{A.32}$$

$\frac{\partial \mu_2}{\partial \tilde{\rho}} \Big|_{\phi_1}$  and  $\frac{\partial \mu_2}{\partial \phi_1} \Big|_{\tilde{\rho}}$  can be obtained from eqs. A.31 and A.32 by exchanging subscripts. The quantities  $\frac{d\epsilon^*}{d\phi_1}$ ,  $\frac{dv^*}{d\phi_1}$ ,  $\frac{dX_{12}}{d\phi_1}$ , and  $\frac{dX_{21}}{d\phi_1}$  are defined as in Chapter IV.

The convergence criterion applied to the Newton-Raphson algorithm was

$$\sum_{i=1}^m F_i^2 \leq 10^{-16}. \tag{A.33}$$

Once the  $m$  values of  $\rho_2$  satisfying eq. A.24 had been found, eqs. A.22 and A.23 were evaluated using the trapezoidal integration formula. The value of  $d\rho_2/d\rho_1$  at a given point was set equal to its finite difference value

$$\frac{d\rho_2}{d\rho_1} = (\rho_2^{i+1} - \rho_2^{i-1})/2\Delta\rho_1; \quad \Delta\rho_1 = (\rho_1^{II} - \rho_1^I)/m.
\tag{A.34}$$

For  $m = 150$  this routine gave results which differed from the Gaussian integration results in the fifth significant figure. One would

expect this technique to require a larger number of points to achieve the same level of accuracy, since the trapezoidal integration formula is less accurate than the Gaussian one.

The numerical procedure applied to eqs. A.22 and A.23 for the case  $\kappa_{12} < (\kappa_{11}\kappa_{22})^{1/2}$  follows the same principle discussed above. In this case the equilibrium condition may be written:

$$\begin{aligned} & [\kappa_{11} + 2\kappa_{12}d\rho_2/d\rho_1 + \kappa_{22}(d\rho_2/d\rho_1)^2][\partial\Delta a/\partial\rho_2(\kappa_{11} + \kappa_{12}d\rho_2/d\rho_1) - \\ & \partial\Delta a/\partial\rho_1(\kappa_{12} + \kappa_{22}d\rho_2/d\rho_1)] - d^2\rho_2/d\rho_1^2 [2\Delta a(\kappa_{11}\kappa_{22} - \kappa_{12}^2)^2] = 0 . \end{aligned} \quad (\text{A.35})$$

If we again assume that component one exhibits a monotonic density profile, we can solve

$$\sum_{i=1}^m F_i = 0 \quad (\text{A.36})$$

where  $F_i$  refers to the left-hand side of eq. A.35 evaluated at  $\rho_1^i, \rho_2^i$  and the  $\rho_1^i$  are defined as previously. The derivatives  $d\rho_2^i/d\rho_1$  and  $d^2\rho_2^i/d\rho_1^2$  are written in the finite difference approximation. Eq. A.34 defines  $d\rho_2^i/d\rho_1$  and

$$d^2\rho_2^i/d\rho_1^2 = (\rho_2^{i+1} - 2\rho_2^i + \rho_2^{i-1})/\Delta\rho_1^2 . \quad (\text{A.37})$$

Due to the forms of eqs. A.34 and A.37,  $F_i$  depends not only on  $\rho_2^i$ , but is also a function of  $\rho_2^{i+1}$  and  $\rho_2^{i-1}$ . The Jacobian matrix which must be set up for the Newton-Raphson iteration is thus



tridiagonal; each row contains  $\partial F_i / \partial \rho_2^{i-1}$ ,  $\partial F_i / \partial \rho_2^i$ , and  $\partial F_i / \partial \rho_2^{i+1}$ . These derivatives are

$$\begin{aligned} \frac{\partial F_i}{\partial \rho_2^{i-1}} = & -[(\kappa_{12} + \kappa_{22} d\rho_2/d\rho_1)/\Delta\rho_1][\partial\Delta a/\partial\rho_2(\kappa_{11} + \kappa_{12} d\rho_2/d\rho_1) - \\ & \partial\Delta a/\partial\rho_1(\kappa_{12} + \kappa_{22} d\rho_2/d\rho_1)] + [\kappa_{11} + 2\kappa_{12} d\rho_2/d\rho_1 + \kappa_{22} (d\rho_2/d\rho_1)^2] \times \\ & [-\partial\Delta a/\partial\rho_1(\kappa_{12}/2\Delta\rho_1) + \partial\Delta a/\partial\rho_1(\kappa_{22}/2\Delta\rho_1)] - \\ & [2\Delta a(\kappa_{11}\kappa_{22} - \kappa_{12})^2]/\Delta\rho_1^2, \end{aligned} \quad (\text{A.38})$$

$$\begin{aligned} \frac{\partial F_i}{\partial \rho_2^{i+1}} = & [(\kappa_{12} + \kappa_{22} d\rho_2/d\rho_1)/\Delta\rho_1][\partial\Delta a/\partial\rho_2(\kappa_{11} + \kappa_{12} d\rho_2/d\rho_1) - \\ & \partial\Delta a/\partial\rho_1(\kappa_{12} + \kappa_{22} d\rho_2/d\rho_1)] + [\kappa_{11} + 2\kappa_{12} d\rho_2/d\rho_1 + \kappa_{22} (d\rho_2/d\rho_1)^2] \times \\ & [\partial\Delta a/\partial\rho_1(\kappa_{12}/2\Delta\rho_1) - \partial\Delta a/\partial\rho_1(\kappa_{22}/2\Delta\rho_1)] - \\ & [2\Delta a(\kappa_{11}\kappa_{22} - \kappa_{12})^2]/\Delta\rho_1^2, \end{aligned} \quad (\text{A.39})$$

and

$$\begin{aligned} \frac{\partial F_i}{\partial \rho_2} = & [\kappa_{11} + 2\kappa_{12} d\rho_2/d\rho_1 + \kappa_{22} (d\rho_2/d\rho_1)^2][\frac{\partial}{\partial \rho_2} (\partial\Delta a/\partial\rho_2)(\kappa_{11} + \kappa_{12} d\rho_2/d\rho_1) - \\ & \frac{\partial}{\partial \rho_2} (\partial\Delta a/\partial\rho_1)(\kappa_{12} + \kappa_{22} d\rho_2/d\rho_1)] + 2[2\Delta a(\kappa_{11}\kappa_{22} - \kappa_{12})^2]/\Delta\rho_1^2 - \\ & d^2\rho_2/d\rho_1^2 [2\partial\Delta a/\partial\rho_2(\kappa_{11}\kappa_{22} - \kappa_{12})^2]. \end{aligned} \quad (\text{A.40})$$

Since

$$\frac{\partial}{\partial \rho_2} (\partial \Delta a / \partial \rho_2) = \frac{\partial \mu_2}{\partial \rho_2} \quad (\text{A.41})$$

and

$$\frac{\partial}{\partial \rho_2} (\partial \Delta a / \partial \rho_1) = \frac{\partial \mu_1}{\partial \rho_2} \quad , \quad (\text{A.42})$$

both of which we have already evaluated, no further quantities are needed. Once the  $\rho_2^i$  have been obtained, the integrals are evaluated in the same way as for the geometric mean case. The initial guesses for the  $\rho_2^i$  which were found to be most likely to result in convergence were the  $\rho_2^i$  which formed the solution in the geometric mean approximation.

As mentioned previously, solutions to eqs. A.22 and A.23 could only be obtained when the density profile of component one is monotonic. For most real systems, one of the components exhibits preferential surface adsorption, i.e. has a nonmonotonic profile. One way to determine which component exhibits this behavior is to "map" eq. A.18 in the same manner as we mapped the spinodal equation previously. The two variables are  $\rho_1$  and  $\rho_2$ , and the contour line along which eq. A.18 changes sign is the path which the solution to the interfacial tension equation must follow. If the same value of  $\rho_2$  corresponds to two different values of  $\rho_1$ ,  $\rho_2$  is the adsorbing component. Fig. 53 is a schematic diagram of such a solution path for a liquid-vapor system. This kind of diagram is also useful for determining whether a solution exists at all. For certain values of

the mixing parameters of polymer-polymer systems, there is no path which connects the equilibrium phase compositions.

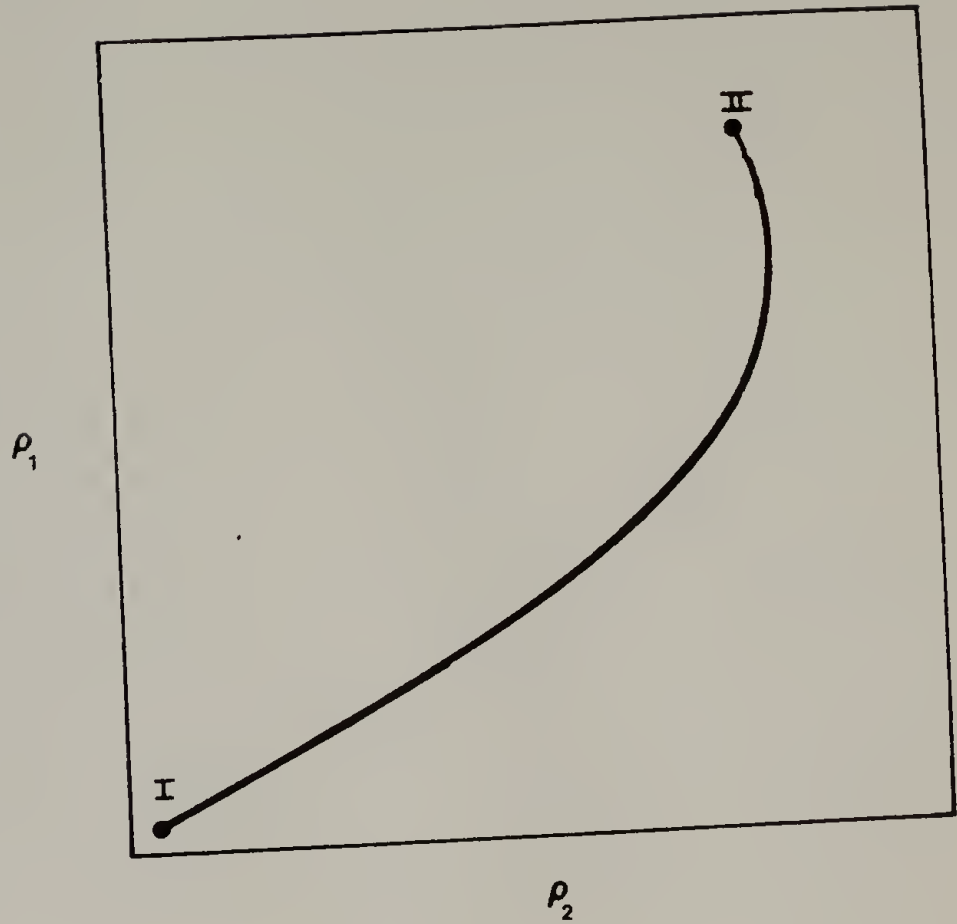


Figure 53. Schematic representation of a solution path for a liquid-vapor interface. Component 2 exhibits surface adsorption.

